NANOSTRUCTURES FOR DONOR-ACCEPTOR PAIR LUMINESCENCE

NANOSTRUCTURES FOR DONOR-ACCEPTOR PAIR LUMINESCENCE

By

FENG CHEN, M. ENG

A Thesis
Submitted to the School of Graduate Studies
in Partial Fulfillment of the Requirements
for the Degree
Doctor of Philosophy

McMaster University

DOCTOR OF PHILOSOPHY (2008)

(Materials Science)

McMaster University

Hamilton, Ontario

TITLE: Nanostructures for Donor-Acceptor Pair Luminescence

AUTHOR: Feng Chen, M. Eng. (Harbin Institute of Technology,China)

SUPERVISOR: Professor A.H.Kitai

NUMBER OF PAGES: XI, 115

Abstract

Commercial success had been achieved with electroluminescent phosphor powders, particularly zinc sulfide activated with copper. The applications of AC Powder EL (ACPEL) are mainly limited to backlighting and lamp applications that require low brightness. This includes low illumination environments, such as nightlights and backlighting for LCDs and keypads in portable electronics and home electronics.

By using nanowires as nanoelectrodes, a novel and self-supported nanostructured powder EL device has been developed in this thesis. The novel structure contains a single layer of ZnS:Cu powder phosphor which is embedded in a polymer matrix with one surface exposed. A dilute layer of conductive nanowires directly contacts the phosphor layer and works as rear electrodes. A highly intensified electric field can be induced in the phosphor region by the metal nanowires if a specific voltage is applied to the device. Simulations of the electric field by using commercial software show that the localized electric field can be at least one order of magnitude higher than the average field depending on the dimensions of the nanowires. As a result, electrons can be injected into the phosphor lattice by high-field-assisted tunneling, hence inducing electron avalanching. The electrons finally are trapped at the donors. When the external field is reversed, the electrons recombine with the holes that are previously injected by the same process and trapped at the acceptors. Therefore, visible light is produced by the recombination of the electron-hole pairs through the donor-acceptor pairs.

The indium nanowires, with diameters of 300 nm and lengths of several microns, have been fabricated by using anodic aluminum oxide (AAO) templates which are known as self-organized porous structures formed by anodization of aluminum in an appropriate acid solution. A hydraulic pressure injection method has been applied to inject molten indium metal into the nanopores of the AAO template and form nanowires. By dissolution of the template, a large number of free indium nanowires is obtained. The nanowires are transferred onto a ZnS-embedded substrate by a wet-coating method. Finally, the entire device is completed by deposition of Au rectangular electrodes on the top of the indium nanowires. The indium nanowires have been characterized by using SEM and XRD.

The tests of the dependence of luminance on voltage at various frequencies for a nanowire contact EL device sample are performed. A peak luminance of 25 cd/m^2 has been achieved for the device driven at frequency of 8.2 kHz and a voltage of 425 V. The EL performance of the nanowire contact EL device is not as good as traditional powder EL devices so far, however, the novel structures have the potential for a lower operating voltage with simultaneous long lifetime and high luminance to overcome limitations of traditional powder EL.

Acknowledgements

The work contained in this thesis could not have been completed without the guidance and support of my supervisor Dr. Adrian Kitai. His enthusiasm throughout the project made the successes that much more exciting and the failures seem not so bad. I have learned much under his direction from which I will benefit in my rest of life. I would also like to thank the members of my supervisory committee: Dr. Igor Zhitomirsky, and Dr. Marek Niewczas for their support and helpful suggestions.
I would like to express my thanks to the staff of the Department of Materials Science and Engineering who aided me throughout my years in graduate school.
Lastly, I would like to thank my wife, Rui Cai, my daughter Cindy, and my parents for their support in my years in McMaster University. I would like to dedicate this thesis to them.

Table of Contents

Section **Page**

List of Figures

Figure Page

Appendix I:

Appendix II:

List of Tables

Table of Abbreviations

Acronym	Definition
n-UV	Near-ultraviolet, wavelength 300-400 nm
MQWs	Muti-quantum walls
ITO	Indium Tin Oxide
CRT	Cathode Ray Tube
UV	Ultraviolet
DUV	Deep Ultraviolet
EUV	Extreme Ultraviolet
SWNTs	Single-wall nanotubes
AAO	Anodic Alumium Oxide
R.F.	Radio Frequency (5-30MHz)

Chapter 1. Introduction

Electroluminescence (EL) is the non-thermal emission of visible light from a crystal (or a system of microcrystals) as a result of current flow or the application of an electric field. Historically, EL was first observed in silicon carbide (SiC) by Captain Henry Joseph Round in 1907 (Round, 1907). Round reported that yellow light was produced when a current was passed through a silicon carbide detector (Gooch, 1973). The second reported observation of EL did not occur until 1923, when O.V. Lossev of the Nijni-Novgorod Radio Laboratory in Russia again reported EL in silicon carbide crystals (Lossev, 1924 and 1928). This type of electroluminescence was known as the "Lossev effect" and is considered nowadays as junction electroluminescence in a semiconductor (Grimmeiss and Allen, 2006), for example, light-emitting diode (LED). The underlying light-emitting mechanism is the injection of minority carriers across a forward-biased p-n junction, followed by radiative recombination of electrons and holes. Consequently, single crystalline materials are required in this kind of device so as to achieve sufficient diffusion length of the minority carriers.

Theoretically, the EL of inorganic materials is classified into the two groups: injection EL and high electric field EL. The high-field EL can be further grouped into different types in terms of the phosphors (powder vs. thin film) and of the driving voltage (DC vs. AC). Due to the requirements for various applications, injection EL, (high intensity lighting-emitting diodes (LEDs), for example,) have a wide application in LCD backlighting and are entering the lighting market. Powder EL has long been used in nightlights and illumination panels since the middle of the last century. Also, thin-film EL is commercially available for environmentally demanding display applications.

This thesis presents a new powder EL device structure combining phosphor powders with a recent nanotechnology platform. Therefore, powder EL devices, including the history, structure, materials and underlying operating principles will be examined in detail in this thesis. By way of introduction, however, injection EL (LED) and thin-film EL will be both reviewed.

1.1 Injection EL (LED)

The term "injection EL" is used to explain the phenomenon of luminescence produced from diode-type devices by the injection of minority carriers. In 1952 Haynes and Briggs (Haynes and Briggs, 1952) reported infrared EL from forward-biased p-n junctions in Ge and Si diodes. This type of EL is classified as injection EL. Later, visible EL was observed in diodes made of wide bandgap semiconductors, such as GaP. These diodes are called light-emitting diodes (LEDs). Since then, many experiments were carried out to generate light emission at the p-n junction of diodes using number of materials. However, the results were disappointing as the light emission was low in intensity, the LEDs were expensive and only a few colors were available. In 1964, GaAsP LEDs were used by IBM on circuit boards in an early main-frame computer as on-off indicator lights (Kitai, A. 2008). This 'tiny' application was considered as a significant breakthrough in the evolution of LEDs as it provided lighting in a new role to both manufacture and end-user. The beauty of this innovation was the LEDs could be mounted directly onto the circuit board, it used little power, and had a long lifetime thereby eliminating maintenance. These attributes are the ones used today to maneuver LEDs into replacing other light sources as the LEDs have become more efficient, cheaper and brighter.

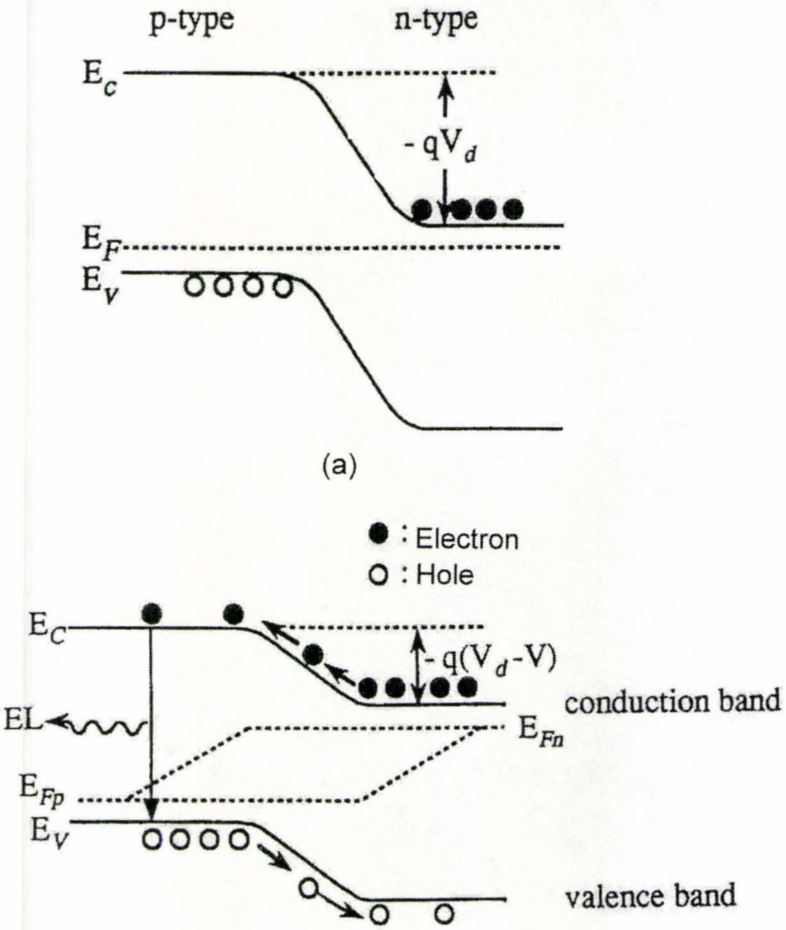

(a)

(b)

Figure 1.1 Energy band diagrams for the p-n junction under (a) thermal equilibrium and under (b) forward-biased conditions

Energy band diagrams for a p-n junction at thermal equilibrium and under forward biased conditions (p-type side: positive) are shown in figure 1.1 (a) and (b), respectively. At the thermal equilibrium, a depletion layer is formed and a potential V_d across the junction is produced. When the p-n junction is forward-biased, the potential

V_d decreases to (V_d-V), and electrons are injected from the n-region into the p-region while holes are injected from the p-region into the n-region; that is, minority carrier injection takes place. Subsequently, the minority carriers diffuse and recombine with majority carriers directly or through trapping at various kinds of recombination centers, producing injection EL. The total diffusion current in the p-n junction is given by:

$$J = J_p + J_n = J_s(\exp(\frac{qV}{nkT}) - 1)$$

$$J_s = q(\frac{D_p p_{n0}}{L_p} + \frac{D_n n_{p0}}{L_n}) \qquad (1\text{-}1)$$

where D_p and D_n are diffusion coefficients for holes and electrons, p_{n0} and n_{p0} are the concentrations of holes and electrons as minority carriers at thermal equilibrium, and L_p and L_n are the diffusion lengths given by $\sqrt{D\tau}$, where τ is the lifetime of the minority carriers.

Due to the dependence of light generation on band-to-band recombination, traps and defects that lead to unwanted, non-emissive recombination events between electrons and holes must be minimized by using high purity, low defect density materials. This means single crystalline materials are generally needed whereby sufficient diffusion length of the minority carriers in a p-n junction can be achieved. Recently efficient InGaN-based blue and n-UV LEDs on patterned sapphire substrates using lateral epitaxy have been fabricated. The structure consists of four periodic MQWs of InGaN/GaN, and the barrier layers are n- and p-type $Al_{0.2}Ga_{0.8}N$ as shown in figure 1.2 (Kitai, A., 2008).

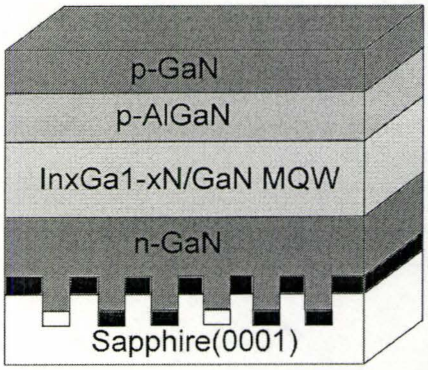

Figure 1.2 A structure of InGaN/GaN MQWs between n-AlGaN and p-AlGaN on a patterned sapphire substrate.

LEDs on the market today are manufactured using III-V semiconductor materials (ternary and quaternary alloys using elements from the periodic table groups III and V) such as GaAlAs, AlInGaP, InGaN and AlInGaN (Nakamura and Fasol, 1997). With recent technological advances, LEDs have evolved from backlighting used in LCDs

(Liquid-Crystal-Displays) into lighting as they have similar lighting efficiency as conventional incandescent bulbs and fluorescent lamps. Moreover, LEDs provide safety as well as other advantages including low operating voltage, compactness and lightweight. Around 1997, prototype white solid-state lighting was presented at international conferences based on using red, green and blue LEDs. LEDs are used as backlights for LCD displays and in outdoor electronic billboards. Issues include the following:

(1) LEDs with different emission wavelengths have different working lifetimes, leading to different ageing of different color LEDs.
(2) Different wavelength emitting LEDs have various brightness (Green window problem).
(3) There is a temperature dependence of emission wavelength of some LEDs. Although for some LEDs the shift of emission is small with temperature, for others it is larger.

Also, LEDs are too expensive for most high-resolution display applications.

1.2 Thin Film EL (TFEL) Devices

In 1967, Russ and Kennedy (Russ and Kennedy, 1967) demonstrated a double insulating layer EL structure. Figure 1.3 shows the structure of a double-insulating layer TFEL device. It consists of a substrate, usually glass, on which a series of thin film layers is grown. There are two electrodes, two dielectric layers and a phosphor layer.

All phosphors for TFEL devices consist of a host material and a luminescent center (or dopant). For a host material, several criteria must be satisfied to enable efficient light emission. Firstly, the host materials must have a band gap large enough to emit visible light. Secondly, the host material must withstand a high electric field of the order of 10^8 V/m without electric breakdown. Meanwhile, once a critical field is reached, an avalanching-type breakdown process can occur in the phosphor. Finally, the host materials must be capable to provide a medium for the efficient transport of high energy (>2ev) electrons.

An efficient EL phosphor also has requirements for the luminescent center. The basic requirement is that the luminescent center should have a large cross section for impact excitation, and the luminescent center must be stable in a high electric field environment. Moreover, the dopant must be properly incorporated into the host materials and have localized quantum states.

The EL emission mechanism for ZnS-based TFEL devices is indicated in figure 1.4. The EL emission occurs in the following way:

(1) Above the threshold voltage, electrons are injected from the interface states between the phosphor layer and insulating layer by high-field-assisted tunnelling.
(2) The injected electrons are accelerated and gain kinetic energy large enough to excite luminescent centers or the host lattice.

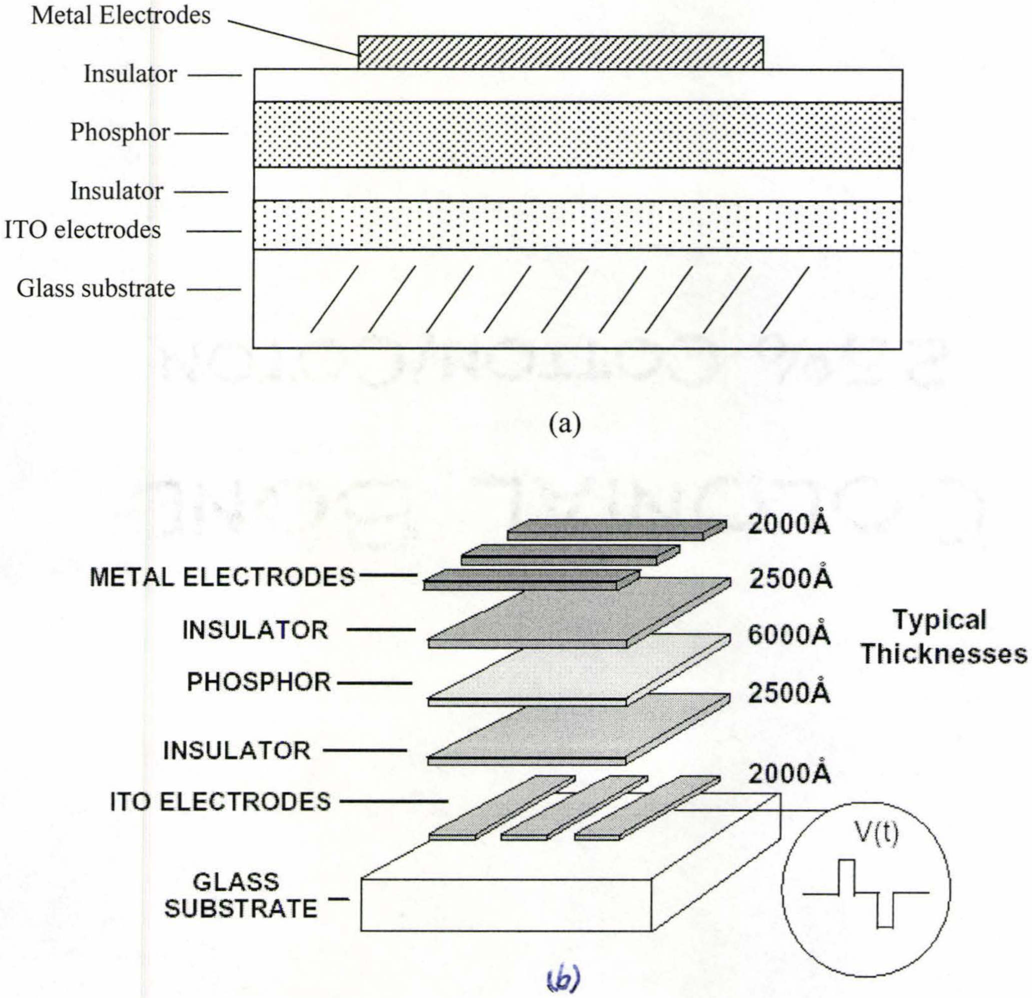

Figure 1.3 (a) Thin film double-insulating-layer TFEL device showing sequence of layers deposited as thin films on a glass substrate. Typical materials used are:

- glass substrate: Corning 1737 glass
- transparent electrode: Indium tin oxide(ITO)
- insulator: Aluminum titanate
- phosphor: Manganese-doped zinc sulfide (ZnS:Mn)
- rear electrode: Aluminum

(b) TFEL display with rows and columns.

(3) High-energy electrons, which are called hot electrons, directly excite luminescent centers through the impact-excitation mechanism. When these electrons in the excited states of the luminescent centers make radiative transitions to the ground state, EL emission is realized.

(4) The hot electrons travel through the phosphor layer and are finally trapped at

the phosphor layer/insulator layer interface states on the anode side, causing polarization.

When the polarity of the ac voltage wave form is reversed, the same process takes place in the opposite direction in the phosphor layer.

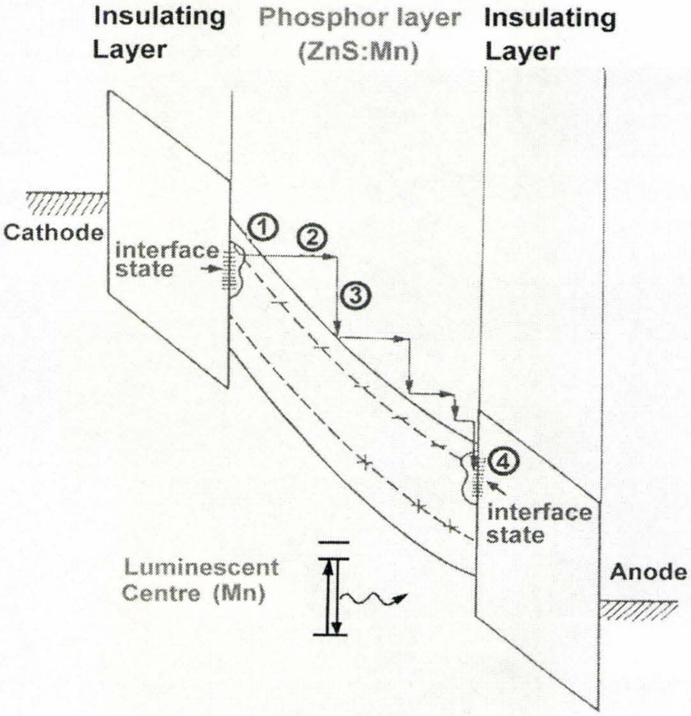

Figure 1.4. Energy-band diagram of the double-insulating-layer-type ac thin-film EL device and the EL emission mechanism; Circled numbers refer to the corresponding features described in the text

The commercialization of LCD and Plasma display panels has currently reduced the large-scale development of TFEL devices, however, the intrinsic characteristics of TFEL devices make them particularly attractive candidates for small to midsize flat panel displays. Since EL displays are emissive, the viewing angle is greater than 160° which has been an inherent problem with LCD displays. Since tunnel injection is temperature insensitive, TFEL devices can be used over a wide temperature range from –100 to 100°C, which in practice is limited by the drive electronics. Solid-state construction makes them inherently more shock and vibration resistant, which is critical in certain military and industrial applications. Display panels have demonstrated device lifetime of over 50 000 h with less than 10% luminance change (Nalwa and Rohwer, 2003). Table 1-1 lists maximum luminance at 1 kHz of some commercial ACTFEL phosphors (Ono, 1993).

More recently, a number of important TFEL structures have been developed, such as Thick Film Dielectric EL (TDEL), Ceramic Sheet Dielectric EL, and

Sphere-supported thin film EL (SSTFEL). These structures offer specific advantages for certain applications. Further developments of TFEL in fundamental physics, materials, fabrication techniques and architectures will continue.

Table 1-1 maximum luminance at 1 kHz of some commercial ACTFEL

Emission Color	Phosphor layer material	Luminance L (cd/m^2)@1 kHz	Luminance efficiency@ 1 kHz η(lm/W)
Yellow	ZnS:Mn	5000	2-4
Red	CaS:Eu	200	0.05
	ZnS:Mn/Filter	1250	0.8
Green	ZnS:Tb, F	2100	0.5-1
	CaS:Ce	150	0.1
Yellow-green	ZnS:Mn/Filter	1300	—
Blue	ZnS:Tm, F	2	<0.01
	$CaGa_2S_4$:Ce	210	—
Yellowish-white	ZnS:Mn/SrS:Ce	2450	1.3

1.3 AC Powder EL (ACPEL)

Inorganic powder phosphor EL is divided into AC powder EL (ACPEL) and DC powder EL (DCPEL) to distinguish the form of the driving voltage. Since DCPEL is not an active field today, and no commercial devices are manufactured, ACPEL is introduced and described in detail in this chapter.

1.3.1 Background

In 1936, French scientist Georges Destriau observed luminescence from ZnS powder phosphor suspended in castor oil when a strong electric field was applied. This type of EL is classified as powder phosphor EL today. It was Destriau who first coined the word "electroluminescence" to refer to the phenomenon he observed.

Figure 1.5 shows the original structure of Destriau cell. At the very beginning, there was a great difficulty in devising a structure in which Destriau could apply high fields to a thin layer of powder to generate visible light since no transparent electrically conductive coating on glass were available on that time. Therefore, a large capacitor with mercury electrodes was used. However, this structure was soon modified to a demountable capacitor as shown in Figure 1.6 (Kitai, 1993). The phosphor powder was mixed with the castor oil and spread in a thin layer on a metal plate. A transparent mica layer was placed as insulation on the top of the phosphor-castor oil mixed layer. Over the mica layer is a layer of salt water used as a top electrode. This structure enabled immediate light emission in a high electric field although the ac voltage could be up to 15 kV and the EL was extremely poor.

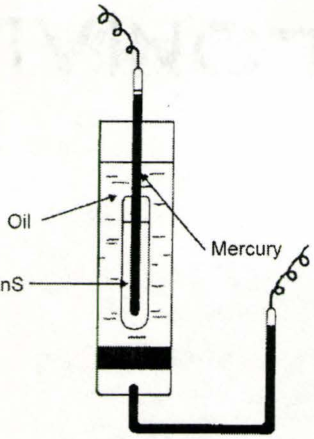

Figure 1.5 The original Destriau cell

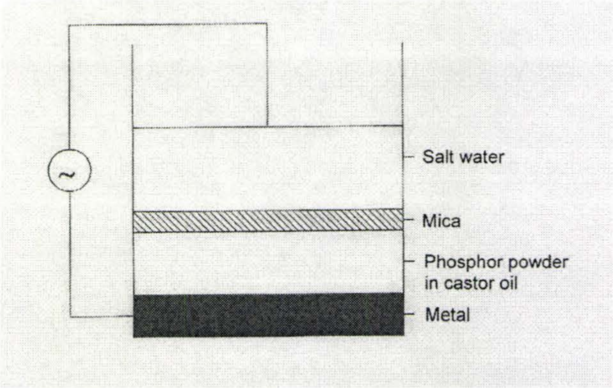

Figure 1.6. The modified Destriau cell

Unfortunately, this EL effect received very little attention in the following decade after Destriau's first reporting. Even in 1950, Leverenz (Leverenz, 1950) questioned the EL mechanism of the light emission. He argued that the powder phosphor might in fact be excited by the UV light emitted by the electrical breakdown of the gases in the fairly porous powder phosphors.

During the Second World War till the late 1940s, development of high performance polymers and ceramics was initiated. More importantly, transparent conducting electrodes were achieved for the first time. These developments triggered a great interest in ac powder electroluminescence (ACPEL). AC EL powders were studied in very many of the world's major electronic laboratories during the period 1950 to 1965 and this was reflected by the two thousand publications of that time (Vecht et al., 1985).

In the search for flat panel displays, the flat panel EL powder display was considered to be the technology and would result in better light sources and flat TV screens. ACPEL has a simple device structure and can be fabricated with a low cost manufacturing method. At a low luminance of 3.4 cd/m^2, its lifetime (operating time for the luminance to drop to half of its original luminance) is near infinite (Tannas, 1985). ACPEL lights have been known to operate continuously for over ten years at 100V rms at 60 Hz. Furthermore, the materials used in powder EL devices are generally inorganic polycrystalline solids rather than the single crystal materials used in LED's. This permits large area devices to be manufactured at a reasonable cost. Highly uniform light emission over large areas is available mainly due to the polycrystalline nature of powder EL devices. The light emitted from each grain of material is normally not seen as a distinct source by the observer, and the light per unit area emitted is the result of numerous grains or crystals. For this reason, a less perfect material than the single crystal LED materials is able to create highly reproducible lighting without requiring the binning associated with LED devices. Last but not the least, EL is particular useful in applications where ruggedness, speed, brightness, high contrast, and a wide viewing angle are needed.

However, ACPEL has several significant challenges for display application:

- Low discrimination ratio, which is defined as the ratio of luminance at V to the luminance at V/2
- Low contrast ratio
- Short lifetime at moderate to high luminance

The low discrimination ratio is due to the fundamental physics of the light emitting mechanism of the AC powder phosphor. It is well known that ACPEL does not have a sharp threshold voltage in its brightness-voltage characteristic. This feature indicates that ACPEL is not suitable for high resolution multiplexed displays. One way to overcome this issue is to incorporate a Thin Film Transistor (TFT) drive circuit into the ACTFEL display as suggested by Fisher in 1971 (Fisher, 1971) and explored by Brody (Brody and Yu, 1975). Unfortunately, experimental devices had a considerable number of blemishes resulting from the poor quality of the TFTs. At that time, TFTs were at their early stage and amorphous silicon technology did not exist. As a result, this technology was soon abandoned.

The low contrast ratio in moderate to high ambient illumination is due to the high reflectivity of the powder phosphor itself. Filters can be used to increase the contrast ratio at the cost of decreased luminance. Therefore, higher voltages and frequencies are required to drive the display, which greatly decreases the lifetime of the ACPEL display.

The short lifetime at moderate to high luminance is due to an exponential decay phenomenon of AC powder EL phosphors. Fisher (Fisher, 1971) explained that the decay in brightness is related to the blunting of microscopic tips of the Cu_2S-decorated imperfection lines inside the ZnS phosphor particles. The blunting spontaneously occurs by the diffusion of the copper ions in the ZnS lattice under the influence of the high AC field. As operating time increases, the Cu_2S-decorated imperfection lines become shorter and approach a final state which does not initiate sufficient electric field to excite luminescence. The degradation is assisted by moisture, high operating temperature and operating frequency. At about 170 cd/m^2, the typical lifetime of ACPEL lamps is only 1000 hours.

In spite of the considerable technical efforts from the 1950s, the inability to improve the lifetime of ACPEL displays led to the end of the first era of ACPEL by the middle of the 1960s. At the same time, other technologies such as gas discharge, light-emitting diodes, vacuum fluorescence, liquid crystals, and thin film electroluminescence attracted more and more research interest. But after a ten years pause, the revival of ACPEL was triggered again because of the development of direct current (DC) powder EL device and then the AC thin-film EL device.

In 1968, Aron Vecht first demonstrated a (DC) powered EL panel using powdered phosphors (Vecht, 1968). The research was then continued by using DC powder EL in watch dials, nightlights and backlights. However, the final results turned out to be quite frustrated and only a few commercially useful devices have been produced so far, such as the car dashboard, dealer room applications and medical scanners.

The first thin-film EL (TFEL) structures were fabricated in the late 1950s by Vlasenko and Popkov (Vlasenko and Popkov, 1960). In 1974, Toshio Inoguchi and his colleagues at Sharp Corporation introduced an alternating current (AC) TFEL approach to EL displays at the annual meeting of the Society for Information Display (SID). The Sharp device used zinc sulfide doped with manganese (ZnS:Mn) as the phosphor layer and yttrium oxide (Y_2O_3) for the sandwiching insulators. This was the first high-brightness long-lifetime EL (10,000 hours) display ever made. Since then, the so-called "second generation" EL device was the subject of much attention and triggered worldwide investigations for the purpose of developing compact flat panel devices for alphanumeric and graphic information displays driven by computer applications.

However, research on ACPEL was very limited and generally confined to two or three laboratories. By reviewing the development of powder EL, from the middle of the 1960s to the present day, very little fundamental work has been reported which has radically changed the characteristics of ACPEL devices although modest improvements in luminance and reliability were made. But for the reasons mentioned above, ACPEL has never been serious considered as a candidate for flat panel displays.

1.3.2 Structure of AC Powder EL Devices

AC powder EL devices were first developed by Sylvania in the first era of EL devices. A typical structure of an AC powder ZnS EL device is shown in figure 1.7. To date, the well-known excitation of powder phosphors by alternating electric field is limited to a comparatively small group of phosphors, mainly of the ZnS type. ZnS is a well-known semiconductor having a valence band as well as a conduction band and an energy gap of about 3.5 eV. As shown in figure 1.7, the EL active phosphor layer consists of suitably doped ZnS powder with particle size of 5 to 20μm suspended in a dielectric, which also acts as a binder. This phosphor layer is 50-100 μm thick and is sandwiched between two electrodes, one of which is transparent, and is supported by a substrate, consisting of either glass or flexible plastic. The EL color of the film depends on the activator of the ZnS phosphors. The most common ZnS phosphor used is the green-emitting ZnS:(Cu, Cl or Al); in this material, the Cu activator acts as an acceptor and is responsible for the color of the emission, while Cl (or Al) works as a donor. The amount of the Cu added in the preparation process of these phosphors is 10^{-3} to 10^{-4}gram per gram of ZnS, and is one order of magnitude larger than that added to ZnS phosphors used in CRTs. As discussed below, the Cu plays an import role in high-field AC powder EL in addition to acting as the activator.

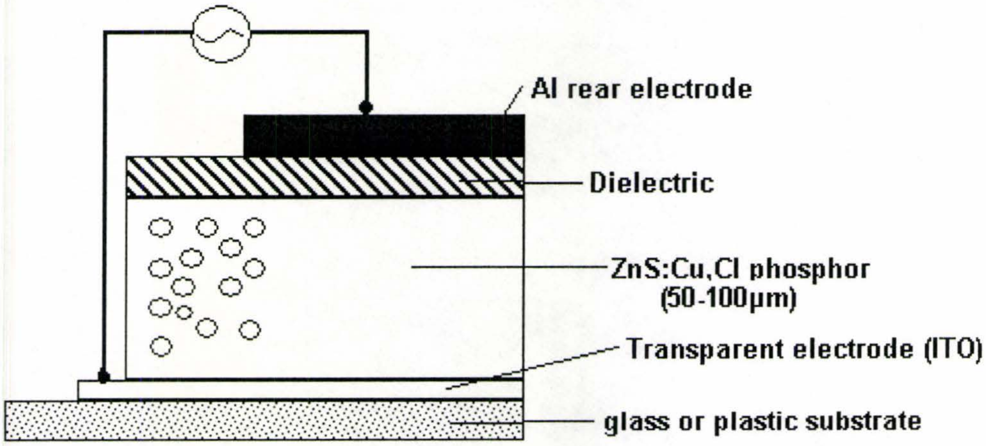

Figure 1.7 Typical AC powder EL structure

Table 1-2 shows some of the binary and ternary systems that have been investigated over the years used for AC powder EL.

The embedding dielectric in the device is an organic material with a large dielectric constant, such as cyanoethylcellulose, or low melting glass (Ono, 1995). In order to increase the stability and protect the EL device against catastrophic dielectric breakdown, an insulating layer, consisting of $BaTiO_3$ powders dispersed in another dielectric materials, is often inserted between the EL active layer and the Al rear electrode.

Table 1-2. Some of the powder phosphors known to exhibit EL under AC

Phosphor	Colour	Reference
ZnS:Cu,Cl(Br, I)	Blue	(Destriau, 1937) (Jaffe, 1961)
ZnS:Cu,Cl(Br, I)	Green	(Destriau, 1937) (Jaffe, 1961)
ZnS:Mn, Cl	Yellow	(Gobrecht et al., 1956)
ZnS:Mn, Cu, Cl	Yellow	(Thornton, 1958)
ZnSe:Cu, Cl	Yellow	(Thornton, 1958)
ZnSSe:Cu, Cl	Yellow	(Thornton, 1958)
ZnCdS:Mn, Cl (Cu)	Yellow	(Vlasenko and Popkov, 1960)
ZnCdS:Ag,Cl (Au)	Blue	(Vlasenko, 1960)
ZnS:Cu,Al	Blue	(Gobrecht et al., 1957)

1.3.3 EL Characteristics of AC Powder EL Devices

EL is observed when an AC voltage of about 100 to 200 V corresponding to an electric field of order of 10^4 V cm^{-1} is applied across the electrodes of the device. Luminance-voltage characteristics of a typical EL device are shown in Figure 1.8 (Shionoya, 1998). The observed dependence of the luminance (L) on the applied voltage (V) is expressed by equation (1-2):

$$L = L_0 \exp\left(-\left(\frac{V_0}{V}\right)^{1/2}\right) \quad (1\text{-}2)$$

The parameters L_0 and V_0 depend on the particle size of the phosphor, the concentration of the powder in the dielectric, the dielectric constant of the embedding medium, and the device thickness. It has been established empirically that one of the key parameters affecting EL characteristics is the particle size, and a critical trade-off between the EL efficiency and the operational lifetimes, defined by the time when the luminance becomes one half of the initial value, exists as follows. The efficiency increases in proportion to $\sim d^{-1/2}$, where d is the particle size. The operational lifetime, however, decreases in proportion to ~d. In addition, the luminance increases with frequency in the frequency region of ~100 Hz to 10 kHz. Luminance of 100 cd m^{-2} has been achieved for devices driven at a frequency of 400Hz and a voltage of 200V (Shionoya, 1998).

A typical voltage dependence of the EL efficiency, η, is also shown in figure 1.8. Typical values of the efficiency are 1 to 10 lm W^{-1}. The efficiency increases initially with increased applied voltage up to a saturation value, but then decreases gradually with further increases in voltage. The EL efficiency dependence on the voltage V is expressed by: $\eta = L^{1/2}V^{-2}$. The maximum efficiency is obtained at a voltage well below the highest luminance level.

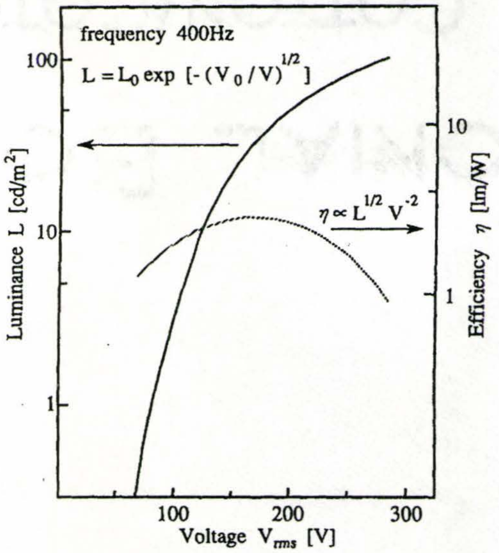

Figure 1.8 Typical luminance-voltage and efficiency-voltage characteristics of AC powder EL device.

1.3.4 Preparation of Powder EL Materials

Most powder EL research has been centered around the II-VI compounds and by far the most important EL lattice is zinc sulphide (ZnS). Zinc sulphide is a semiconductor material and has two structural variants, namely a cubic phase (zinc-blende) with bandgap energy of 3.7 eV at low temperature and a hexagonal phase (wurtzite) with bandgap energy of 3.8 eV at high temperature (Figure 1.9). Actually, these two phases differ only in terms of second-nearest neighbours, and both phases are excellent EL phosphors. In either phase, each Zn^{2+} ion is coordinated by 4 S^{2-} ions in a tetrahedral configuration. ZnS is a relatively stable sulphide in that it may be stored in ambient atmospheric conditions without degradation, however it does require moisture protection when it is subjected to high electric fields in an EL device. This may be due to the field-assisted dissociation of water to form OH^- ions which hydrate the ZnS material. Generally, ZnS is ideal for being used as phosphor material by doping with transition metals or rare-earth metals due to its excellent electrical properties such as the large band-gap energy, direct recombination and low leakage current (McClure, 1963) (Shrader et al., 1971). In addition, owing to the advantage of the simple manufacturing process, the convenience of being able to print large areas and the intrinsic high power efficiency, ZnS phosphor powders are suitable for back lighting of liquid crystal panels or for flat panel displays (Nien et al., 2006) also.

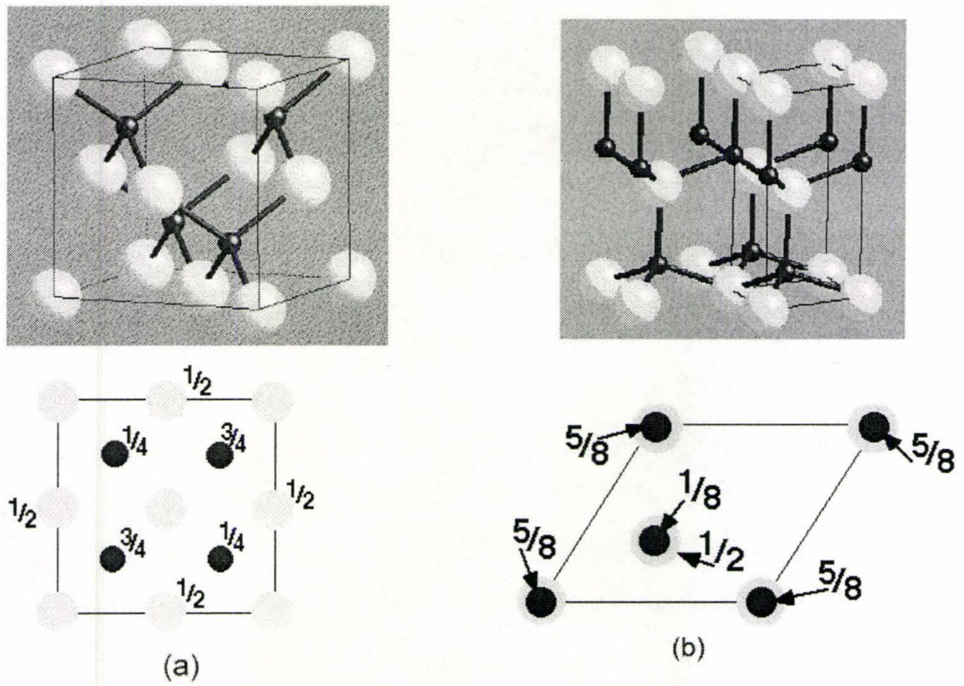

Figure 1.9 (a) Cubic zinc blende and (b) hexagonal wurtzite modifications of ZnS

Therefore, ZnS type phosphors such as green-emitting ZnS:(Cu, Al) are very important from a practical point of view. Luminescence centers in these phosphors are formed from deep donors or deep acceptors, or by their association at the nearest-neighbour sites.

The energy levels of ZnS: (Cu, Al) are shown in Figure 1.10.(Suzuki and Shionoya, 1971). To luminesce, a charge transfer processes occurs. Before excitation, Cu (acceptor) is monovalent (1+), while Al (donor) is trivalent (3+), so that charge compensation is realized in the lattice. When excited, a hole is trapped by Cu and an electron is trapped by Al, resulting in both Cu and Al becoming divalent (2+). In the process of the relaxation due to the reverse of the electric field, the electron trapped by

Al^{2+} recombines with the hole trapped by Cu^{2+}. Therefore, luminescence is generated and Al and Cu become monovalent and trivalent respectively again. This process is called a trap-assisted electron-hole recombination process.

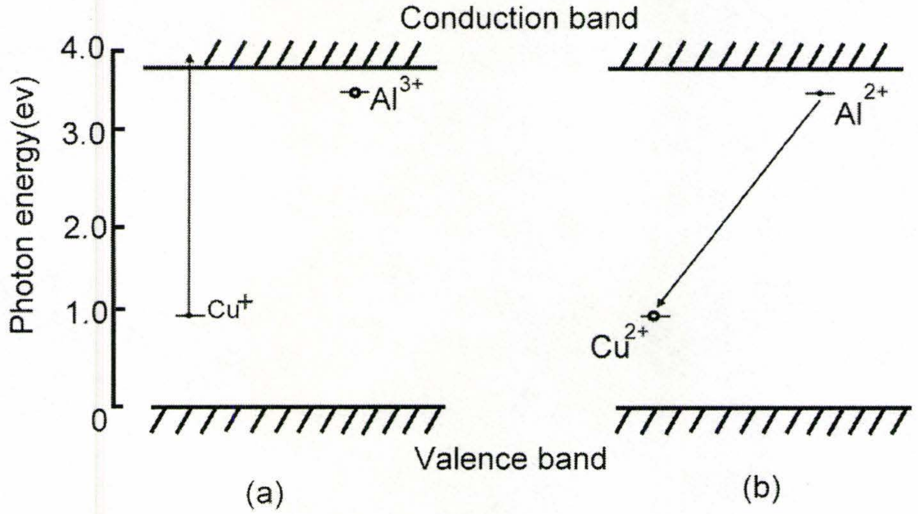

Figure 1.10 Energy levels and absorption transitions of Zn:Cu,Al phosphor before excitation (a) and during excitation (b)

1.3.4.1 Preparation of pure II-VI compounds (starting materials)

The techniques used for preparation of AC powder phosphors are described below. The recipes originally developed for the preparation of CRT phosphors are modified for the manufacture of AC powder EL phosphors. Most luminescent and optoelectronic II-VI materials are prepared by the addition of controlled amounts of specific impurities (dopants), called 'activators' and ' co-activators', to high purity II-VI compounds.

In order to prepare high purity starting materials, three methods have been developed so far.

In the first method the direct reaction of the group II and VI elements, such as pure elemental S and Zn is used. However, this method is not practical since the reaction is difficult to control and is explosive especially if the reagents are in form of finely divided powders.

The second method relies on thermal decomposition of suitable organometallic precursors such as zinc or cadmium diethyldithiocarbte. The drawback of this method is the production of the toxic organic residues and traces of carbon due to the decomposition of the organometallic compounds. As a result, this method is also not recommended for the preparation of the powder II-VI compounds although this method has been used successfully for the deposition of thin films of ZnS (Vecht et al., 1990).

The last developed method is to use the reaction of the aqueous group II salt solutions with gaseous hydrogen sulphide, selenide or telluride. The reaction between group II salt in aqueous medium with, for example, thiourea or thioacetamide that provides the sulphur also yields high purity ZnS. So far, this method is the most widely used for preparation of powder II-VI phosphors compared with the other two methods mentioned above.

ZnS can be precipitated using a purified solution of a Zn salt and hydrogen or ammonium sulphide in alkaline or acidic conditions. The phosphor made using this technique contains only a few parts per million of heavy metal impurity. The firing of the dried precipitate in a nitrogen atmosphere reduces the non-metal impurity level to about 500 ppm. The firing also leads to an increase in the particle size and an improved crystallinity of the lattice. Methods for the preparation of the ZnS have been described in detail by Levernz (Leverenz, 1950).

1.3.4.2 Activators (dopants)

All phosphors consist of a host material and a light-emitting dopant called an activator or a luminescent center. Pure, stoichiometric ZnS, for example, does not luminesce. Luminescence can be caused by the introduction of lattice defects, by deviation from the stoichometric Zn-S ratio, and by the addition of certain atoms to the system. Often, when impurity atoms are introduced, defects and deviations from stoichiometry are simultaneously produced, either by the rearrangement of the crystal lattice or by the physical and chemical processing conditions under which the impurity is added. Typical examples of impurity atoms (activators) are Mn and Cu. Other impurities leading to the reduction of the EL phenomenon are termed ‘ killers’ or ‘ quenchers’. Co, Fe and Ni, for example, are well known quenchers in CRT- type phosphors.

In normal AC powder EL phosphor preparation, the incorporation of the impurity atoms is carried out by adding the dopants either in a slurry form or by milling (dry or wet). If the addition is carried out by slurrying or wet milling, the mixture has to be dried out completely before firing at elevated temperatures to assist the diffusion of the dopants into the host material lattices. Sometimes, fluxes such as MgO, $BaCl_2$, and NaCl are also added in order to lower the activation temperature. Elements from group IB or VB (activators) are normally introduced with group IIIB or group VIIB impurities (co-activators). The primary reason for the addition of two or more types of impurities simultaneously is related to charge compensation in the II-VI phosphor lattice. In AC powder phosphors, Cu from group IB is the most important activator giving rise to both green and blue EL. Halide coactivators are normally employed, with Cl^- being preferred for luminance (Kitai, 1993).

1.3.5 EL emission spectra

The emission spectra of ACPEL devices are shown in figure 1.11 (Shionoya and Yen, 1998). Emission colors depend on the different luminescent centers incorporated in the phosphors. When the ZnS lattice is activated with Cu (activators) and Cl, I, and Al (co-activator), donor (co-activator)-acceptor (activators) pairs are formed. As mentioned above, the EL is due to the radiative recombination of electron-hole pairs at donor-acceptor (D-A) pair sites. The combination of Cu and Al (ZnS: Cu,Al) produces green(~550 nm)emission color. The combination of Cu and Cl (ZnS:Cu, Cl) gives blue (~460 nm) and green emission bands, their relative intensities depending on the relative amount of Cu to Cl. ZnS:(Cu,I) shows a blue emission. It should be noticed that ZnS:Cu in which no co-activators are incorporated shows a red emission. By further incorporating Mn^{2+} ions into ZnS:Cu,Cl phosphors, the resultant ZnS:Cu,Mn,Cl shows a yellow emission(~ 580 nm) due to Mn^{2+}.

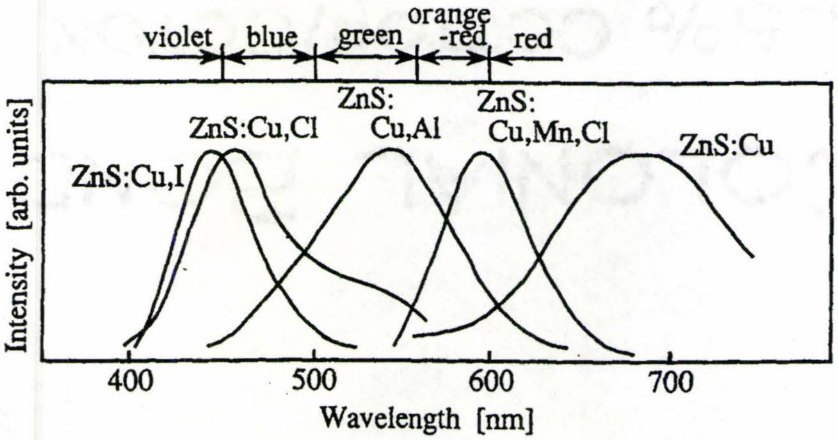

Figure 1.11.The emission spectra of AC powder EL devices

1.4 Powder Contact EL

Lehmann (Lehmann, 1957) reported that many powdered crystal phosphors which are normally non-EL become EL if they are simply mixed with suitable powdered metals, or with some non-metals of good electrical conductivity. This phenomenon is termed as "contact electroluminescence " or "contact EL".

The arrangement of contact EL is shown in figure.1.12. Powdered phosphors which are unable to EL under usual conditions in a strong alternating electric field have been mixed mechanically with metal powders. This mixture, with castor oil as the embedding dielectric, is placed in a normal plaque cell consisting of a front electrode of conducting glass over-coated with a thin, transparent, insulating film and a back electrode of Al. When an alternating voltage is applied to the cell, the mixture of phosphor and metal is electroluminescent.

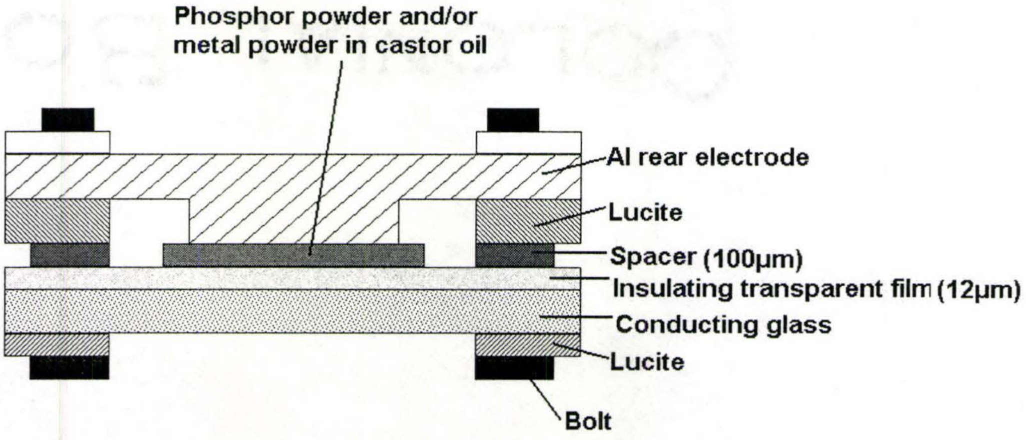

Figure 1.12. The arrangement of Lehmann's contact EL

Generally a great variety of phosphors are able to show this contact EL. A qualitative survey of some results obtained with mixtures of various phosphors with metal powder is given in Table 1-3 (Lehmann, 1957) for an applied sinusoidal voltage of 600 v rms and a frequency of 10,000 cps. The embedding dielectric material here was castor oil; similar results are obtained, however, with other organic dielectric materials or even with air as the embedding material (Lehmann, 1957). The emission colour of some phosphors is different for photo- and electroluminescence, indicating that the phosphors have been excited by the electric field instead of u.v radiation generated by a glow discharge in the cell. Although no direct relation could be found between the nature of the phosphor and its ability to be excited by contact EL, the crystallinity, the activator concentration (if activators are necessary), and other properties may have an influence on contact EL in addition to the general type of material.

An experiment similar to Lehmann's contact EL was performed in our lab. In this case, CRT phosphor powders of ZnS:(Cu, Al) were embedded into a polymer which was supported by a glass substrate coated with a thin layer of indium tin oxide (ITO). Spherical silver metal powders with diameter of 1 to 3 µm are pressed onto a conducting tape and put on the top of the phosphor layer. When both the pressure and the alternating electric field are applied to the cell, green light can be generated from the phosphor layer. We call this phenomenon "powder contact EL". The arrangement of powder contact EL is shown in figure 1.13. Appendix I of this thesis introduces and describes the experimental procedures and results in detail.

Table 1-3. Photoluminescent and electroluminescent emission of various phosphors
Intensities: br= bright, m= moderate, w= weak, vw= very weak

Phosphor	Photoluminescence		Electroluminescence	
	2537 Å	3650 Å	Pure Phosphor	Mixed with metal powder
ZnS-Cu (0.03%)	br green	br green	—	m blue
ZnS-Cu (0.1%)	Br blue green	br blue green	m blue	br blue
ZnS-Cu (0.01%)	br green	br green	—	M green
ZnS-Ag (0.03%)	br blue	br blue	—	br blue
ZnS-Mn (1 %)	M yellow	br yellow	—	br yellow
(ZnCd)S-Cu	br yellow	br yellow	—	w green
(ZnCd)S-Ag	br yellow	br yellow	—	br yellowgreen
CaS-Bi	M blue	m blue	—	w blue
(CaSr)S-Bi	M blue	m blue	—	w blue
Zn_2SiO_4-Mn	br green	vw green	—	br green
Zn_3GeO_5-Mn	br green	—	—	m green
$CaWO_4$-Pb	br white	—	—	vw blue
$Cd_2B_2O_5$	br red	w red	—	vw red
Cd_2SiO_4-U-Sm	br pink	w red	—	w green
$CaPO_4$-Tl	br white	br white	—	m white
$UO_2(NO_3)_2\cdot 6H_2C$	br green	br green	—	w green
Anthracene	br blue	br blue	—	w blue

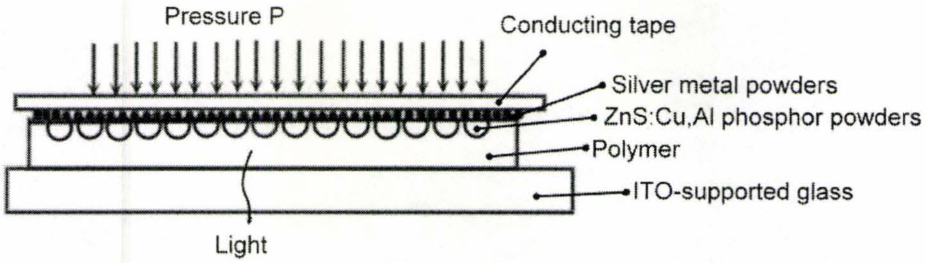

Figure 1.13. Arrangement of powder contact EL device

1.5 Future of the Powder EL

Due to the low brightness and short lifetime, the applications of powder EL devices are mainly limited to backlighting and lamp applications that require low brightness. This includes low illumination environments, such as nightlights and backlighting for LCDs and keypads in portable electronics and home electronics. A unique feature of powder EL is the plastic cell structure that provides great versatility in product design. Flexible powder EL lamps can be folded, creased and pierced while maintaining complete functionality- allowing design concepts unachievable with other lamp types. This feature makes powder EL the only truly thin and flexible light-emitting device in the current market. Powder EL continues to be the most commercially successful high-field EL device. Furthermore, the intrinsic high luminous efficiency of powder EL results in low power consumption.

Chapter 2. Objectives of Present Work

Exploring the contact EL idea and taking advantage of the concentration effect of electric field on conductive nanowires, a novel powder EL device based on ZnS:Cu phosphors has been fabricated. In this thesis, the device structures, the fabrication processes and the final results are elucidated in detail.

2.1 Nanowire Contact Powder EL Device Structure (NCPEL)

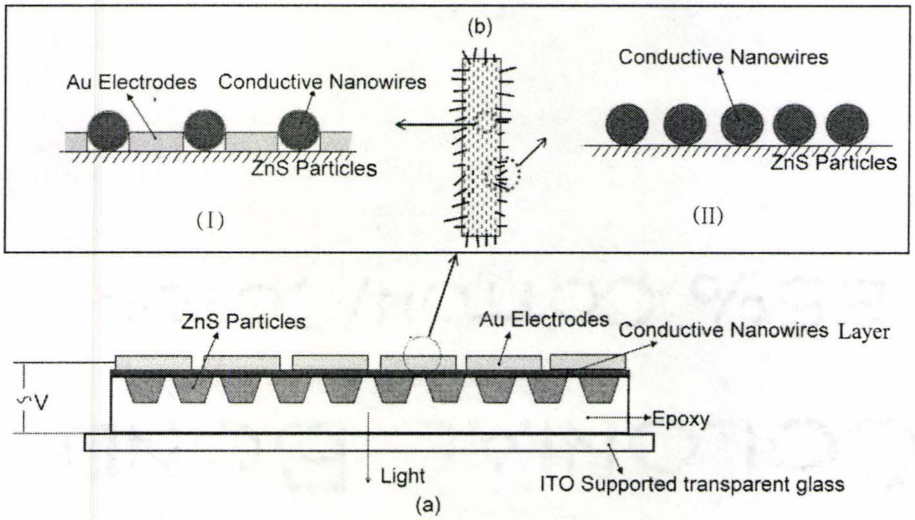

Figure 2.1. Proposed nanostructured contact powder EL device. (a) Cross-sectional view of the device; (b) Top view of one Au rectangular electrodes. Due to the deposition of Au on the nanowires, two kinds of nanowire profiles are formed: (b-I) nanowires from the inner area of Au; (b-II) nanowires extending beyond the perimeter of the Au electrodes.

As shown in Figure 2.1, CRT ZnS phosphor particles with diameter of 3-20μm are embedded into, but not covered by, a polymer film with a thickness of 10 to 20 μm, which is supported by ITO-coated transparent glass. The exposed surfaces of the phosphor particles are covered by a dilute layer of metal nanowires. Two kinds of metal nanowire profiles are formed simultaneously at the vicinity of the top vacuum-deposited Au rectangular electrodes. The top view of one Au rectangular electrode is shown in figure 2-1 (b): (b-I) the nanowires from the inner area of the Au electrodes separated from each other and connected by Au; (b-II) the nanowires extending beyond the perimeter of the Au electrodes, but electrically contacted by Au electrodes. In these structures, the metal nanowires directly contact with the phosphor and function as rear nanoelectrodes.

2.2 Features of Nanowire Contact Powder EL Device (NCPEL)

As mentioned above, the nature of short lifetime at high luminance of traditional ACPEL devices has severely limited their practical uses for higher brightness applications in lamps or flexible displays. However, NCPEL is proposed as an alternative way to address this challenge by combining modern nanotechnology with traditional powder EL technology. The structural combination of the conductive nanowires with the phosphor powders potentially enables NCPEL device to break through the current technical limitations on the development of high performance ACPEL devices. As summarized, the contributions of NCPEL include the following aspects:

1. The device is self-supported with a very simple structure. Therefore, it can be fabricated with a low cost manufacturing method.
2. The phosphor powder is embedded into but not covered by a polymer by using a vacuum lamination method. This method allows ease of processing and low cost. By using this method, the phosphor powder can be uniformly pushed into the polymer under atmospheric pressure. Samples air-bubble-free have been made.
3. The technique, namely template synthesis, used to fabricate the conductive nanowires with uniform dimensions is a low-cost and high-yield method, resulting from commercially available porous alumina (PA) templates and cost-effective hydraulic pressure injection. A large quantity of metal nanowires has been prepared.
4. The conductive nanowires can induce a highly intensified electric field and hence generate electron injection and avalanching in the phosphor. Therefore, low average fields that are easy to produce can generate luminescence. As a result, NCPEL devices have the potential for a lower operating voltage with simultaneous long lifetime and high luminance.
5. The conductive nanowires are more stable and reliable than the Cu_2S precipitates and function as the field emitters in the device, indicating that NCPEL device has potential of long operating time although moisture protection is still desirable.
6. Rugged nanostructured powder EL devices are possible since a polymer can be used as a vehicle for the phosphor powders.
7. CRT phosphor is used for this powder EL device. ZnS:Cu CRT phosphor, for example, can not be excited under the normal EL conditions due to the low composition of the Cu dopant. The amount of the Cu added in the preparation process of CRT phosphor is 10^{-4} to 10^{-5}gram per gram of ZnS, and is one order of magnitude lower than that added to ZnS phosphors used in EL, and Cu_xS precipitates do not form in the ZnS lattice. However, by introducing conductive nanowires, the phosphor can be excited under normal EL conditions as the nanowire can induce a highly localized electric field in the phosphor region.

2.3 Summary of Contributions of This Thesis

(1) Indium nanowires with very high aspect ratio of 300:1 have been fabricated using the hydraulic pressure injection method for the first time.
(2) A monolayer of ZnS:Cu /polymer composite film has been achieved using a vacuum double-lamination method for the first time.
(3) A dilute layer of nanowires has been deposited on ZnS particles using a wet-coat method for the first time.
(4) The use of conductive nanowires to achieve EL in ZnS:Cu powder EL devices has been demonstrated for the first time.

After reviewing the background theory of EL, the mechanism of ACPEL is described in detail in the third chapter. The recent developments of nanotechnology are reviewed in Chapter 4, in particular nanowires. Chapter 5 is the experimental part. Components of NCPEL, processing parameters, electric field modeling, working principles and EL performance of NCPEL are discussed in detail in chapter 6. A summary of the conclusions and an observation of the future development of NCPEL are presented in the last section.

The other research in the process of developing the nanowire contact powder EL device, including powder contact EL and growth of thin films on the porous alumina substrate are summarized in Appendix I and Appendix II, respectively.

Chapter 3 Theory of Operation

3.1 Basic Underlying Principles of EL Devices

The conversion of certain forms of energy to optical photonic energy is termed luminescence. If the energy supplied by application of an electric field, the resulting luminescence is called electroluminescence (EL). There are many ways by which electrical energy can be used to generate photon emission in a solid. In LEDs an electric current causes the injection of minority carriers into regions of the crystal where they can recombine with majority carriers, resulting in the emission of recombination radiation. This effect is called injection EL. The emission of photons by certain phosphors, such as ZnS, in an alternating field is an alternative means of conversion of electrical energy to optical photonic energy since majority charge carriers, usually electrons, play a key role rather than the minority carriers in the emission processes.

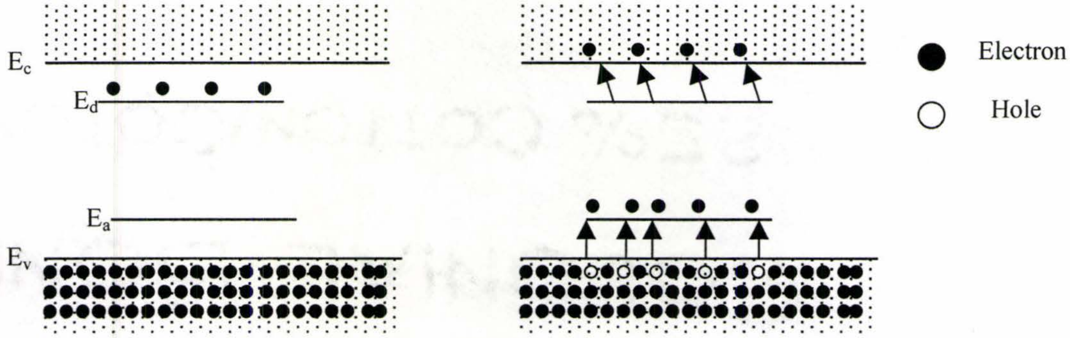

Figure 3.1 Energy band model in semiconductors. E_c, E_v, conduction band, valence band edge; E_a, E_d, acceptor, donor energy level.

According to the band theory of solids, when individual atoms bond together in a crystal network, their energies form a series of 'bands'. Within a band there is essentially a continuum of energy states. In a perfect non-metallic crystal the individual bands are separated by gaps devoid of any energy levels. The gap between the highest occupied band (the valence band) and the lowest unoccupied band (the conduction band) is termed the bandgap, E_g. Luminescence can be divided into two categories in terms of the transitions across or within the bandgap: (1) intrinsic, fundamental or edge emission and (2) extrinsic, activated or characteristic emission. Intrinsic luminescence is due to electron-hole recombination across the energy gap of a material, with associated excitation formation. The peak in intensity of the emission occurs at an energy approximately equal to the energy gap. However, if radiative recombination is localized within the energy gap of a material due to energy levels introduced by crystal imperfections or impurity atoms, extrinsic luminescence can be observed. Most commercial phosphors luminesce by an extrinsic mechanism rather than an intrinsic one.

Doping is a process in which impurities are purposely introduced into the semiconductor crystal to create carriers. When impurities (or lattice defects) are incorporated, interstitially or substitutionally, into an otherwise perfect crystal additional levels are created in the energy band structure, usually within the bandgap. If an intentional impurity introduces an energy level very near the conduction band, very little thermal energy is required to excite the electrons "trapped" at this level to the conduction band. Such an impurity is called "donors". If the energy level introduced by the impurity is very near to the valence band, electrons are very easy to be thermally excited from the valence band to the impurity level, leaving behind holes in the valence band. Then such impurity is called "acceptor". Donor and acceptor in semiconductor can be visualized as shown in figure 3.1.

In quantum mechanics, quantum tunneling is a micro and nanoscopic phenomenon in which a particle violates the principles of classical mechanics by penetrating or passing through a potential barrier or impedance higher than the kinetic energy of the particle. When an extremely high electric field of over 10^6 V/cm is applied to a Schottky barrier, defined as a potential barrier formed in the contact region of a semiconductor with metal, or to electron traps, the barrier width becomes very thin, with a thickness in the neighborhood of 100 Å. In this case, electrons tunnel directly into the conduction band as illustrated in figure 3.2 (Shionoya, 1998).

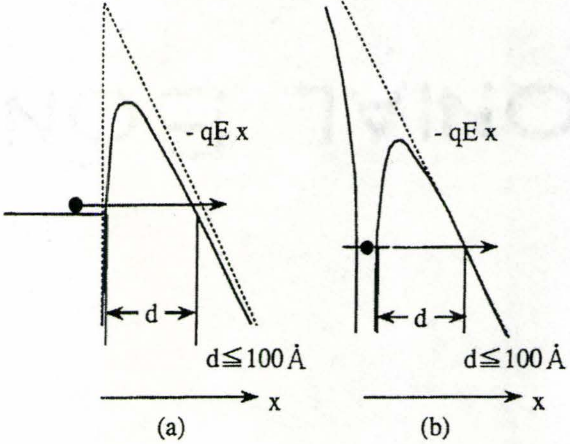

Figure 3.2. Energy band diagram for (a) Schottky barrier and (b) deep electron traps under high electric field. Electron injection due to the tunnelling effect is illustrated

The current density due to this process depends only on the electric field and does not depend on temperature, and is described by equation (3-1):

$$J \cong V^2 \exp(-\frac{b}{V}) \quad (3\text{-}1)$$

After Cu and Al atoms are intentionally introduced into a ZnS lattice, the Cu atoms act as the acceptors and are the combination centres responsible for the emission, while Al atoms work as the donors, trapping and de-trapping electrons as well as compensating the charges induced by the Cu. It is known that thin embedded Cu_xS conducting needles are formed in the ZnS lattice. The detailed structure of the contact between conduction Cu_xS inclusion and ZnS matrix is still uncertain. We may have an abrupt transition from the conducting phase to the luminescent ZnS as shown in figure 3.3. Although the average electric field in the device is about 10^4-10^5 V/cm, the electric field is concentrated at the tips of these needles and the local electric field can be 10^6 V/cm or more. Then electrons can be injected by high-field-assisted tunneling from one end of the needle and holes from the other end. This mechanism is known as the bipolar field-emission model (see later section). The injected electrons are finally trapped at the donors (Al) and recombined with holes that were injected by the same process and were trapped at luminescent centers (Cu) previously, resulting in EL.

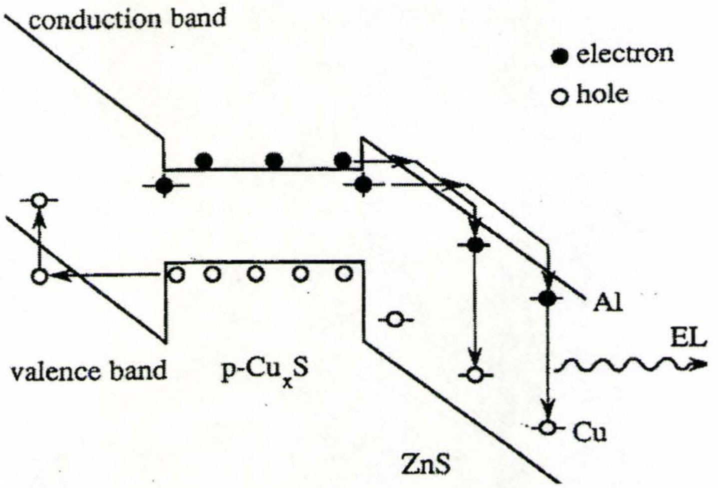

Figure 3.3. Schematic band model of simultaneous injection of electrons and holes from the opposite ends of a Cu_xS needle into the ZnS:(Cu, Al) surrounding lattice (Fisher, 1963)

3.2. Electric Field Modeling for Conductive Spheroid in the Insulating Phosphor Particle

When a uniform electric field is applied to a dielectric in which conductive material is dispersed, the electric field is disturbed and a very high field may be produced. It is of great interest to investigate the field distribution around the conductive material to further understand the mechanisms and characteristics of powder electroluminescence (EL).

During the preparation of the powder phosphor, a conductive phase is formed and incorporated as small segregations within the phosphor particles. Although the shape of individual conductive substance is irregular, it is reasonable to assume simple models, i.e., oblate spheroids and prolate spheroids. The surface of the conductive phase likely has a form which is intermediate between the two simple spheroids assumed here. These spheroids are further assumed to be isolated from each other and embedded in an ideal insulative medium. It should be noted that the detailed structure of the boundary between the conductive substance and ZnS may not be abrupt due to, for example, diffusion, however for the present discussion, we will assume that the boundary is abrupt.

When the conductive spheroid is placed in a uniform electric field E_0 with its major axis parallel to the field, i.e., in the x direction, the potential φ around it can be determined by solving Laplace's equation (Frankl, 1986) with ellipsoidal coordinates.

The equation:

$$\frac{x^2}{a^2}+\frac{y^2}{b^2}+\frac{z^2}{c^2}=1 \quad (a>b>c)\,(3\text{-}2)$$

is that of an ellipsoid whose semiprincipal axes are of length a,b, c. Then

$$\left.\begin{aligned}
&\frac{x^2}{a^2+\xi}+\frac{y^2}{b^2+\xi}+\frac{z^2}{c^2+\xi}=1 \quad (\xi>-c^2),\\
&\frac{x^2}{a^2+\eta}+\frac{y^2}{b^2+\eta}+\frac{z^2}{c^2+\eta}=1 \quad (-c^2>\eta>-b^2)\\
&\frac{x^2}{a^2+\zeta}+\frac{y^2}{b^2+\zeta}+\frac{z^2}{c^2+\zeta}=1(-b^2>\zeta>-a^2)
\end{aligned}\right\} \quad (3\text{-}3)$$

are the equations respectively of an ellipsoid, a hyperboloid of one sheet, and a hyperboloid of two sheets, all confocal with the ellipsoid from equation (3-2) as shown in figure 3.4.

Through each point of space there will pass just one surface of each kind, and to each point there will correspond a unique set of values of ξ,η,ζ. The variables

$$u^1=\xi,\ u^2=\eta,\ u^3=\zeta,$$

are called ellipsoid coordinates. The surface, $\eta = cons\tan t$, is a hyperboloid of one sheet and $\zeta = cons\tan t$, a hyperboloid of two sheets. The transformation to rectangular coordinates is obtained by solving simultaneously for x, y, z. This gives

$$\left.\begin{aligned}
x&=\pm\left[\frac{(\xi+a^2)(\eta+a^2)(\zeta+a^2)}{(b^2-a^2)(c^2-a^2)}\right]^{\frac{1}{2}},\\
y&=\pm\left[\frac{(\xi+b^2)(\eta+b^2)(\zeta+b^2)}{(c^2-b^2)(a^2-b^2)}\right]^{\frac{1}{2}},
\end{aligned}\right\} \quad (3\text{-}4)$$

$$z = \pm\left[\frac{(\xi+c^2)(\eta+c^2)(\zeta+c^2)}{(a^2-c^2)(b^2-c^2)}\right]^{\frac{1}{2}}$$

In ellipsoidal coordinates Laplace's equation can be transformed to

$$(\eta-\zeta)R_\xi\frac{\partial}{\partial\xi}(R_\xi\frac{\partial\phi}{\partial\xi})+(\zeta-\xi)R_\xi\frac{\partial}{\partial\eta}(R_\xi\frac{\partial\phi}{\partial\eta})+(\xi-\eta)R_\xi\frac{\partial}{\partial\xi}(R_\xi\frac{\partial\phi}{\partial\zeta})=0 \quad (3\text{-}5)$$

where $R_\xi = \{(a^2+\xi)(b^2+\xi)(c^2+\xi)\}^{1/2}$ (Stratton, 1941).

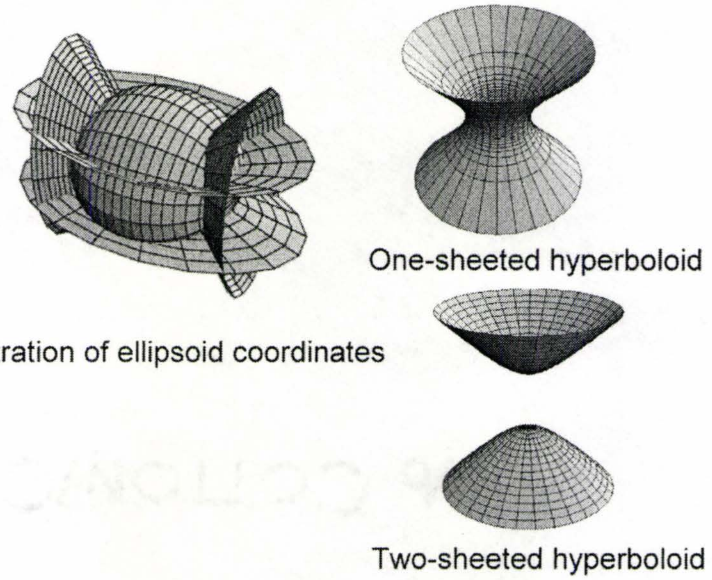

Figure 3.4 Illustration of ellipsoid coordinates

Since the applied field is uniform, the potential of it is:

$$\phi_0 = -E_0 x = -E_0\left[\frac{(\xi+a^2)(\eta+a^2)(\zeta+a^2)}{(b^2-a^2)(c^2-a^2)}\right]^{1/2} \quad (3\text{-}6),$$

with the value of x expressed instead using ellipsoidal coordinates being substituted from Equation (3-4). This primary potential is a solution of Laplace's equation in the form of a product of three functions:

$$\phi_0 = C_1F_1(\xi)F_2(\eta)F_3(\zeta),\ C_1 = -E_0\frac{1}{\sqrt{(b^2-a^2)(c^2-a^2)}} \quad (3\text{-}7)$$

Now if the boundary conditions are to be satisfied, the potential ϕ_1 of the induced distribution must vary functionally over every surface of the family $\xi = constant$ in exactly the same manner as ϕ_0 in its regularity at infinity. We presume, therefore, that ϕ_1 is a function of the form

$$\phi_1 = C_2 G_1(\xi) F_2(\eta) F_3(\zeta) \quad (3\text{-}8)$$

where

$$F_2(\eta) = \sqrt{\eta + a^2}\,, \quad F_3(\zeta) = \sqrt{\zeta + a^2} \quad (3\text{-}9).$$

To find the equation satisfied by $G_1(\xi)$ we need only substitute (3-8) and (3-9) into (3-5), obtaining as a result

$$R_\xi \frac{d}{d\xi}\left(R_\xi \frac{dG_1}{d\xi}\right) - \left(\frac{b^2 + c^2}{4} + \frac{\xi}{2}\right) G_1 = 0 \quad (3\text{-}10)$$

Equation (3-10) is an ordinary equation of the second order and as such possesses two independent solutions. One of these we know already to be $F_1 = \sqrt{\xi + a^2}$. There is a theorem which states that if one solution of a second-order linear equation is known, an independent solution can be determined from it by integration(Stratton, 1941). If y_1 is a solution of

$$\frac{d^2 y}{dx^2} + p(x)\frac{dy}{dx} + q(x) y = 0 \quad (3\text{-}11),$$

then an independent solution of y_2 is given by

$$y_2 = y_1 \int \frac{e^{-\int p dx}}{y_1^2} dx\,. \quad (3\text{-}12)$$

In the present instance,

$$p(\xi) = \frac{1}{R_\xi}\frac{dR_\xi}{d\xi} = \frac{d}{d\xi}\ln R_\xi \quad (3\text{-}13);$$

hence,

$$G_1(\xi) = F_1 \int \frac{d\xi}{F_1^2 R_\xi} \quad (3\text{-}14)$$

The potential of the induced charge is, therefore,

$$\phi_1 = \phi_0 \frac{C_2}{C_1} \int_\xi^\infty \frac{d\xi}{(\xi + a^2) R_\xi} \quad (3\text{-}15)$$

The constant C_2 is determined finally from the condition that on the ellipsoid $\xi = 0$ the potential is a constant ϕ_s.

$$\phi_s = \phi_0 \left[1 + \frac{C_2}{C_1} \int_0^\infty \frac{d\xi}{(\xi + a^2) R_\xi}\right] \quad (3\text{-}16)$$

As a result, at any external point, the potential is given by

$$\phi = \phi_0 + \frac{\phi_s - \phi_0}{\int_0^\infty \frac{d\xi}{(\xi + a^2) R_\xi}} \int_\xi^\infty \frac{d\xi}{(\xi + a^2) R_\xi} \quad (3\text{-}17)$$

By substituting equations (3-6) and (3-16) into equation (3-17), we finally can obtain the potential around the conductive spheroids.

$$\phi = -E_0 x \left\{ 1 - \int_{\xi}^{\infty} \frac{d\xi}{(a^2+\xi)R_{\xi}} \Big/ \int_{0}^{\infty} \frac{d\xi}{(a^2+\xi)R_{\xi}} \right\} \quad (3\text{-}18)$$

For the conductive spheroid around which high field is produced, the major axis is much larger than the minor axis; i.e.,

$a = b >> c$ for oblate spheroid

and

$a >> b = c$ for prolate spheroid.

The field distribution along the extension of the major axis is calculated from equation (3-18) the for oblate spheroid:

$$E = \frac{4E_0}{\pi} \left\{ \frac{a}{\sqrt{c^2 + 2ax}} + \frac{x}{c} \right\} \quad \text{for} \quad x \le c \; (3\text{-}19)$$

and similarity for the prolate spheroid:

$$E = \frac{E_0}{\{\log(2a/b) - 1\}} \left\{ \frac{a^2}{b^2 + 2ax} + \frac{1}{2}\log(1 + \frac{2ax}{b^2}) \right\} \quad \text{for} \quad x \le a \quad (3\text{-}20)$$

where x measures the distance from the surface of the spheroid (Stratton, 1941).

From equation (3-19) and (3-20) respectively, we can confirm that the maximum field happens at the surface of the spheroid, i.e., $x = 0$, and can be expressed as:

$$\frac{E_{\max}}{E_0} = \frac{4}{\pi}\frac{a}{c} \quad \text{(Oblate spheroid) (3-21)}$$

and

$$\frac{E_{\max}}{E_0} = \frac{1}{\{\log(2a/b) - 1\}} \left(\frac{a}{b} \right)^2 \quad \text{(Prolate spheroid) (3-22)}$$

Therefore, the ratio of the maximum field at the surface of the spheroid to the average field is nearly equal to the ratio of major axis to minor axis for the oblate spheroid and to the square of the axis ratio for the prolate spheroid. Hence, the local high field exceeding the average by two or more orders of magnitude is conceivable near the edge of an actual conductive substance.

It is an inherent property of powder EL that EL emission intensity is highly localized. This means an extension of high field over some distances; i.e., the potential drop with position in the high field region must be larger than a certain value. For the local high field expressed in equations (3-19) and (3-20), the extent of the high field region cannot be defined unambiguously. However, we can compare the field strength at the position, where the first and the second term are equal in equations (3-19) and (3-20) respectively, with the maximum field at the surface. Denoting this position by $x = \delta$, we have for the oblate spheroid

$$\delta = \left(\frac{ac^2}{2} \right)^{1/3} \quad \text{and} \quad \frac{E(\delta)}{E(0)} = \left(\frac{2c}{a} \right)^{2/3} \quad (3\text{-}23)$$

and for the prolate spheroid

$$\delta = \frac{a}{n} \text{ and } \frac{E(\delta)}{E(0)} = \frac{1}{n}\left(\frac{b}{a}\right)^2 \quad (3\text{-}24)$$

where n is defined by $(a/b)^2 = ne^n/2$.

It is noticed that the field decreases considerably at δ for the spheroid with large axis ratio. Therefore, δ gives a rough estimate of dimension of the luminous spot.

Table 3-1 Examples of local high field around conductive spheroid.

	Oblate spheroid		Prolate spheroid	
axes	$a = b = 1\,\mu\text{m}$	$c = 0.1\,\mu\text{m}$	$a = 1\,\mu\text{m}$	$b = c = 0.1\,\mu\text{m}$
$E(0)/E_0$	13		50	
δ	0.17 μm		0.25μm	

As examples, the ratio of maximum field to the average and the length of luminous spot for an oblate spheroid with $a = b = 1\,\mu\text{m}$ and $c = 0.1\,\mu\text{m}$ and for a prolate spheroid with $a = 1\,\mu\text{m}$ and $b = c = 0.1\,\mu\text{m}$ are calculated respectively as shown in table 3-1. The above dimensions of the conductive spheroids are chosen since the actual phosphor particles are of the order 10 μm in length. Exactly speaking, however, the shape and size of the conductive substance within phosphor particles are quite random, the local field varies from spot to spot.

If the high local field can induce electron tunneling from the conductive substance-phosphor junctions, the momentary field-emission current I through the junctions follows the Fowler-Nordheim equation:

$$I = A\frac{E^2}{W^{3/2}}\exp\left(-B\frac{W^{3/2}}{E}\right) \quad (3\text{-}25)$$

where A and B are constants, E is the field strength, and W is the work function.

For ZnS:Cu phosphor, the work function W corresponds to the energy difference between the electron affinity of ZnS and that of the conductive substance.

A powder EL device can be approximately represented by a circuit model as shown in figure 3.5, consisting of a resistor and a capacitor in series. The resistor, representing the field-emitting junctions, is variable with a voltage dependence:

$$R_r = \frac{V_r}{I} = \frac{V_r W^{3/2}}{AE^2 \exp(-BW^{3/2}/E)} \quad (3\text{-}26)$$

where V_r is the voltage drop over the resistor.

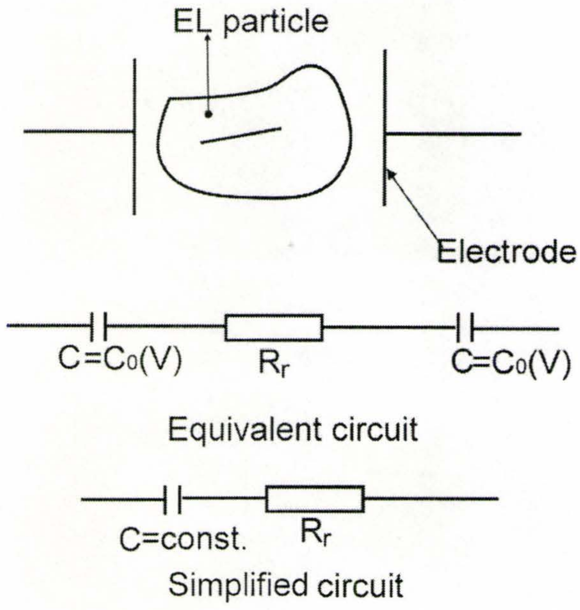

Figure 3.5 Equivalent circuit for AC powder EL

Theoretically, the capacitor, which represents the finite capacitance of the EL particles, is also voltage-dependent. However, to simplify the model, we shall assume that the capacitance is constant, thus $R_c = \frac{1}{j\omega C}$. Then the total impedance is then

$$R = \sqrt{R_r^2 + R_c^2} \quad (3\text{-}27)$$

We let U be the total A.C. applied voltage which is divided into the voltage across the nonlinear resistor, V_r, and the voltage across the capacitor, V_c, so that $U=V_r+V_c$.

If the resistor were constant, the corresponding A.C. current through the circuit would be:

$$I = \frac{\omega C U}{\sqrt{\omega^2 C^2 R_r^2 + 1}} \quad (3\text{-}28)$$

3.3 Bipolar Field-Emission Model

Many theories have been proposed to explain AC-excited EL of embedded ZnS-type powders, such as the impact ionization model, Zener emission model, inverted impact ionization model. However, the accepted theory is this bipolar field-emission model, which was proposed by Fisher in 1963 (Fisher, 1963). A careful study of the interior of ZnS:(Cu,Cl) particles using an optical microscope was performed. It was observed that the shape of the lighting-emitting region within a single EL particle takes the form of double lines with shapes similar to twinkling tails of a comet, as illustrated in Figure 3.6.

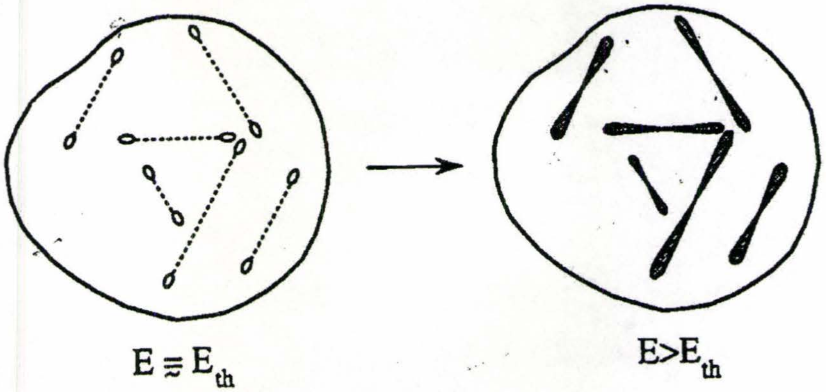

Figure 3.6 Typical microscopic view of EL from ZnS:(Cu,Cl) particles. Double lines at threshold voltage and above the threshold voltage are illustrated (Fisher,

Further observing the ZnS phosphor particles under the microscope, Fisher found that there were many dark segregations and precipitates inside the phosphor particles as shown in figure 3.7.

According to these observations, Fisher proposed the following model for the EL mechanism. ZnS EL powders are typically prepared by firing at high temperature (1100-1200℃) where the hexagonal wurtzite phase predominates. When the powders

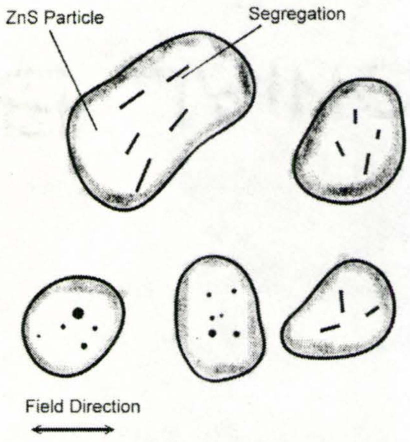

Figure 3.7 Phosphor particles containing dark segregations and emitting spots

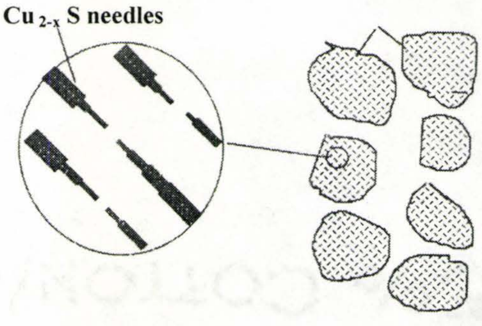

Figure3.8 Illustration of $Cu_{2-x}S$ precipitate needles embedded in the ZnS lattice

are cooled, there is a phase transition to the cubic zinc-blende structure. Copper preferentially precipitates on defects formed in the hexagonal-to-cubic transformation with the reduction of their solubility in ZnS. The Cu forms thin embedded $Cu_{2-x}S$ needles with innumerable small roughness in the crystal matrix, as shown in figure 3.8 (Kitai, 1993). $Cu_{2-x}S$ is known to be a p-type semiconductor with high conductivity. Between these $Cu_{2-x}S$ precipitates and the ZnS, hetero-junctions are formed as previously shown in figure 3.3.

When an external electric field is applied to the phosphor particles, it relaxes in the $Cu_{2-x}S$ conducting needles, which have a component parallel to the field, so that the needles remain at equal potential. This gives rise to a field-intensification from the center of the line, where the field is zero, to the tips, where the field is much higher than the applied field as shown in figure 3.9 (Fisher, 1963). As described before, the intensity of electric field at the tips can be up to 50 times higher or more than the average field in other regions.

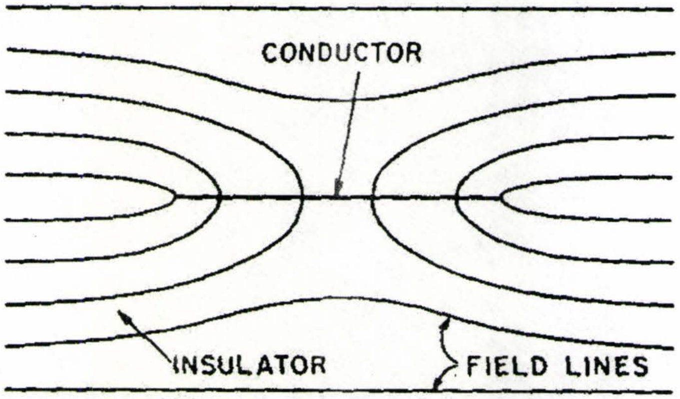

Figure 3.9.Conducting needle embedded in insulator. A uniform electric field is applied parallel to the needle. Geometrical field intensification occurs at the ends.

Therefore it is possible that an applied field of 10^4-10^5 V/cm can induce a local field of 10^6 V/cm or more. This electric field is strong enough to induce tunneling of holes from one end of the needle and electrons from the other to the ZnS:(Cu, Al) lattice. The electrons are captured in shallow traps in Al donor sites, while the holes are trapped by the Cu recombination centers (acceptor sites). When the field is reversed, the emitted electrons recombine with the trapped holes to produce EL. Figure 3.10 shows the illustration of the basic principle of the bipolar field-emission model.

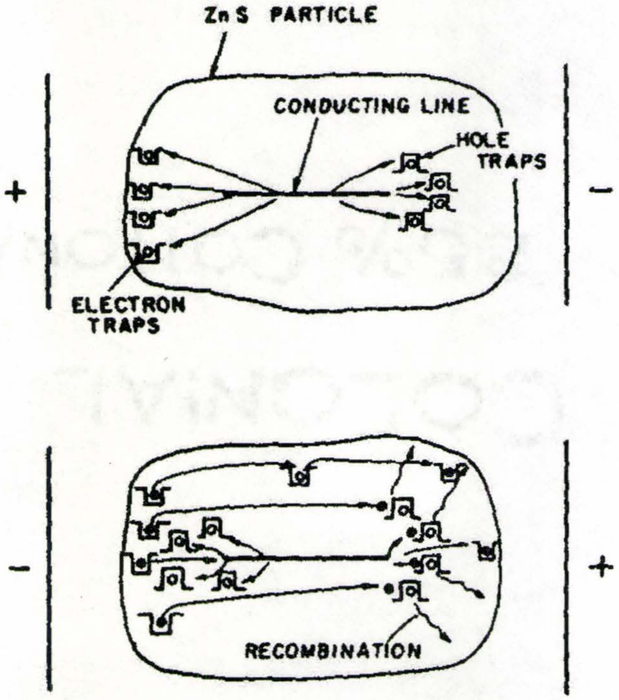

Figure 3.10 Illustration of the basic principle of field-emission model. Above, at field application, electrons and holes are ejected from the opposite ends of the conducting inclusion, where the field is intensified, into the ZnS lattice. Holes are trapped after a short path. Electrons can travel farther. Below, at field reversal, trapped electrons flow back to recombine with trapped holes (light emission). Other electrons are field-emitted into the trapped holes. New holes are field-emitted at the other end of the conducting line.

As a conclusion to the bipolar field emission model, EL emission from a ZnS-powder-EL device is caused by the radiative recombination of electron-hole pairs though donor acceptor pairs.

The bipolar field-emission model can plausibly explain the degradation in ACPEL devices in terms of copper ion diffusion in a ZnS lattice under the influence of a high alternating electric field. The diffusion is caused by the outward drift of copper ions, or by attraction of ions from the adjacent host crystal, or, most likely, by sideward-drift of copper ions in front of the tips during their back-and-forth oscillation under the influence of the high AC field in front of the tips. As a result, the copper sulfide needles are blunted (not only the end tips but also the innumerable little roughnesses). As operating time increases, the copper sulfide needles become shorter and approach a final state which does not initiate sufficient electric field to excite luminescence.

Experimental evidence has been provided by Ono et al. (Ono et al., 1990) for the validity of Fisher's model by carefully examining ZnS:Cu phosphor particles showing EL using a transmission electron microscope (TEM). Black speckles in the shape of narrow needles with diameters of 20 to 40 nm along the boundaries of micro-twin crystals inside a ZnS particle were observed under TEM. The speckles were believed to be the Cu_2S further confirmed by measuring the wavelength of characteristic X-rays emitted from the precipitates. Cu_2S is well known to be a p-type semiconductor with high metallic conductivity. Therefore, these observations confirm the prediction of Fisher.

As we know, one of the necessary requirements for contact EL is that the conducting powders must have relatively sharp edges. The explanation of powder contact EL can be found in the bipolar field-emission model. The electric field near sharp edges of the conducting powders which contact with the phosphors is considerably higher than the average electric field across the phosphor crystals. Therefore, the sharp-pointed powders perform the same role as the conducting Cu_xS imperfection lines embedded in ordinary EL ZnS powders. When an electric field is applied to the mixture, electrons will be ejected from the edges of the conducting powders into the ZnS lattice and recombine with the holes which are trapped by luminescent centers to produce EL with the reversion of the field.

Chapter 4 will review the recent developments of nanotechnology, in particular nanowires, including the materials and methods of fabrication in general, because the powder EL devices discussed in this thesis are fully based on conductive nanowires.

Chapter 4 Nanotechnology – Nanostructure Design and Fabrication

4.1 Introduction

The field of nanotechnology represents an exciting and rapidly expanding research area that crosses the borders between physical, life and engineering sciences (Timp, 1999). One of the frontier areas in nanotechnology involves the design and use of quasi-one-dimensional (quasi-1 D) materials as building blocks for nanoscale devices. By whatever name these nanostructures are known (nanowires, nanobelts, nanorods, nanoribbons, nanowiskers,..), they are clearly a hot commodity in nanoscale science and technology and are certain to remain a focus of research activity for the next decade or more due to their unique physical properties and potential to revolutionize broad areas of nanotechnology. One feature of nanowires, for instance, compared to other low dimensional systems, is that they have two confined directions and one unconfined direction for electrical conduction. This gives nanowires potential applications where electrical conduction rather than tunneling transport is required. Because of the unique density of electronic states, nanowires in the limit of small diameters are expected to exhibit significantly different optical, electrical and magnetic properties from their bulk 3D crystalline counterparts (Shankarn and Raychaudhuri, 2005). In addition, nanowires can also be used as building blocks to assemble new generations of nanoscale electronic circuits and photonics (Hu, et al., 1999). In this regard, semiconductor nanowires, including carbon nanotubes, have shown particular promise (Franceschetti and Zunger, 1996).

Many methods for fabrication of nanosturctures have been developed for diverse applications, ranging from electron beam lithography (Yoon, et al., 2008), nanosphere lithography (Milne, et al., 2002) (Solak, et al., 2003), soft lithography (Xia and Whitsides, 1998), nanoimprint lithography (Chou, et al., 1996), thin-film micropatterning using polymer microspheres or submicron spheres (Lenzmann, et al., 1994), Vapor-Liquid-Solid (VLS) method (Wu, et al., 2002), to template-synthetic method using polycarbonate track-etch membrane (Hulteen and Martin, 1997) or anodic aluminum oxide (AAO).

This chapter focuses on the current state of the art in template-based approaches for the preparation of conducting nanowires due to the real application of indium nanowires on powder EL devices in this thesis. These methods involve the synthesis of a desired material within the pores of a nanoporous membrane. However, a limited number of methods used in nanostructure design and fabrication is reviewed in general because while many nanotechniques have only emerged recently, most of their characteristics – fidelity, resolution, speed and cost – are still under development.

4.2 Strategies in Nanotechnology

4.2.1 Nanostructures Prepared by Lithography with Photons, Particles, and Scanning Probes

To date, preparation of nanostructures or nanoscale patterns based on lithographic techniques is the most universal route (Jung, et al., 2005). The lithographic methods, which are characterized as top-down, all share the same operational principle: exposure of an appropriate material to electromagnetic radiation (UV, DUV, EUV, or X-ray), or energetic particles (electrons or ions) using a scanned beam introduces a latent image (usually a difference in solubility) into the material as a result of a set of chemical changes in its molecular structure; this latent image is subsequently developed into relief structures through etching. The nanopattern achieved by lithography then can be used as a template or mask to deposit a selective catalyst for nanowire growth followed by other techniques such as Electrochemical Deposition (Ji, et al., 2006), Evaporation (Vazquez-Mena, et al., 2008), or Molecular-Beam Epitaxy (MBE) (Toyli, 2006).

The lithographic technology features high resolution, tailorable patterning and good reproducibility. Therefore, this technique, particularly photolithography, is an invaluable tool for microfabrication in a broad range of applications in science and technology and one of the most widely used and highly developed of all technologies now practiced with microelectronics being perhaps the best example today. (Moreau, 1998). However, costly equipment is required and is not practical and efficient in the case of a large area or a large throughput production although such method might work efficiently in the preparation of structures of small areas. Conventional lithography with focused beams of electrons or ions (FIB), for example, is performed serially and is so slow that typical electron-beam patterning of a 4-inch wafer that has a high density of features requires ~ 1h (Gibson, 1997). Furthermore, the physics of diffraction and of interactions of high-energy photons or particles with matter is the intrinsic limitation for lithography and may be hard to overcome. As a result, it is worth considering nonlithographic methods for nanofabrication of patterning and nanostructures, such as self-assembly, vapor-liquid-solid (VLS) deposition and templated-direct deposition.

4.2.2 Nanostructures Prepared by Self-Assembly

One family of approaches to fabrication of nanostructures is based on self-assembly (Whitesides et al., 1991). The idea of self-assembly originally came from biological processes such as the formation of the DNA helix (Sanger, 1986) and the formation of cell membranes from phospholipids (Ringsdorf, et al., 1988). In self-assembly, subunits (molecules or meso-scale objects) spontaneously organize and aggregate into stable, well-defined structures based on noncovalent interactions. The final self-assembly structures form the lowest free energy arrangement, and are close to or at thermodynamic equilibrium.

A variety of strategies for self-assembly have been demonstrated and employed for nanopatterning and nanowires. For example, cylindrical domains of self-assembled monolayers of block copolymers on silicon surfaces were utilized as structural elements for the production of parallel metal nanowires (Chai and Buriak, 2008). The metal ions loading with the block copolymers lead to a high local concentration of metal complexes within the cylindrical domain. A subsequent brief plasma treatment simultaneously removes the polymer and produces metallic nanowires. The morphology of the patterns can modulated by controlling solution concentration, deposition time, and molecular weight of the block copolymers, as well as other factors. The self-assembled aligned single-wall nanotubes (SWNTs) were achieved by dipping a gold (111) ball into a functionalised SWNTs suspension in ethanol, followed by ultrasonication and drying in nitrogen (Liu et al., 2000). The final structure obtained was stable and ultrasonication could not remove the nanotubes from the gold substrate.

Self-assembly is now being examined intensively for patterning at scales >1 μm, and applications are moving to smaller dimensions. Demonstrations, including microcontact printing of self-assembly monolayers (Xia, et al., 1996), reactive ion etching with thin films of block copolymers as masks (Park, et al., 1997), and synthesis of mesoporous materials with aggregates of surfactants as templates (Trau, et al., 1997), illustrate the capability and feasibility of self-assembly as a strategy for fabricating nanostructures. However, integration of these methods into practical routes to useful patterned nanostructures still requires great effort. In microcontact printing, for example, the formation of the defects, the distortion of patterns, the dimensional stability of the stamps, and registration must be understood and controlled.

4.2.3 Nanostructures Prepared by Vapour Phase Growth

In general, nanostructures, e.g. nanowires, are not thermodynamically stable relative to their bulk materials. Therefore, a critical issue in nanowire growth is how to kinetically promote anisotropic growth. A well-accepted mechanism of nanowire growth via a gas phase reaction is the so-called vapour-liquid-solid (VLS) process proposed by Wagner in 1960s during his studies of large single-crystalline whisker growth (Wagner, 1964 and 1970). According to this mechanism, the anisotropic growth is promoted by the presence of the liquid alloy/solid interface. This process is illustrated in figure 4.1 for the growth of Ge nanowires by using Au clusters as the solvent at high temperature.

Based on the Ge-Au phase diagram (figure 4.1 a), Ge and Au form a liquid alloy when the temperature is higher than the eutectic point (363℃) (figure 4.1 a-I). The liquid surface has a large accommodation coefficient and is, therefore, a preferred deposition site for the incoming Ge vapour. After the liquid alloy becomes supersaturated with Ge, precipitation of Ge nanowire occurs at the solid-liquid interface as shown in a-II-III of figure 4.1. Recently, real-time observation of Ge nanowire growth was conducted in a high-temperature in-situ TEM (Wu and Yang, 2001). The experimental results clearly demonstrated the validity of the VLS growth mechanism. There are three growth stages: metal alloying, crystal nucleation and axial growth.

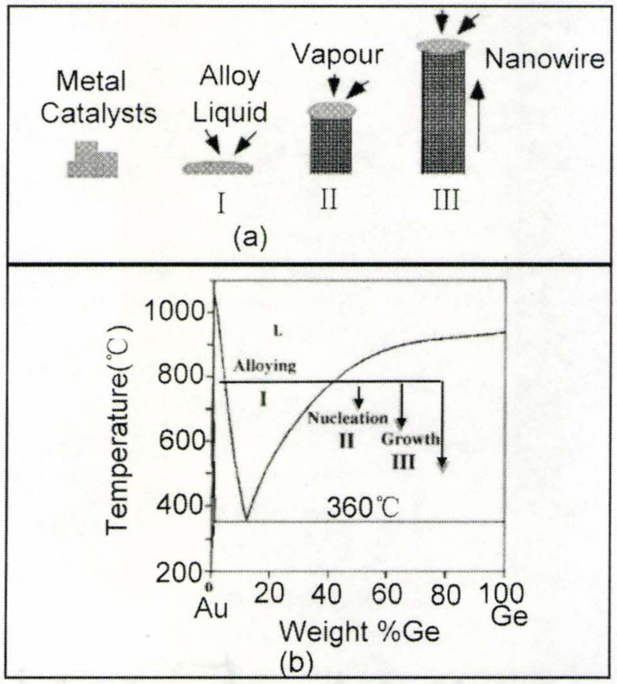

Figure 4.1(a) Schematic illustration of the three stages in vapour-liquid-solid (VLS) mechanism:
(I) Alloying
(II) Nucleation and
(III) Axial growth
The three stages are projected onto the conventional Au-Ge phase diagram: The compositional and phase evolution during the nanowire growth process is shown in (b)

Since the diameter of the nanowires is confined by the diameter of the catalyst particles, VLS is an efficient method to obtain uniform-sized nanowires. Knowing the phase diagram of the reacting species, the growth temperature can be set in between the eutectic point and the melting point of the material. Physical methods such as laser ablation or thermal evaporation as well as chemical methods such as CVD are used to generate the reactant species in vapour form, required for nanowire growth. Catalyst particles are sputtered on the substrates or metal nanoparticles prepared by solution-based routes used as the catalysts. An advantage of VLS is that patterned deposition of catalyst particles yields patterned nanowires. Using the VLS growth mechanism, nanowires of materials, including elements (Ge and Si), oxides (ZnO, MgO, SiO_2), carbides, phosphides (GaP, InP), etc., have been successfully obtained (Rao and Govindaraj, 2005).

Controlling the growth orientation is desirable for many proposed applications of nanowires. By integrating the conventional epitaxial crystal growth technique into the

VLS process, it is possible to precisely control the growth orientation of the nanowires. Therefore, this technique, vapour-liquid-solid epitaxy (VLSE), is particularly powerful in controlled synthesis of nanowire arrays (Wu, at el., 2002). Si nanowires, for example, prefer to grow along the <111> direction. As a result, if the substrate is properly selected and the reaction conditions are precisely controlled, Si nanowires can be grown epitaxially and vertically on the substrate. A nanowire array is formed.

Before the nanowire array growth, generally a thin film of gold is deposited as a solvent/catalyst for the nanowire growth. Upon heat-up, this gold thin film will self-aggregate into high density of Au clusters. The diameters and the density of these clusters are determined by the thickness of the thin film and the growth temperature. This is possible to control the area density of the nanowires by varying the thin film thickness. Figure 4.2 shows the AFM image of clusters obtained by annealing Au thin film on Si substrate at high temperature in argon atmosphere.

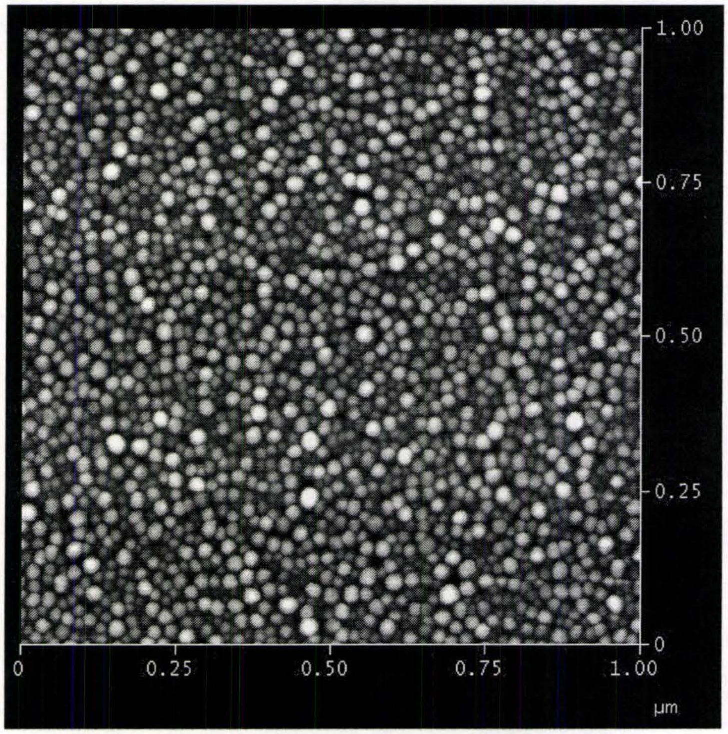

Figure 4.2 AFM image of Au clusters obtained by annealing Au thin film at high temperature. Experimental conditions:

- Au sputtered on Si chip with thickness of 15 nm
- Au thin film annealed at 540℃ for 40 minutes at Ar atmosphere, then cooled with furnace.

Alternatively, the density of the nanowires can be controlled by using solution-based Au clusters. By dispersing a different density of Au clusters on the substrate, it is possible to obtain nanowire arrays with different densities. However, the patterning of the nanowires/Au clusters may resort to lithographical techniques, for example, soft lithography, e-beam, and photolithography. This limits the real efficiency of the process. In addition, VLS process usually needs high temperature for the nanowire growth, so that temperature-sensitive substrates can not be used.

4.2.4 Template Synthesis of Nanostructures

The template method involves synthesizing a desired material within the pores of a porous membrane. If the membranes that are used have cylindrical pores of uniform diameter, a nanocylinder of the desired material is obtained in each pore. Depending on the properties of the material and the chemistry of the pore wall, this nanocylinder may be solid (a nanowire) or hollow (a nanotubule) (Hulteen and Martin, 1997).

There are a variety of interesting and useful characteristics associated with template synthesis. Firstly, the beauty of this method is that it is extremely general with regard to the types of materials that can be prepared. For example, nanowires composed of conductive polymers (Liang and Martin, 1990), metals (Guo, et al, 2003), semiconductors (Lakshmi et al., 1997), carbon (Sung, et al, 1999), and other materials have been prepared by the template method. Secondly, the diameter of the nanostructure is determined by the pore size of the template so that nanowires with diameter as small as 3 nm have been prepared by this method (Wu and Bein, 1994). In addition, nanowires of desired material with uniform diameter can be easily achieved due to the intrinsic uniform pore size of the template membrane. Finally, the nanostructures obtained by the template method can be used as a building block in various applications. For example, if the nanowires remain inside the template membrane, a nanowire array is obtained. Alternatively, the nanowires can be freed from the template membrane and collected as an ensemble of free nanoparticles. Also, if the nanostructure-embedded membrane is attached to a surface and the membrane is removed, an ensemble of micro- or nano-structures that protrude from the surface like the bristles of a brush can be obtained.

To date, most of work in template synthesis has focused on the use of two types of nanoporous membranes, 'track-etch' polymeric membranes and porous alumina membranes. However, there are a variety of other templates that could be utilized.

4.2.4.1 Track-etch polymeric membranes

Polymeric membranes with microporous or nanoporous structures have been prepared by a track-etch method (Fleisher, et al., 1975). This method involves bombarding a non-porous sheet of the desired material with nuclear fission fragments, leaving damaged tracks in the materials, and then followed by chemically etching these tracks into pores. The resulting membranes contain randomly distributed cylindrical pores of uniform diameter, as shown in figure 4.3.

Owing to the random nature of the bombarding process, the angle of the pores with respect to the surface normal can be as large as 34° (Poretics Corporation, 1995).

Therefore, a number of pores maybe actually intersect within the membrane.

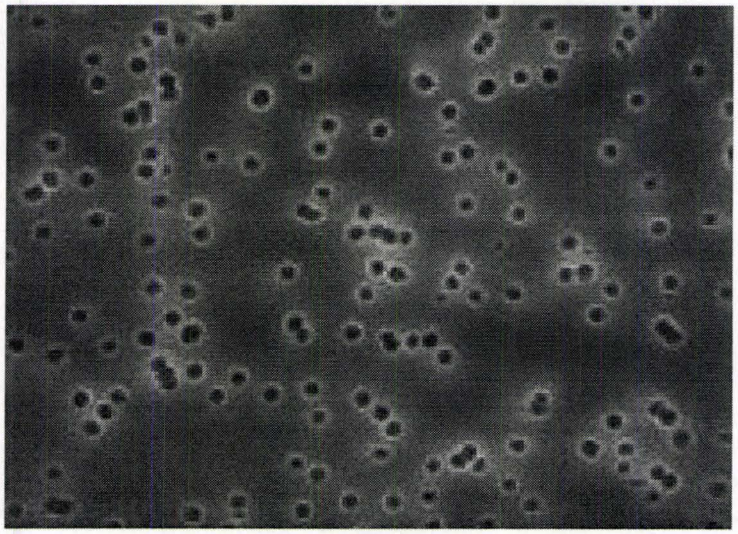

Figure 4.3 SEM image of Isopore™ polycarbonate porous membrane prepared by track-etch.

4.2.4.2 Anodic aluminum oxide (AAO) membranes

Anodic aluminum oxide (AAO), which is formed by anodizing high-purity aluminum in an appropriate acid solution has been studied extensively over the last five decades and is characterized as a self-organized porous structure with uniform pore diameter and depth (Shingubara, 2003). Unlike the track-etch membranes, the pores in AAO have little or no tilt with respect to the surface normal resulting in an isolating, non-connecting pore structure.

The history of electrochemical oxidation of aluminum dates back to the beginning of the last century. Anodic oxidation of aluminum has attracted considerable attention because of its wide application in various fields of technology. Traditionally, aluminum is "anodized" in order to protect the metal against corrosion, to improve its abrasion and adsorption properties, etc. (Wernick and Pinner, 1976) The more recent and rapidly growing applications of anodic alumina in electronics due to their excellent dielectric properties, perfect planarity, and good reproducibility in production have enhanced the interest in anodic alumina (Despic et al., 1989).

Formation of nonporous oxides spontaneously occurs upon contact of aluminum metal with neutral (pH 7-8) solutions of borates, citrates, tartrates, phosphate, etc (Thompson and Wood, 1983) (Ammar et al., 1981). They are limited to a thickness of several hundred nanometers due to their virtually insolubility in the solutions. Porous oxides are created in electrolytes promoting oxide dissolution, i.e., aqueous sulfuric, oxalic, or phosphoric acid solutions, with a thickness of up to hundreds of microns (Fukushima et al., 1974). Nowadays, it is generally accepted that the structure of porous oxides is a close-packed array of columnar hexagonal cells, each containing a central pore normal to the substrate surface and separated from it by a layer of a hemispherically shaped barrier-film as shown in figure 4.4 (Keller et al., 1953).

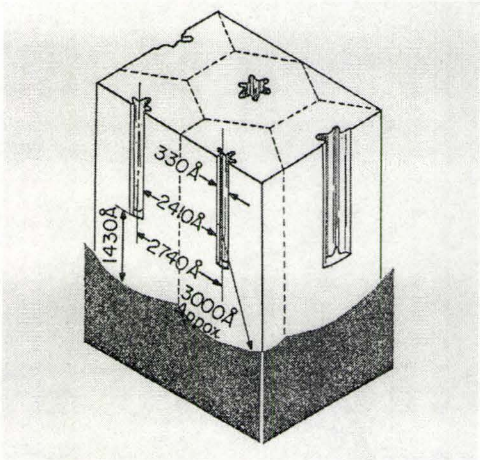

Figure 4.4 Illustration of a porous oxide film formed in a phosphoric acid solution (4wt%) at 120 V and 24℃

As illustrated by figure 4.5, an electrolytic cell consists of a high purity aluminum anode and a noble metal, such as platinum, cathode. The electrolyte can be phosphoric, sulfuric, chromic or oxalic acid. Under a DC voltage, the aluminum is electrochemically anodized, and an oxide consisting of pores grows at the anode electrode (Bard, 1973),

$$2Al(s) + 3H_2O(l) = Al_2O_3(s) + 6H^+ + 6e^-,$$

and hydrogen evolves at the cathode

$$6H^+ + 6e^- = 3H_2(g).$$

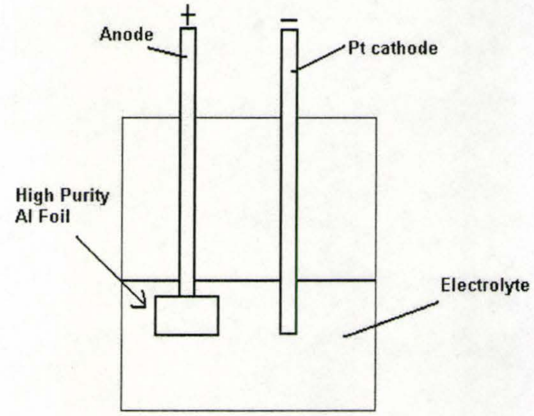

Figure 4.5 Schematic illustration of anodizing aluminum. Highly ordered structure can be produced.

The pore formation mechanism is shown schematically in figure 4.6.At the beginning of the anodization, a barrier film, which consists of a non-conductive oxide, covers the entire surface of the aluminum (figure 4.6 a). The electric field is focused locally on fluctuations of the surface (figure 4.6 b). This leads to field-enhanced or/and temperature enhanced dissolution in the formed oxide and thus to the growth of pores (figure 4.6 c). Finally, an equilibrium state is approached and pores grow in a stable manner, induced by the decrease of current (figure 4.6 d).

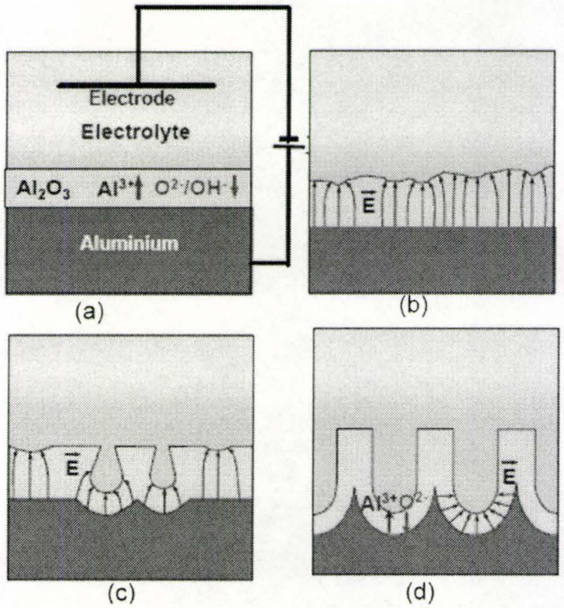

(a) (b)

(c) (d)

Figure 4.6 Schematic of the pore formation at the beginning of the anodization

A mechanical stress model (Jessensky et al., 1998)(Li et al., 1998) was proposed to explain the formation of AAO. The atomic density of aluminum in alumina is by a factor of 2 lower than in metallic aluminum if the formed alumina by anodization is Al_2O_3. Consequently, the volume of the anodized alumina expands to about twice the original volume. This volume expansion leads to the compressive stress during the oxide formation in the oxide/metal interface. Since the oxidation takes place at the entire pore bottom simultaneously, the material can only expand in the vertical direction, so that the existing pore walls are pushed upwards by the stress.

In experiment, due to the mobility of Al^{3+} in the oxide under the electric field, the degree of the volume expansion of aluminum can be controlled by means of varying the applied potential, resulting in the formation of either self-ordered pores or disordered pores. It was concluded that self-ordered porous alumina is best formed when the volume expansion coefficient is approximately 1.2 (Li et al., 1998).

AAO finds steadily growing application in various fields. Traditionally, it is most popular in civil industrial engineering for producing protective and decorative surface finish in panels and different objects. These applications are well reviewed in the literature (Kape et al., 1984). Moreover, AAO membranes are also produced and used in various spheres, such as molecular separation (Vlassiouk et al., 2004), electronics

(Rahman et al., 2007), masks for growing structures (Yang et al., 2007). Furthermore, AAO membrane is a good support for the deposition of a variety of thin films with nanoporous structures which show anomalous optical, electronic, magnetic and other properties different from those of their corresponding bulk materials. Nanoporous Pd (Ding, et al. 2006) and WO_3 (Gorokh, et al., 2006) thin films, for example, have been prepared using AAO as substrates by sputtering method. It was reported that these films are highly sensitive to the specific gas and have promising sensor applications. Based on this idea, porous SiO_2 thin films grown on the AAO membranes have been prepared by us during the course of this work. Due to the intrinsic nature of the AAO support, SiO_2 thin films with a self-organized porous structure have promise as microporous(<100nm) materials for catalysts and molecular separation. Since this part of work has no direct relationship to the EL device preparation, the detailed experimental procedures and results are summarized in Appendix II.

Recently, since the pioneering work of Martin's group (Martin, 1994), AAO membranes with pore sizes ranging from 4 nm to 200 nm are widely used as template materials for synthesis of regularly ordered nanowires or nanotubes by inserting metals such as Au (Matsumoto et al., 2004), Ag (Lee et al., 2005), Bi (Riveros et al., 2006), Sn (Huber et al., 2000), In (Chen et al., 2006), Al (Huber et al., 1994), or semiconductors such as Se, Te, GaSb (Huber et al., 1994), Bi_2Te_3, Si (Lew et al., 2003), and Bi_2S_3 (Xu et al., 2007) thanks to its monodisperse controllable diameter and thickness.

However, porous alumina is not a perfect candidate for a template. Although it is commercially available now, an inherent defect of the membrane is the high aspect ratio (the ratio of the thickness to the diameter of the pore), which means innovative strategies are needed to insert desired materials into its holes to obtain nanostructures. The traditional physical evaporation techniques such as sputtering, electron beam evaporation do not work ideally for AAO membrane although ZnO films have been achieved on the membrane by using Atomic Layer Deposition (ALD) (Elam et al., 2003).

4.3 Template-synthesized Nanowires Using AAO Template

Theoretically, nearly any material can be synthesized within the nanoporous membrane, AAO or track-etch membrane, as long as a suitable process can be developed. To date, numbers of routes have been developed to insert various materials into the pores of membrane, such as electrochemical deposition, electroless deposition, chemical polymerization, sol-gel deposition, physical/chemical vapour deposition, and pressure injection, etc. The following is a general outline of four selective chemical/physical strategies that have been used in our lab or elsewhere to conduct template synthesis nanowires within AAO membranes.

4.3.1 Electrodeposition

Electrodeposition or electro-plating inside AAO, pioneered by Possin in 1970s

(Possin, 1970) and Martin (Martin, 1994) in 1990s, is a 'bottom-up' method and is

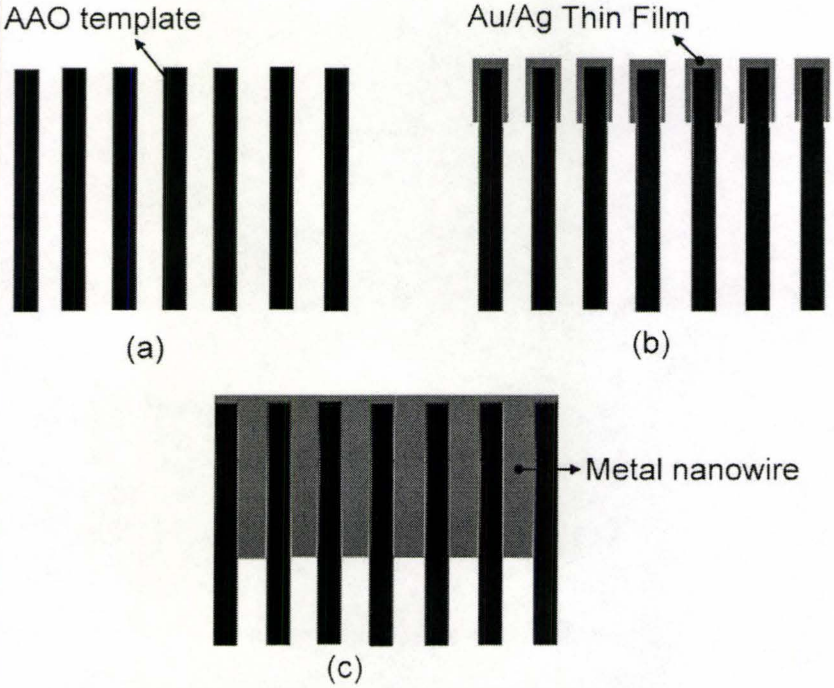

Figure 4.7 Schematic illustration of electroplating metal into AAO template. AAO template (a); Metal thin film, e.g, Au/Ag grown on the surface of AAO (b); Electroplating metal inside AAO (c)

widely used because of its low-cost and high-yield producing nanowires from various materials (Matsumoto et al., 2004), (Lee et al., 2005), (Riveros et al., 2006). Electrodeposition is one of the best candidates to grow conductive materials due to the fact that electrodeposition is based on electron transfer, which is fastest along the highest conductive path (He et al., 2003). In practice, one side of AAO was covered with a very thin metal such as gold by performing sputtering or evaporation. This metal film provides electrical contact and is to be used as a cathode for electrodeposition. After this, electrodeposition is conducted in a specific electrolyte under a specific DC voltage or current. Figure 4.7 illustrates the processes for electrodeposition of metal inside AAO. By this method, silver nanowire arrays have been fabricated by Choi et al. (Choi et al., 2003) as shown in figure 4.8. In this case,the length of these nanowires can be controlled by varying the amount of metal deposited. Small amount of metal deposited can get short wires, whereas, large quantities of metal can introduce long needle-like wires.

Electrodeposition is a relatively simple and inexpensive method. Nanowires of large aspect ratio can be grown within pores of AAO. However the conducting substrate and the requirement of the appropriate chemical precursor limit the application of this technique. Therefore, electroless deposition was introduced.

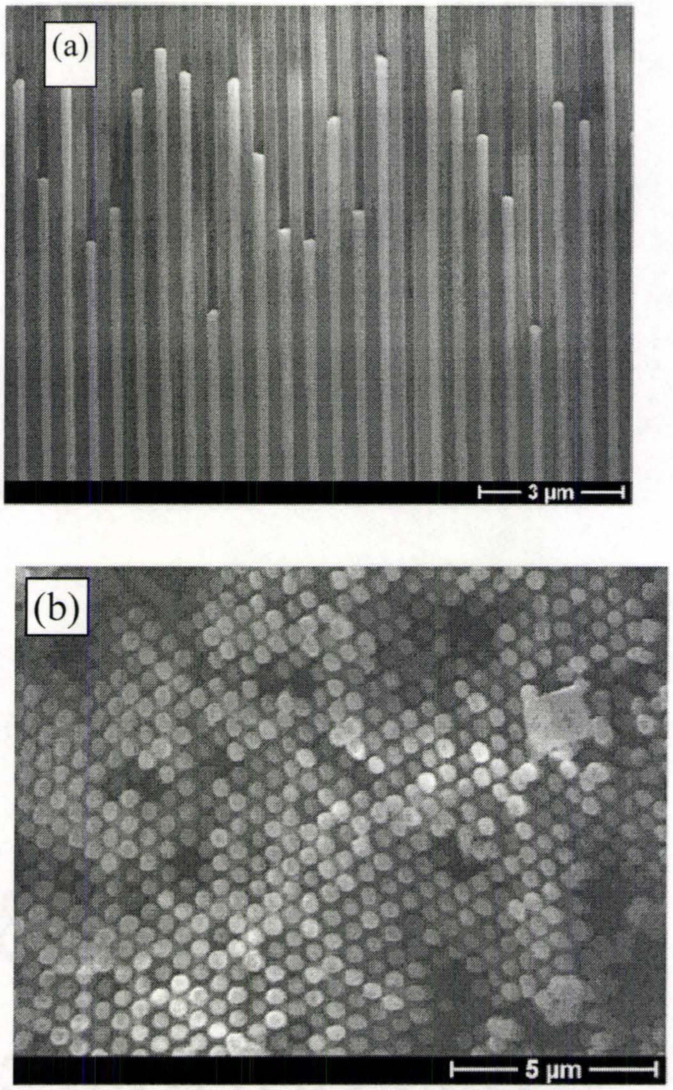

Figure 4.8 SEM images of silver inside AAO template fabricated by Jinsub Chol et al using electrodeposition method. The difference in the darkness of color in(b) indicates fluctuations of the height of the silver rod. The higher the rods, the brighter they appear (Choi, et al., 2003)

4.3.2 Electroless Deposition

Electroless metal deposition involves the use of a chemical reducing agent to plate a metal from solution onto a surface. This method differs from electrodeposition in that the surface to be coated need not be electronically conductive. The key feature of the electroless deposition process is that the metal deposition in the pores starts at the pore wall. Therefore, the structures yielded by this method run the complete thickness of the AAO template. Meanwhile the inside diameter of the metal can be controlled at will by varying the metal deposition time. In practice, three steps are followed by Martin et al. to grow Au nanowires inside AAO by the electroless deposition (Kohli, 2004):

(a) Activation: Immerse the AAO in a Sn^{2+} solution to chemically bind Sn^{2+} to the pore walls.

(b) Catalyst deposition: Immerse the Sn^{2+}-activated AAO into a solution of Ag^{+}. The following surface redox reaction occurs, yielding catalytic metallic Ag nanoparticles on the pore walls:

$$Sn^{2+} + 2Ag^{+} \rightarrow Sn^{4+} + 2Ag$$

(c) Electroless deposition: This involves immersing the AAO in the Au plating bath, where the Ag nanoparticle acts as a catalyst for the reduction of Au (I) by the reducing agent.

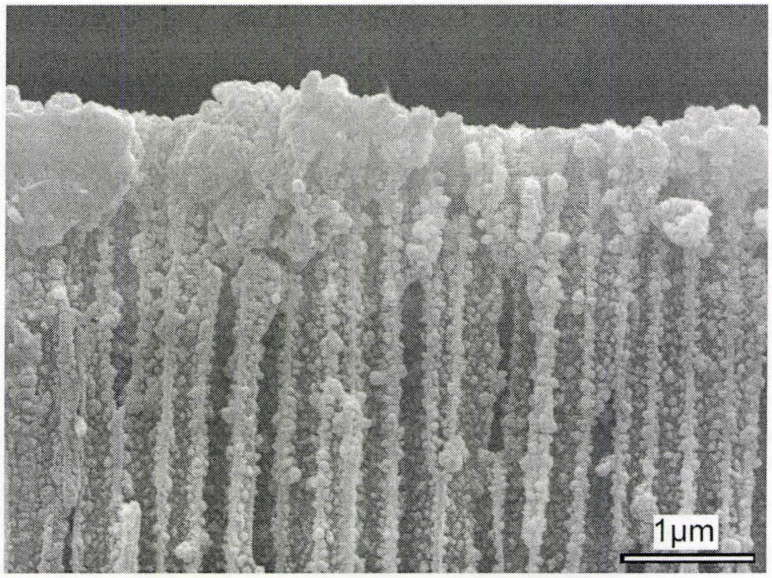

Figure 4.9 Electroless deposition of Ag nanoparticles into AAO template after 10 cycles.

Based on these processes, a similar experiment was conducted to fabricate Ag nanoparticles inside AAO template in our lab. The following is the outline of the experimental procedures:

(1) Dip AAO template into a mixture of $SnCl_2$ (0.02M) and HCl (0.01M) (1:1, V/V) for 2 minutes;
(2) Rinse the Sn^{2+}-activated AAO by DI water several times;
(3) Rinse the Sn^{2+}-activated AAO by acetone and dried at 70 ℃ for 1

minute;

(4) Immerse the dried AAO membrane into $AgNO_3$ (0.02M) solution for 2 minutes and completed one cycle;

(5) Return to step 2, starting another cycle.

Figure 4.9 shows preliminary result of Ag particles embedded in the pores of AAO obtained in our lab after 10 cycles.

4.3.3 Chemical/Physical Vapour Deposition (CVD/PVD)

Vapour deposition is a simple and convenient method of filling the pores of the template to prepare nanostructures. It is a good route to fabricate nanocomposites of metals and metal oxide semiconductors which are difficult to deposit by usual electrochemical processes. Particularly, the use of the vacuum deposition of semiconductors into the holes of anodic porous alumina contributes to the enlargement of the application field of anodic porous alumina.

A typical CVD process, for example, preparing carbon nanotubes involves placing an alumina membrane in a high-temperature furnace (ca.700℃), and passing a gas such as ethane or propene through the membrane. Thermal decomposition of the gas occurs throughout the pores, resulting in the deposition of carbon film along the length of the pore walls. Therefore, carbon nanotubes are obtained and the thickness of the wall of the carbon tubes is dependent on the total reaction time and the precursor pressure. Physical vacuum deposition can be directly applied to template synthesis in fabrication of metal or metal oxide nanostructures. Vacuum evaporation has been reported for preparing Au nanodots/nanotubes (Jung, et al., 2005) and Ag/Ni nanowires (Yasui, et al., 2005) with AAO membranes.

By adjusting the anodization conditions, AAO membranes can be synthesized with pore diameters ranging from d= 4 to 200 nm and pore lengths in the range of L= 1 to over 200 μm. Consequently, the AAO nanopores may have aspect ratios as high as $L/d = 2.5 \times 10^4$. Therefore, the ultrahigh aspect ratios seriously challenge the traditional chemical/physical vapour deposition method as the surface of the pores becomes blocked before the vapour can traverse the length of the pore and the deposition rates are often too fast. To address this problem, atomic layer deposition (ALD) has been reported to fabricate ZnO and Al_2O_3 on AAO membrane (Elam et al., 2003) owing to the good thermal stability of the membrane. The final thickness of ZnO/Al_2O_3 coatings on the wall of pores can be 129 Å with respect to the AAO aspect ratios of 800.

4.3.4 Metallization of AAO using Gas/Hydraulic Pressure Injection Method

Hydraulic pressure injection method is a different approach to fabricate metal nanowires. This method takes advantage of high gas (Zhang et al., 1998),(Zhang et al., 1999) /hydraulic pressure(Chen et al., 2006),(Chen et al., 2005) to force the molten metal into the pores of AAO template. It features easy handling and high repeatability to overcome most of the problems associated with electrochemical methods. In practice, the metal and the template are heated up to the metal melting point, and then the molten metal is injected into the template by high gas/hydraulic pressure, overcoming the surface tension force. Sn nanowires, 15 nm and 60 nm in diameter respectively, fabricated by the hydraulic injection method are continuous, dense and have uniform length (10 μm). In addition, the filling ratio is very high and can be up to 100% (Chen et al., 2006). In this thesis, the hydraulic pressure injection method is used to fabricate indium nanowires and is described in detail in the following section.

Chapter 5. Experimental Procedures

5.1 Nanowire contact EL device preparation

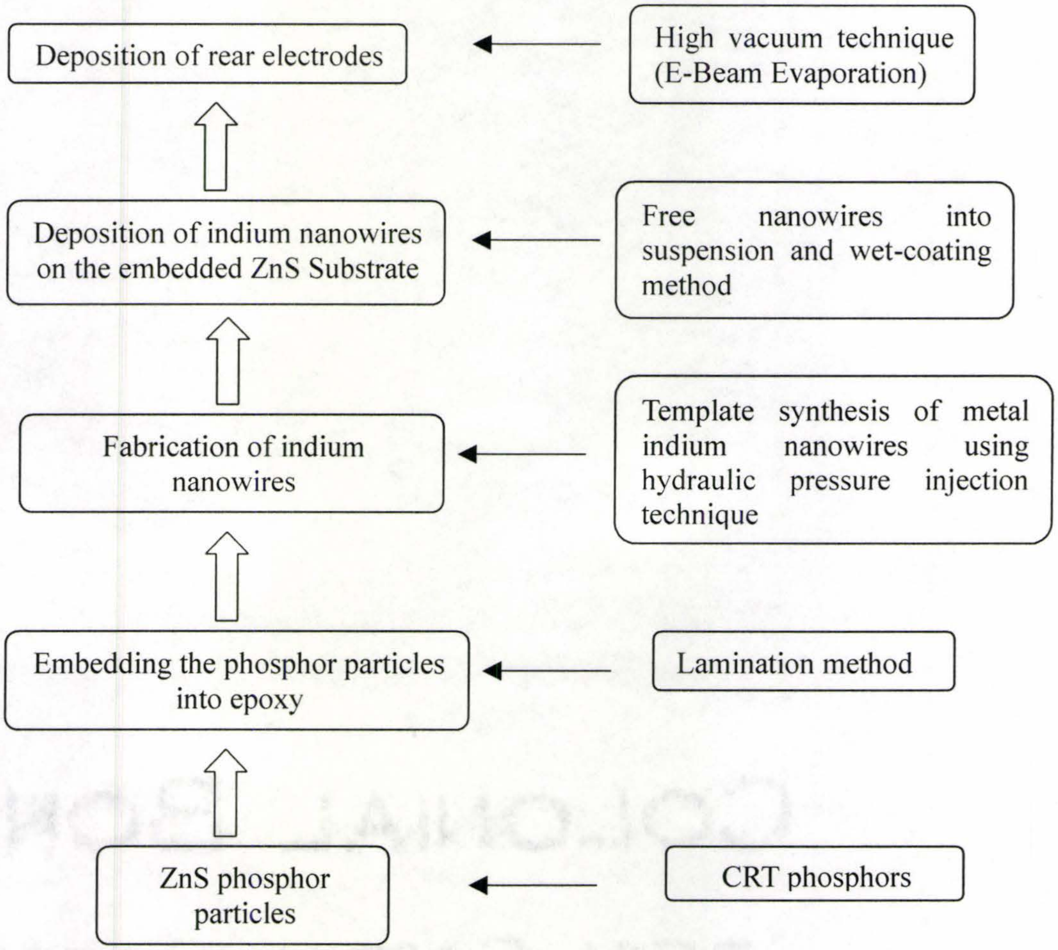

Figure 5.1 Flow chart of the fabricating processes for nanowire contact EL

The experimental procedures for preparing a nanowire contact EL (NCEL) device are shown in figure 5.1. The right column in the figure shows the techniques used in each step. The experimental process begins using Sylvania type 1260 green ZnS:(Cu, Al) CRT phosphor. This phosphor has a very strong PL emission under u.v. excitation of 254 nm, but no electroluminescence under usual conditions in a high electric field. The phosphor particles have faceted morphology with a particle size of 3-20 μm.

5.1.1 Separation of ZnS phosphor particles

Coarse particles have a larger effective contact area with the nanowires which function as nanoelectrodes in the device compared to fine particles. Consequently, large particles and narrow distribution of particle size are expected to improve the performance of the EL device. A sedimentation method is used to remove the small particles according to Stokes' law given by:

$$v = (1/18)(\rho_p - \rho)gD_p^2/\eta \quad (5\text{-}1)$$

where v is the sedimentation terminal velocity of a spherical particle in a viscous liquid, ρ_p and ρ are the density of the particle and the medium, respectively, η is the viscosity of the medium, D_p is the diameter of the particle, and g is the acceleration due to gravity. The sedimentation speed increases in proportion to D_p^2, resulting in the separation of coarse particles and fine particles in the sedimentation process.

If the particle diameter is 5 μm, the medium is pure water with viscosity of 0.89 mpa·s at 25 ℃, the particle density is 4090 kg/m^3, the sedimentation terminal velocity is estimated approximately 4.7×10^{-5} m/s. Therefore, the time for the particle to travel a 10 cm depth in water is ~1 hour.

In the experiment, deionised water is used as the medium. First, ZnS particles are added into a beaker containing water 10 cm deep. Thorough stirring of the suspension is performed. Then the suspension becomes still, allowing the particles to travel 45 minutes in the water. Due to the difference in the sedimentation speeds of particles, large particles settle down onto the bottom first, resulting in layer separation in the suspension. The upper layers of the suspension mostly consisting of fine particles are smoothly decanted, leaving coarse particles coating the beaker bottom. After repeating the steps described above 5 times, the water is evaporated and the powder is dried by placing the beaker on a hot plate at 120℃ for 10 hours.

5.1.2 Embedding the phosphor particles into the epoxy

The epoxy used in this work is Epo-Tek 301(Epotek), a two-part, optically transparent epoxy system with viscosity of 100-200 cP at 100 rps/23℃. In order to get a uniform embedding force and remove the air trapped by the epoxy, a method called the double-lamination method is used to embed the phosphors into the epoxy as shown in figure 5.2.

The double laminator consists of two metal plates stacked together and separated by a mylar film into two chambers: top and bottom, respectively. Each chamber is sealed by gaskets and connected with a vacuum, controlled by a valve. At the beginning, the epoxy is uniformly coated on ITO-coated glass, and the phosphor powders are deposited on a sticky tape (Gel-pak). Excess powder is removed by shaking the tape in order to get a single layer of particles staying on the tape. Then the epoxy-coated glass and powder-coated tape are placed face to face into the bottom chamber of the laminator (figure 5.2 a). Sequentially, the following three steps are employed:

(1) Open valve 1 and close valve 2. The mylar with the powder moves up due to the evacuation of the top chamber of the laminator (figure 5.2 b).

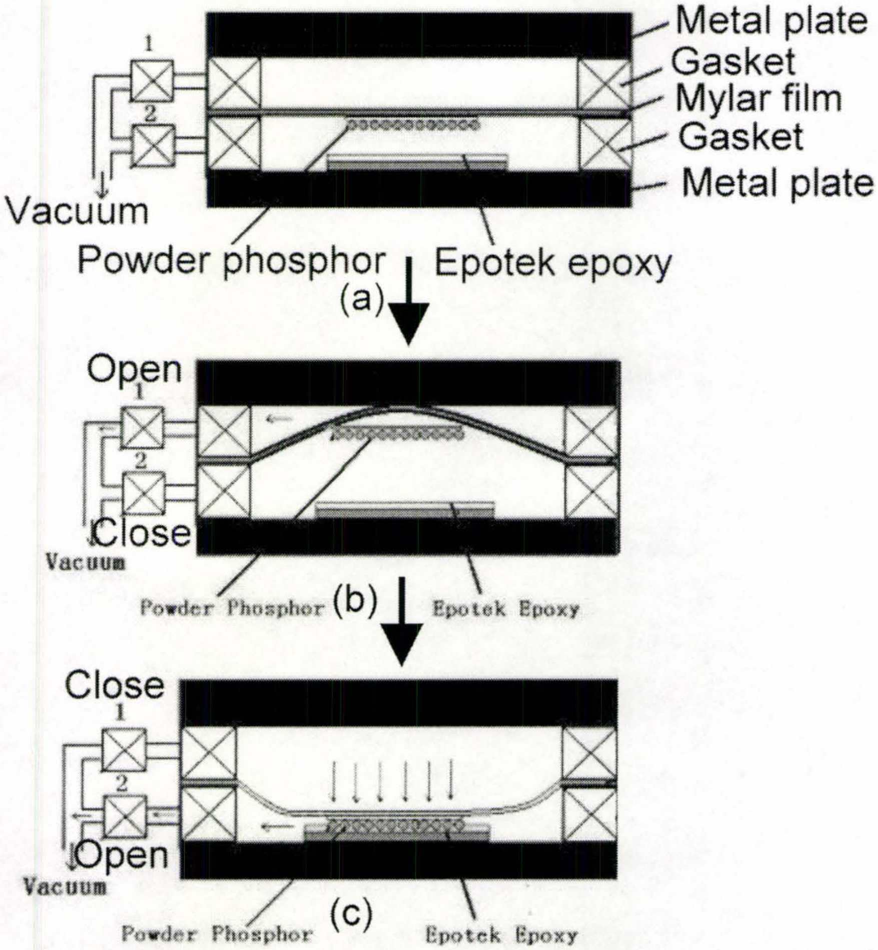

Figure 5.2 Illustration of double-laminator method

(2) Open valve 2 and keep valve 1 open. Air in the bottom chamber of the laminator and air bubbles trapped by the epoxy liquid are removed by the vacuum process.

(3) Close valve 1 and keep valve 2 open, and meanwhile let the air go into the top chamber of the laminator. As a result, the powders are pushed into the epoxy by atmospheric pressure during the vacuum process (figure 5.2 c).

Finally, after the epoxy is fully cured, the tape is removed and the phosphor powders are embedded into the epoxy, but not covered by epoxy.

5.1.3 Fabrication of Anodic Aluminum Oxide Membrane

High purity aluminum foils (8×7×0.25mm, 99.9995%, annealed, Alfa Aesar) are used as starting material. Firstly, the foils are mechanically polished with progressively finer grit sand papers and then further polished using SiO_2 solution with a mean particle diameter of 50 nm. To obtain a smooth surface, the foils are then electropolished in a mixed solution of perchloric acid (60%) and ethanol (1:9) under a constant voltage condition of 20 V at room temperature for 5 minutes. A two-step anodization process (Masuda and Satoh, 1996) is employed so that highly ordered pore arrays can be achieved. The first anodization step is carried out in a 0.9M sulphuric acid solution at room temperature by applying a constant voltage of 20 V for 30 minutes. Then, the resulting alumina layer is removed by immersing the specimens in a mixture of phosphoric acid (5 Wt%) and chromic acid (1.8 Wt%) with the ratio of 4:1 at 60℃ for 30 minutes. A relatively ordered indent pattern was produced on the surface of the aluminum foils after this step. The second anodization of the foils is then performed under the same anodization conditions as the first one for 30 minutes.

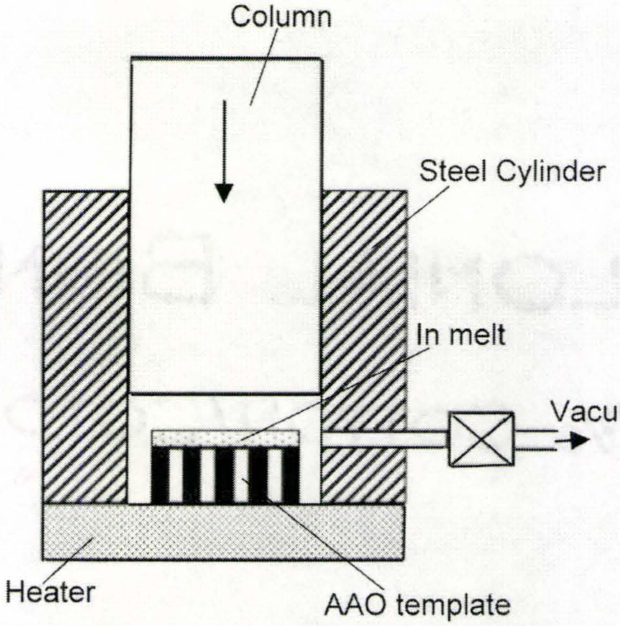

Figure 5.3. Schematic illustration of the set-up for injecting In into AAO template

5.1.4 Fabrication of indium nanowires using AAO templates by hydraulic pressure injection method

Porous alumina filter discs (Whatman) with a nominal pore size of 0.1 μm are used as indium nanowire templates. The thickness of the discs is approx. 60μm. A hydraulic pressure injection method is used to metallize the discs. The detailed set-up is shown in figure 5.3.

In the experiment, a piece of indium foil (5×8×0.1mm, Alfa Aesar, 99.9975%) and an AAO template are placed in a stainless steel chamber which is connected with a high vacuum (less than 5×10^{-5} Torr) and placed on a hot plate. When the chamber is heated to 160℃, slightly above the indium melting point (156℃) for 20 minutes, the indium melts and spread over the AAO surface. Then the chamber is removed from the hot plate and a hydraulic force is applied to the column by a hydraulic jack. As a result, the metal indium is injected into the AAO template. Finally, the chamber is fan-cooled down to room temperature. Figure 5.4 shows the step-by-step fabrication procedures of indium nanowires.

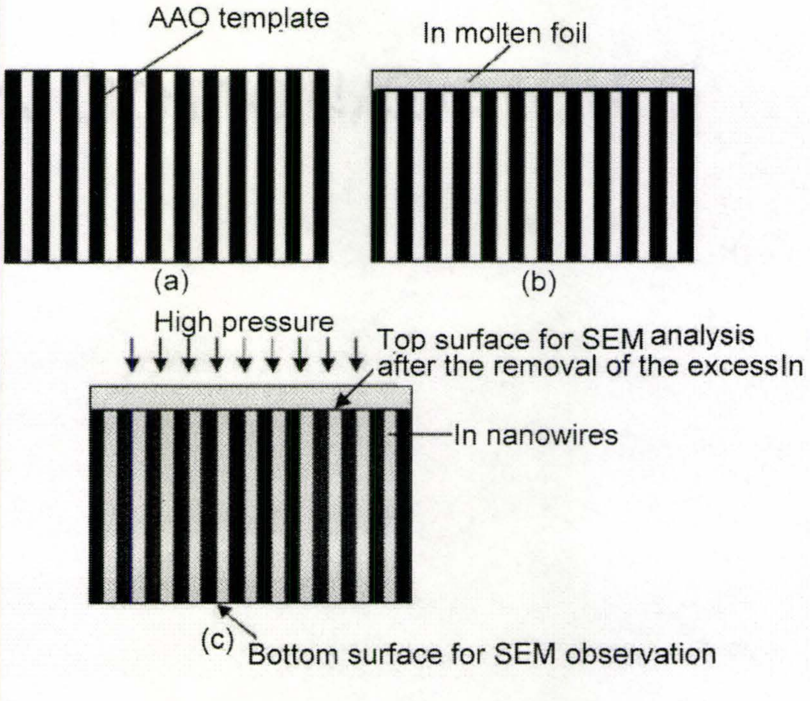

Figure 5.4. Scheme for the injection of In into AAO. Bare AAO template (a), In foil is put on the AAO surface and heated to its melting point (b), under high pressure, the molten In is injected into the AAO template and nanostructures are formed (c)

The critical pressure P needed for the molten metal to permeate into the AAO can be obtained from the Washburn equation: $D = -4\gamma\cos\theta / P$, where γ is the surface tension of the liquid indium, θ is the contact angle between the indium liquid and the alumina substrate ($\theta > 90^{\circ}$ for nonwetting liquids) [49] and D is the diameter of the channel. In this paper, γ of In is estimated as 573 mNm^{-1}[22]. If the mean diameter of the channel is assumed to be 100 nm, the maximal critical pressure P, which is reached in the nonwetting case ($\theta = 180^{\circ}$)(Lee et al.,2005), can be calculated as 23 MPa. Considering additional work to overcome the friction between the metal and the channels, and the force from the air trapped in the channels, 110 MPa pressure is applied to impregnate the In into the AAO channels in the current work to make sure all In nanowires run through the thickness of the template.

After the experiment, the bottom surface of the In-embedded AAO is slightly polished to remove the excess bulk indium from the AAO channels. The sample is then post processed by etching in 0.3 wt% NaOH solution at room temperature for 60 minutes. As a result, the excess surrounding bulk indium on the top surface is removed. In addition, the indium nanowires are exposed on both surfaces because of the dissolution of the AAO template.

The AAO/indium nanowire composite samples are characterized by a scanning electron microscope (SEM) and x-ray diffraction (XRD).

5.1.5 Deposition of the indium nanowires on the ZnS embedded substrate

In order to transfer the indium nanowires to the embedded ZnS substrate, the following four steps are employed:

(1) Dissolve the porous AAO/In nanowire composite using NaOH solution (~0.2wt%). An ultrasonator is used to help the dissolution of the composite in solution. A small piece of AAO/In composite is put into NaOH solution. After 60 minutes they are transferred into an unltrasonator. The ultrasonication time is 15 to 20 minutes with an interruption of 1 minute every 2 minutes at high amplitude. Indium nanowires are released into the solution since amorphous alumina is very sensitive to NaOH solution.

$$Al^{3+} + 3OH^{-} = Al(OH)_3 \downarrow$$

(2) Transfer the nanowires onto the surface of a porous alumina filter. The AAO membrane is used as a filter in this step because of its nanoporous structure. Nanowire-containing solution is dropped onto the surface of an AAO membrane (0.1 μm pore size with 60 μm thick). The solvent can pass through the pores of the membrane, leaving the free nanowires lying on the surface.

(3) Rinse the nanowires using deionised water and make nanowire suspension. Deionised water is used to rinse the nanowires, removing the residual solutions. After that, the nanowire suspension is prepared. The transparency of the solution can suggest the density of the nanowires in the suspension. High transparency indicates low density of nanowires.

(4) Wet-coat the embedded ZnS powder substrate using the In nanowire suspension. Wet-coating method features ease of handling and low cost. In nanowire suspension is dropped on the embedded ZnS powder substrate. By solvent evaporation, a dilute layer of indium nanowires is formed on the ZnS particles.

5.1.6 Deposition of the rear electrodes

Electron beam deposition is used to grow the Au rear electrodes on the devices at room temperature. A stainless steel mask with rectangular pads 0.5 mm by 5 mm is employed to obtain the patterned Au electrodes. The Au electrodes with various thicknesses ranging from 80 nm to 300 nm are prepared to investigate the effect of thickness on the device performance.

5.2 Calculation of the electric field in the phosphor

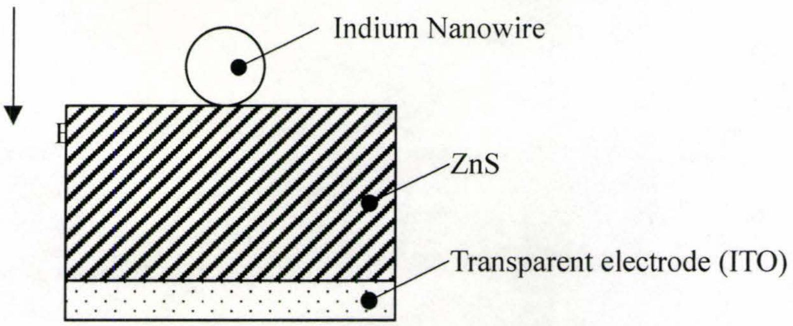

Figure 5.5. Illustration of the geometry of a conductive nanowire on the ZnS

A simple model can be set up corresponding to the nanowires extended beyond the perimeter of the gold strip electrodes, but electrically contacted by the gold electrodes (Figure 5.5).

Calculation of the electric field in the phosphor due to the contact with conductive nanowires is performed with electromagnetic field simulation software. This software (2D Maxwell SV from An Soft Inc.) is powerful and accurate for two-dimensional electromagnetic and electrostatic-field simulation through the finite element method (FEM). It can also perform 3D simulations on symmetrical devices with a rotation axis.

It is assumed before simulation that the ZnS particle is a linear and isotropic material with a relative permittivity of 8.0 and the nanowire contact nanoelectrodes are perfect conductors. Furthermore, there is no electrical breakdown in the phosphor and the nanowire is infinitely long in the Z direction. The electrostatic simulator is based on Poisson's Equation.

$$\nabla \cdot (\varepsilon_r \varepsilon_0 \nabla \phi(x,y)) = -\rho(x,y)$$

where $\phi(x,y)$ is the electric potential

ε_r is the relative permittivity

ε_0 is the permittivity of vacuum, 8.854×10^{-12} F/m

$\rho(x,y)$ is the charge density

The first step in simulation is mesh generation. The solution volume is divided into a large number of elements and vertices as shown in figure 5.6.

A given potential value is assigned to the top nanoelectrodes and the bottom electrode (ITO) is set to 0 V. Once the potential $\phi(x,y)$ is generated, the electrostatic field simulator automatically computes the E field using $E(x,y) = -\nabla\phi(x,y)$ according to the following boundary conditions for any two media.

Tangential E $E_{1t}=E_{2t}$; Normal E $\varepsilon_1 E_{1n} - \varepsilon_2 E_{2n} = \rho_s$;

Where

E_{1n} is the normal component of electric field directed away from medium 1

E_{2n} is the normal component of electric field directed away from medium 2

ρ_s is the surface charge density at the interface.

The total field energy is calculated with equation

$$U = \iiint \frac{\varepsilon_r \varepsilon_0}{2} E^2 dv$$

Starting from a few hundred triangles, the number of triangles continuously increases until the field energy error between two iterations is less than 0.5% which is considered as convergence and computation is finished.

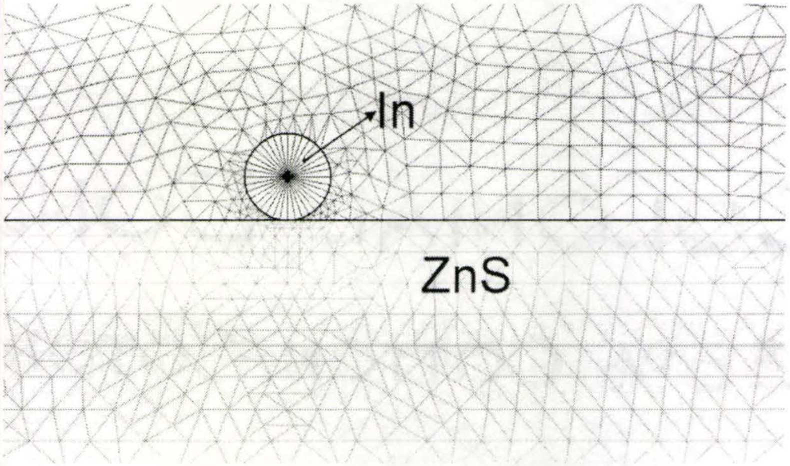

Figure 5.6 Illustration of the mesh generation in naonowire/ZnS system

5.3 Characterization Techniques

5.3.1 Scanning Electron Microscopy (SEM)

SEM (JEOL 7000F) is the main tool to characterize each component of the nanostructured EL device, such as AAO templates, ZnS powders, In/AAO composites, free indium nanowires, the ZnS/epoxy composite etc. All images were collected using the secondary electron detector, with a 15 keV acceleration voltage. Energy dispersive x-ray spectra were collected using a Si:Li detector with 20 keV acceleration voltage

5.3.2 X-Ray Diffraction (XRD)

The structure of the indium nanowires is determined by comparing observed x-ray diffraction (XRD) patterns to those in the Joint Committee on Powder Diffraction (JCPD) Database. The diffraction patterns were collected with a Nicolet diffractometer using a copper K_α radiation of 0.154 nm (Bruker D8 Advance).

5.3.3 Electroluminescent Performance

The nanowire contact EL devices were driven by a sinusoidal waveform with various frequencies ranging for 744 Hz to 9.2 kHz. The brightness was measured with a Minolta LS-100 photometer. The transferred charge was measured with a standard Sawyer-Tower circuit, using a 6.82 nF capacitor. Meanwhile, the charge-voltage (Q-V) loop was recorded by an oscilloscope with two channels (Tektronix TDS1002B). Since the leakage currents were observed across the nanostructured devices, an extrapolating method was employed to estimate the luminous efficiency of the devices.

Chapter 6. Experimental Results and Discussion

6.1 ZnS: (Cu, Al) phosphor powder

ZnS: (Cu, Al) CRT phosphor (Sylvania type 1260) is used as the emitting layer in the device. As described in Chapter 4, this phosphor has a very strong PL emission under u.v excitation of 254 nm, but no electroluminescence under a high electric field. The phosphor particles have a faceted morphology with a particle size of 3-20 μm (Figure 6.1). The particle shape is quite irregular.

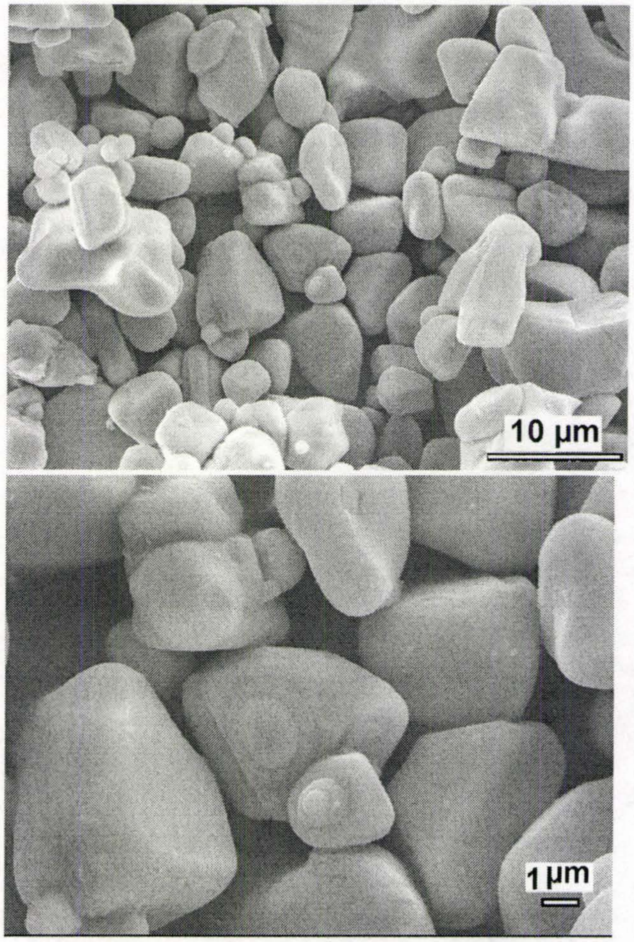

Figure 6.1 SEM observation of ZnS:(Cu, Al) CRT phosphor particles

Figure 6.2 shows the distribution of the particle size before and after the sedimentation selection measured by a particle analyzer. Before selection, most particles are in the range of 5 to 11 μm. However, after 5-times sedimentation, particles less than 5 microns have been removed and most particles are 8 to 14 microns.

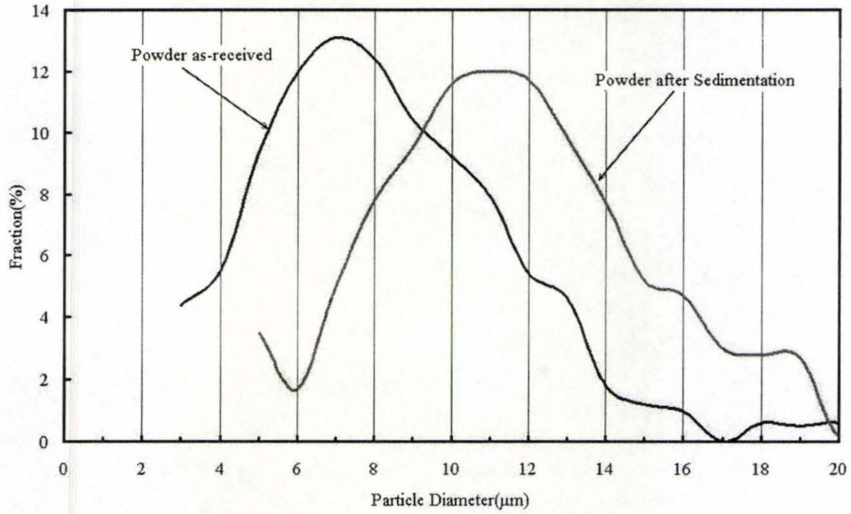

Figure 6.2 Particle size distribution (by area). The particles were measured by the Horiba CAPA-700 particle analyzer.

According to Fisher's bipolar-emission model, large phosphor particles are not preferred for powder EL in terms of the efficiency and brightness since the efficiency increases in proportion to ~ $d^{-1/2}$.where d is the particle size. In addition, the brightness of cells made of uniform small phosphor particles rises more steeply with voltage and reaches higher value than the brightness of comparable cells made with selected large particles. The reason is that long conducting lines embedded in the ZnS lattice as dislocations shield the short lines from the electric field. However, in the nanowire contact EL device, large particles can offer more effective contact areas with the nanowires than that of small particles, suggesting that more area is available to be excited by the contacted conductive nanowires to luminesce.

6.2 ZnS/Epoxy composite

Figure 6.3 shows a film of ZnS particles embedded into the epoxy by using the lamination method.

It is easy to confirm that the particles are embedded into but not covered by the epoxy. The density of particles in the epoxy can be characterized by measuring phosphor area density, namely the number of particles in a unit area. The average phosphor area density is approximately $\sim 4\times10^{10}/m^2$ determined from figure 6.3 a. High phosphor density indicates that a large effective contact area is available between the phosphor and the metal nanowires. The thickness of the film varies from 10 μm to 21 μm as shown in figure 6.3 c and d.

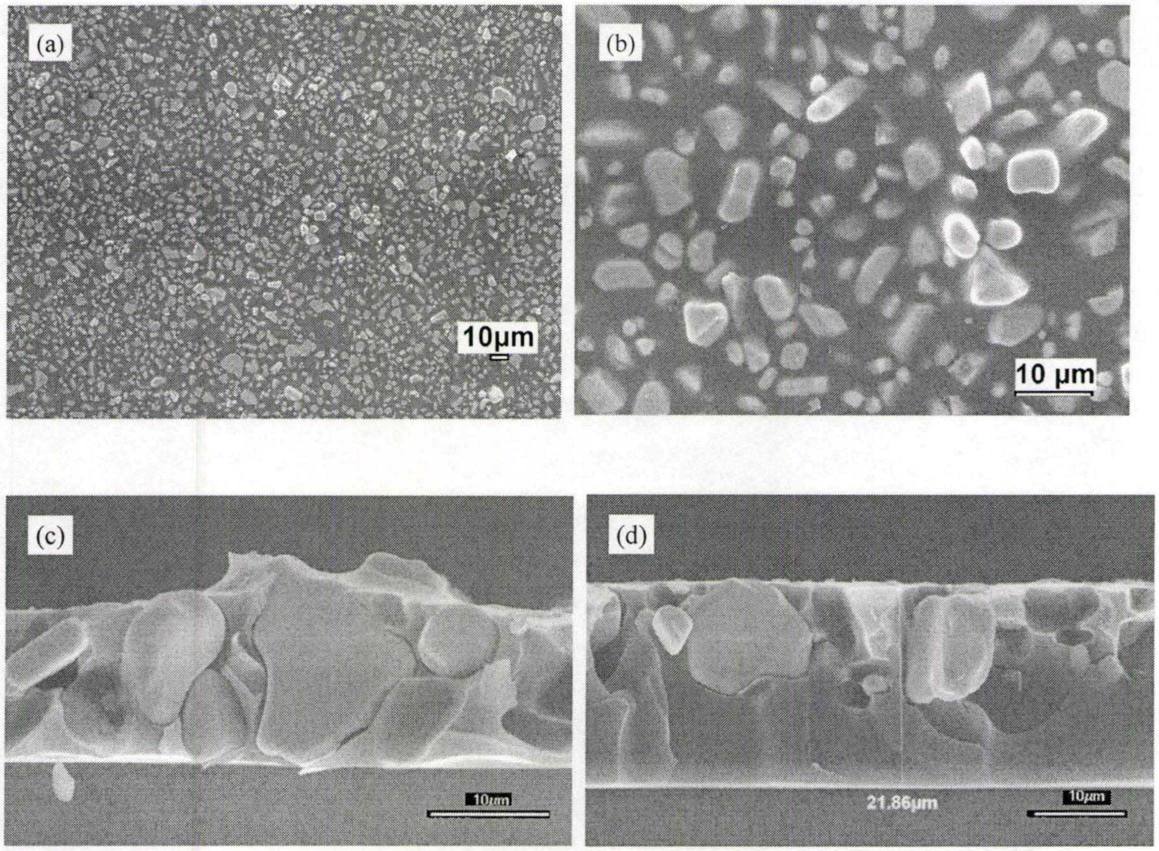

Figure 6.3 ZnS particles embedded in the epoxy film using the double-lamination method. Top-view with low magnification (a); Top-view with high magnification (b); Cross-sectional view (c) and (d).

6.3 Anodic Aluminum Oxide (AAO) Membranes Made in Our Lab

The porous alumina membranes obtained by using the two-step anodization process have a highly uniform and perfect hexagonal ordered nanopore array within domains of micron size. Figure 6.4 shows the SEM images of the surface view of the resulting anodic porous alumina membrane. The average pore diameter is 19.9 nm. The interpore distance (center to center) is measured to be 49.9 nm. Compared to the commercial product as discussed in the following section, the AAO membranes made in our lab have a smaller pore size with a better regularity. However, in the present work these membranes are not used for templated synthesis of the nanowires due to the complicated post-processes. For example, after anodization, the remaining aluminum substrate is removed using $HgCl_2$ solution and the pore bottoms are opened by chemical etching in acid, such as dilute phosphoric acid. Compared to direct use of commercial product all these processes are quite difficult to handle and were not pursed in this thesis. However, the AAO membranes made in our lab could be used to fabricate nanowires in the future.

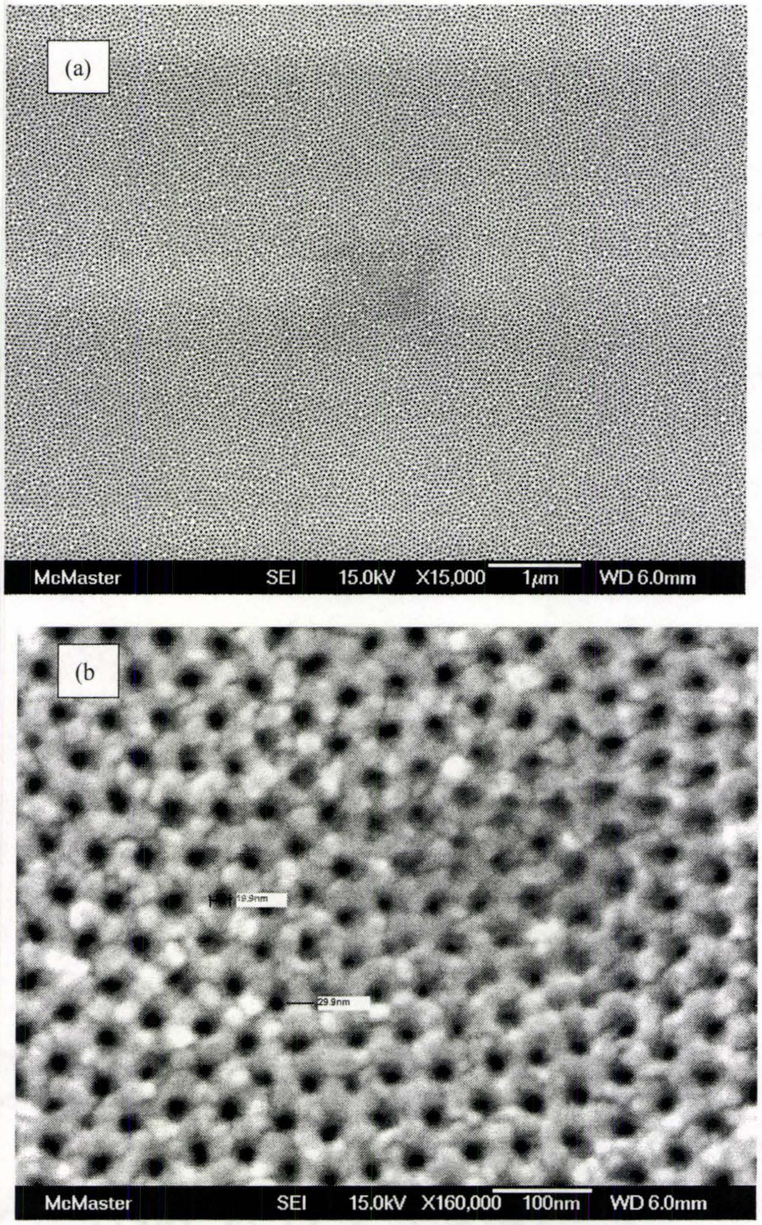

Figure 6.4. SEM images of the surface view of the AAO membrane obtained by two-step anodization process. (a) Magnification: 15,000×.(b) Magnification: 160,000×.

6.4 Template synthesis of indium nanowires using AAO template

6.4.1 Characterization of the AAO membrane template

In this thesis, Whatman Anodisc membranes 13 mm in diameter and 0.1 μm pore size without a polypropylene support ring are used as templates. These membranes have two well defined faces: a branched side formed by interconnected channels with a nominal diameter of 100 nm (corresponding to the pore size claimed by the manufacturer) and a thickness of approximately 1.6 μm, and the other face (denoted as the front side in this thesis) formed by unconnected cylindrical pores of ~ 200 nm mean diameter, with pore density of 1×10^9 pores/cm^2 and an ordered pattern. The membrane thickness is about 58 μm. Figure 6.5 shows the SEM images of the AAO membranes. The AAO membranes are amorphous as confirmed by x-ray diffraction. In the experiment, the AAO branched side and front side are designated as the top surface and the bottom surface for the injection process respectively.

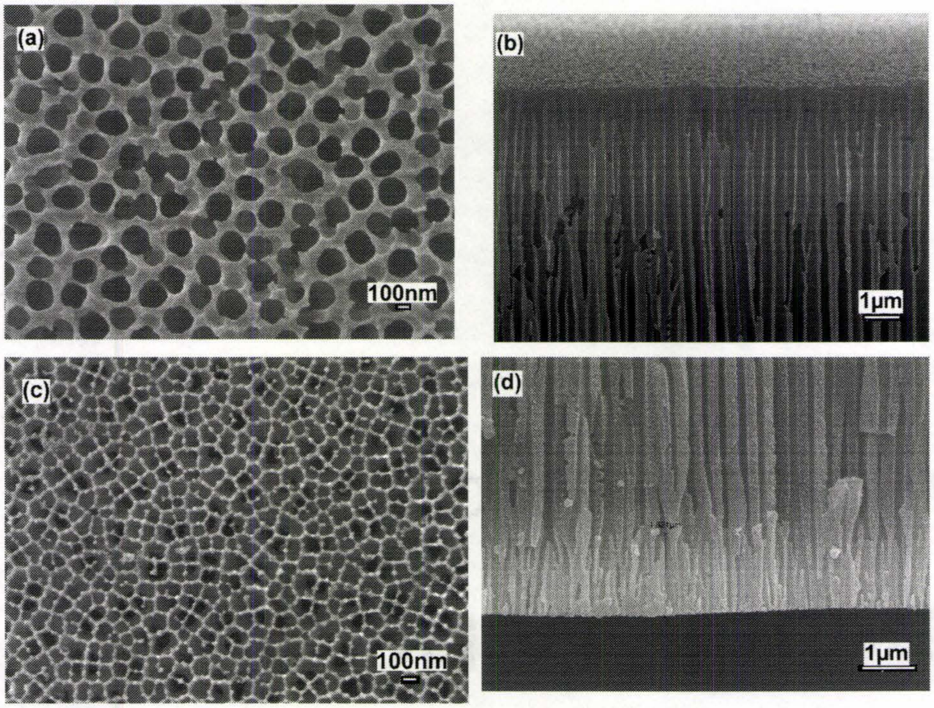

Figure 6.5. SEM images of the AAO template. Top view of the AAO front side (a), cross-sectional view of the AAO front side (b), top view of the AAO branch side (c), cross-sectional view of the AAO branched side (d).

6.4.2 SEM study of the In nanowires embedded in the AAO template

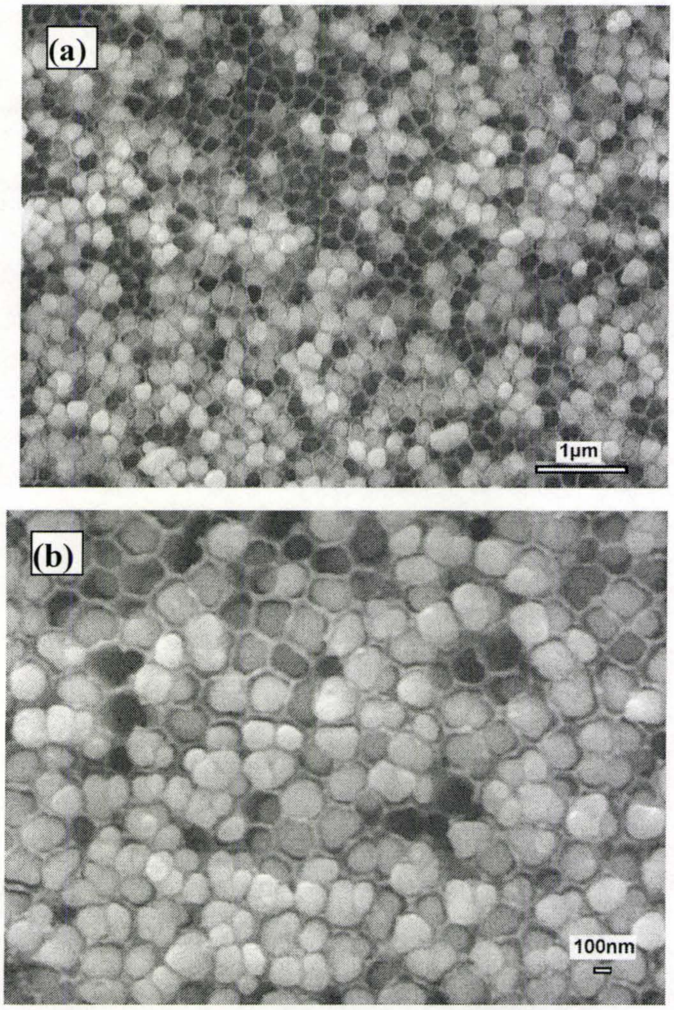

Figure 6.6. SEM micrographs of the top surface of the In-embedded AAO. (a) Magnification: 16,000×.(b) Magnification: 33,000×. The white regions are In-filled AAO channels, while the black regions are empty AAO channels.

Figure 6.6 shows SEM graphs of the top surface of the In-embedded AAO. It can be observed in the figure that the metal indium is impregnated into the AAO channels. The diameter of the nanowires is ~ 200 nm, as defined by the mean diameter of the AAO template (~ 200 nm).

The filling ratio is estimated as 62%. The proposed reasons that the filling ratio is less than 100% even though the pressure is almost 5 times larger than the analytical expression from the Washburn equation are the friction between the In nanowires and the AAO channels, the residual air trapped in the channels, and the uneven applied force.

The uneven force, which is believed to be the dominant factor, comes from two sources: one is the hydraulic jack, and another one is the non-uniformity of the contact between the AAO surface and the column surface. This can be confirmed by the optical microscope observation and by measuring the surface conductivity of the sample bottom surface. Parts of the sample bottom surface are very shiny, covered with excess bulk indium and have a very good surface conductivity, while other parts are not shiny and nonconductive.

Figure 6.7 and Figure 6.8 show SEM images of the In-embedded AAO sample before and after post-processing respectively.

It can be observed in Figure 6.7 that the indium nanowires come out from the AAO membrane bottom surface, spread out, tend to form continuous structures and cover the whole AAO bottom surface. This indicates that the In nanowires run through the entire thickness of the AAO template with the length of 59.6 μm. After polishing and etching in NaOH solution, the In nanowires individually stand up normal to the surface and the diameter of the wires is approximately 300 nm, larger than the mean diameter of the AAO template (~ 200 nm) as shown in Figure 6.8.

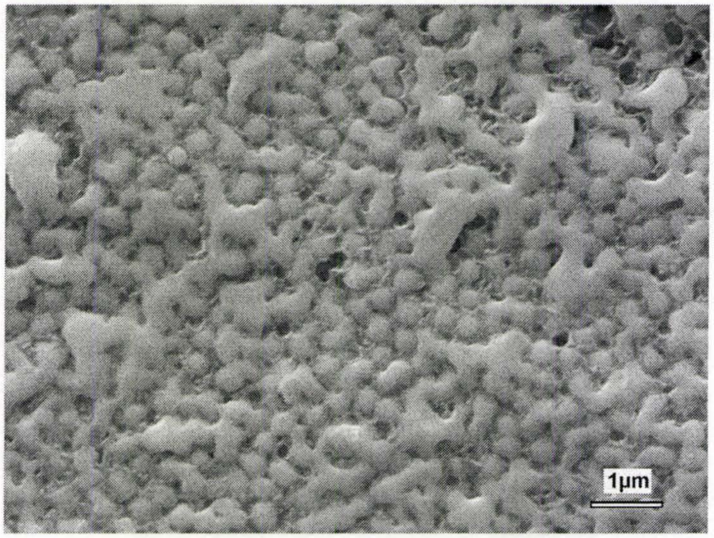

Figure 6.7. SEM image of the bottom surface of the In-embedded AAO before post-processing.

Figure 6.9 shows the SEM cross-sectional views of an In-embedded AAO sample. The structure of the nanowires is not continuous due to the SEM sample preparation. The interface between the In nanowires and the AAO template is incoherent because there is no interaction between the two phases: the AAO template is essentially stable at temperatures lower than 800℃ (Mardilovich et al., 1995). This indicates that there is no strong bonding between the In nanowires and the AAO template. Considering the softness and the low mechanical strength of the In metal, the In nanowires embedded in the AAO channels were definitely broken and damaged when the sample

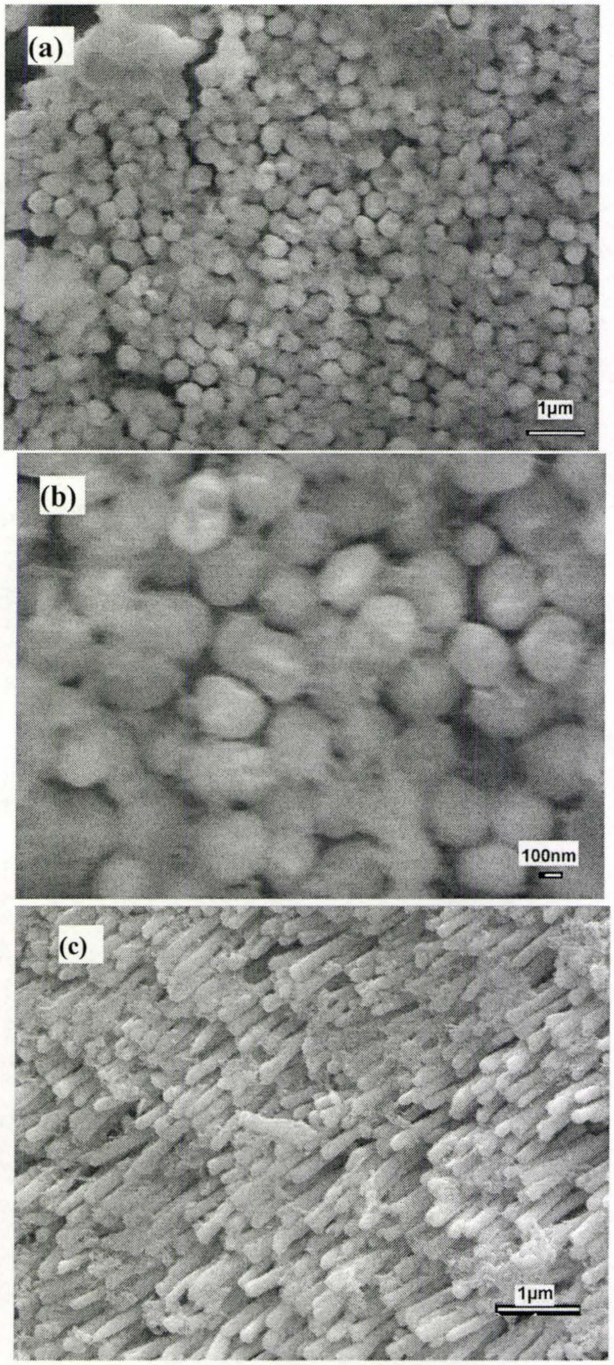

Figure 6.8. SEM images of the bottom surface of the In-embedded AAO after post-processing. (a) Magnification: 14,000×, (b)Magnification: 40,000×,(c) some In nanowires are released from the AAO template. The surface was mechanically polished to remove the excess bulk indium and etched by 0.3wt% NaOH solution at room temperature for 1 hour.

was broken for SEM observation. The In nanowires are brighter than the AAO matrix in the SEM.

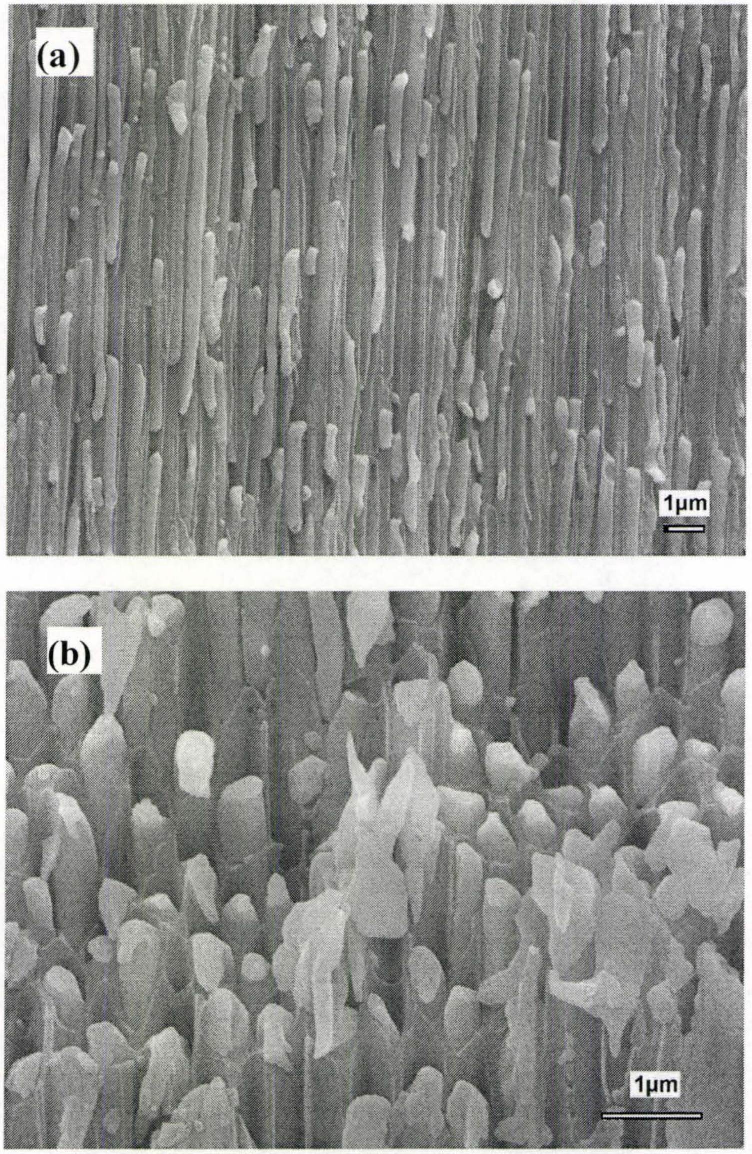

Figure 6.9. SEM images of cross-sectional views of In-embedded AAO. The cross section of the sample is normal to the surface (a) and the cross section of the sample is tilted to the surface (b). Indium nanowires are brighter than the AAO matrix.

After the AAO template is completely dissolved in NaOH solution, the nanowires are transferred onto a new AAO membrane surface as shown in Figure 6.10. A randomly selected single nanowire is measured with a diameter of 331nm and length of 2.9 μm. The reason that the average lengths of the nanowires is shorter than the thickness of the AAO template is that the nanowires have been broken to form shorter nanowires during dissolving the AAO template in NaOH solution with the help of ultrasonication. It is worth noting that no branched-structured nanowires are observed under SEM although the AAO templates have the branched structure as shown in Figure 6.5.

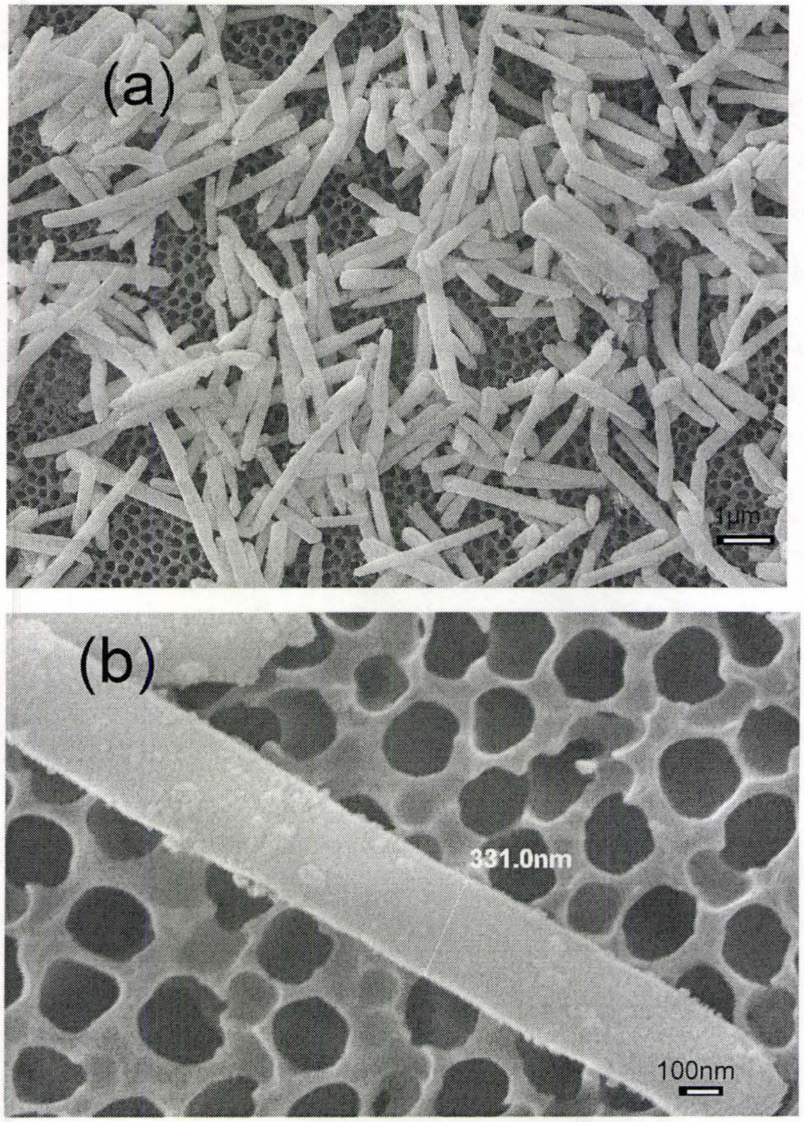

Figure 6.10. SEM pictures of indium nanowires deposited on a new PA membrane after the PA template is completely dissolved (a) and a randomly selected single nanowire on PA membrane (b)

6.4.3 X-ray diffraction of In nanowires embedded in the AAO template

Figure 6.11 shows the X-ray diffraction (XRD) patterns of the In nanowires. One X-ray experiment is performed on the bottom surface of the In/AAO sample (Figure 6.11 a), and another experiment is performed on the indium nanowires randomly deposited on a Si substrate after the AAO is completely dissolved by hydroxide solution (Figure 6.11 b). The crystal structure of the nanowires can be confirmed as body-centred-tetragonal (BCT) structure with the lattice constant $a = b = 3.25\dot{A}$; $c = 4.95\dot{A}$; $c/a = 1.52$ with reference to the JCPDS standard diffraction pattern (Figure6.11 c).

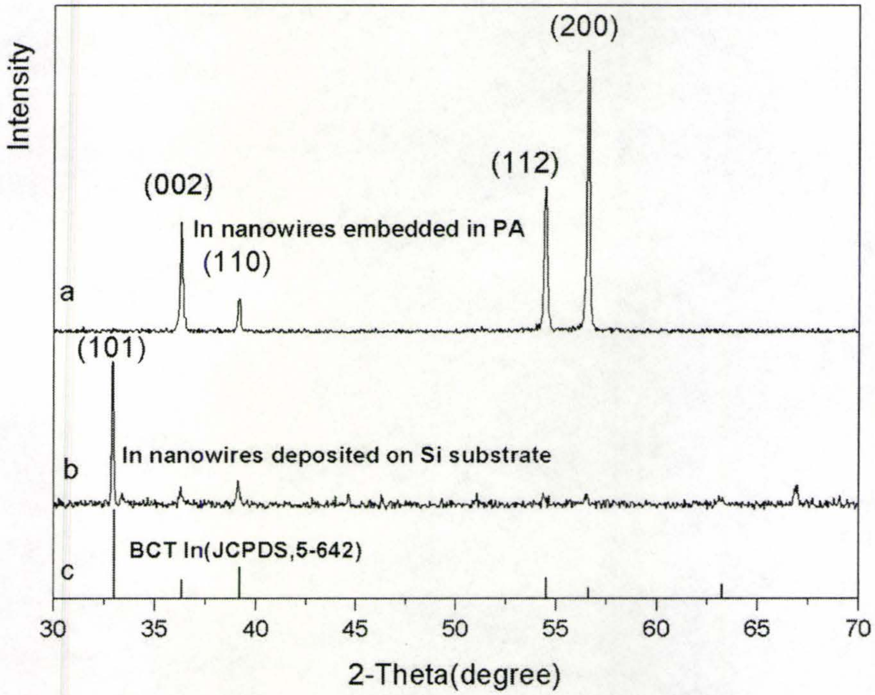

Figure 6.11. XRD patterns of the In nanowires (a) Indium nanowires embedded in PA template. (b) Indium nanowires randomly deposited on the Si substrate after the complete dissolution of the PA template by NaOH solution.

It should be noticed that there is a considerable difference between the characteristics of the indium wires embedded in the AAO template and those deposited on the Si substrate. In Figure 6.11 a, the intensity of the (200) peak is much higher than that of others and the (101) peak almost can not be detected, which indicates that the In nanowires have a preferred orientation. In Figure 6.11 b, however, the pattern matches with the standard diffraction pattern (Figure 6.11 c) except that the (101) peak is stronger relative to other peaks than the standard pattern. This may be explained since the nanowires are lying down on the silicon substrate in a manner similar to that as shown in Figure 6.10 a (although in that case the substrate is an AAO membrane). Therefore, we conclude that a preferred alignment with [100] direction parallel to the nanowire axis exists.

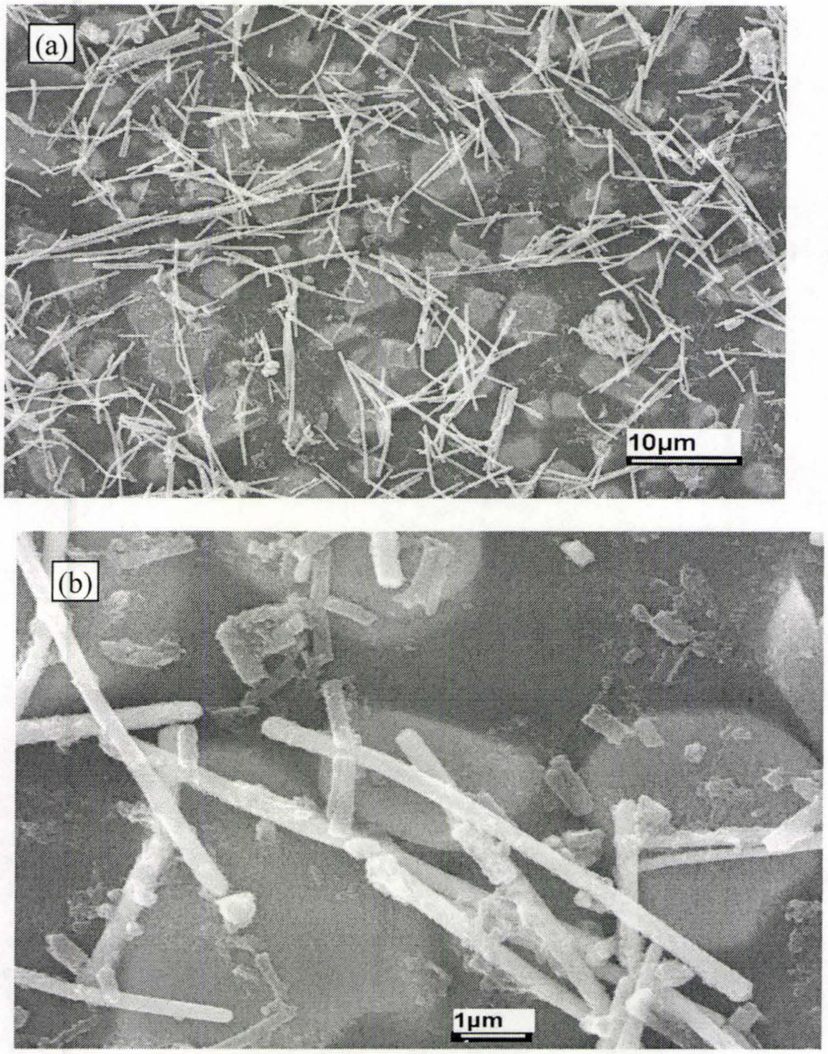

Figure 6.12 Indium nanowires lying on ZnS particles embedded in the epoxy film (a); and (b) Nanowire bundles

An explanation for the preferred nanowire crystallographic orientation is currently lacking; however, the process steps are as follows:

1. Indium melting
2. Liquid penetration into nano-pores
3. Solidification

It can be conjectured that during the solidification process, the heterogeneous nucleation process of indium crystalline material is initiated at the indium-alumina interface, however we do not have an understanding of the details of the nucleation and growth of the nanowires. For the formation of tin nanowires, TEM results suggest that the predominant growth direction of the Sn nanowires is along the [100] direction (Chen, et al., 2006).

6.5 Deposition of indium nanowires on the embedded ZnS substrate

Figure 6.12 shows the indium nanowires deposited on the embedded ZnS substrate using a wet-coating method. The indium nanowires directly contact the ZnS particles. Nanowires bundles are observed because of the electrostatic force between nanowires. It can be expected that better separation of the nanowires will benefit the concentration of the electric field intensity, and hence improve the performance of the EL devices.

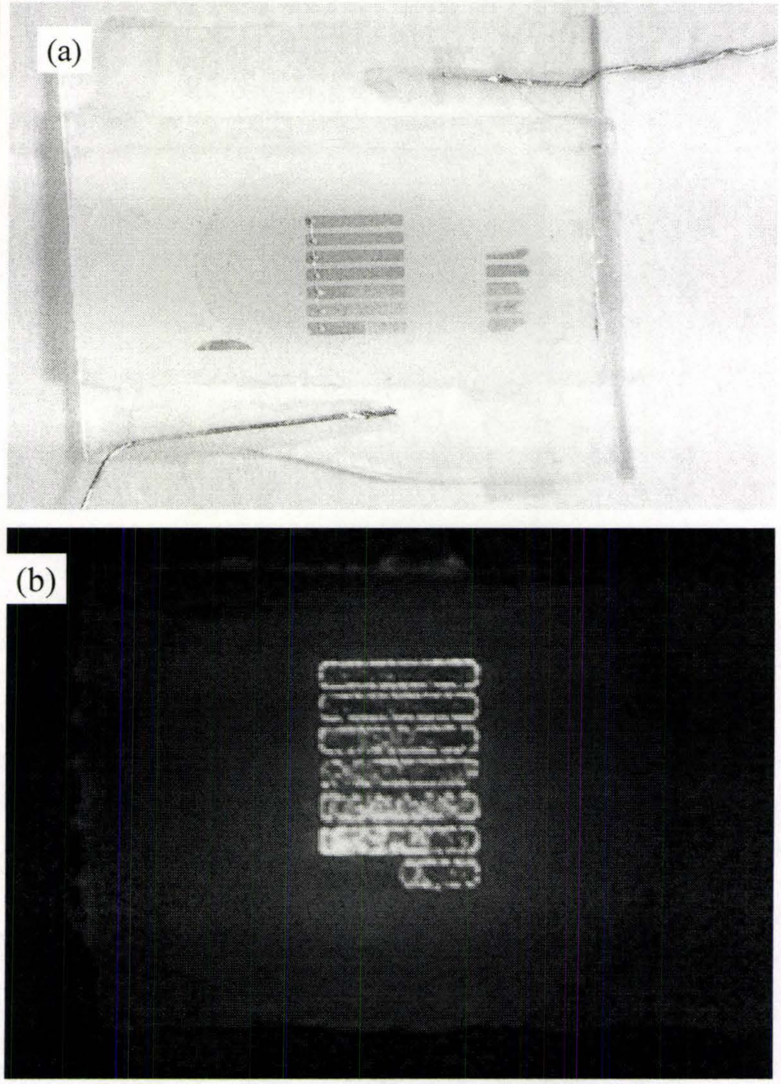

Figure 6.13 Nanowire contact powder EL device. Without applied voltage (a) and with applied voltage (b). Device is viewed through the glass substrate in (b).

6.6 Growth of Au rear electrodes on the device

Electron beam deposition was used to grow the rear strip electrodes. Figure 6.13 shows the resultant self-supported nanowire contact powder EL device. When an AC voltage is applied across the ITO and the gold strip electrodes, light is generated from the device as shown in Figure 6.13 (b).

6.7 Profiles of the nanowires after deposition of Au

After deposition of Au, the metallurgical reactions at phosphor/electrodes interfaces are not discussed in this thesis due to the lack of heat treatment. However, the nanowires have three profiles as shown in figure 6.14: (1) nanowires fully covered by Au; (2) nanowires partially covered by Au at the edges of the Au electrodes, which are electrically connected by Au, resulting the light generation from the edges of the Au electrodes (figure 6.13 b); (3) nanowires lying on the regions among the Au electrodes, which are not electrically connected each other. Therefore, they are not responsible for the light generation. It should be noticed that light could be generated from the inner of Au, which can be related to the nanowires fully covered by Au (figure 6.15). The electric field strongly depends on the profiles of the nanowires. Simulations of the electric field due to the nanowires with different profiles are performed in the section 6.8.2.

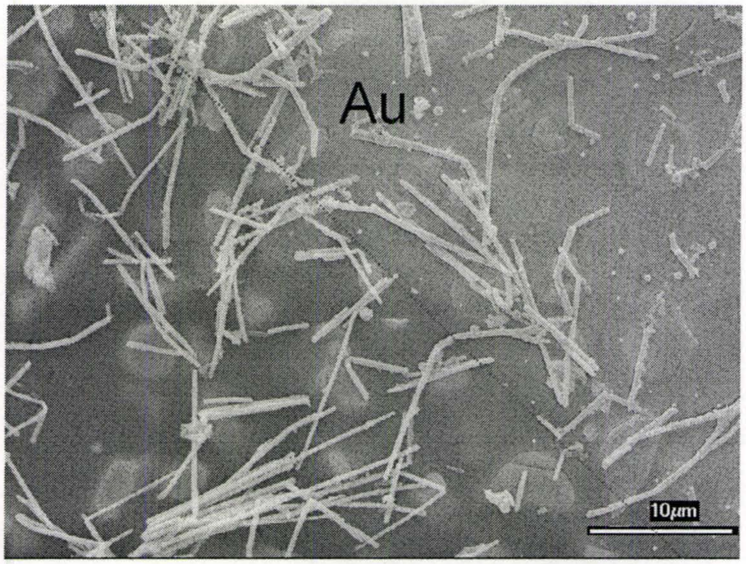

Figure 6.14 Indium nanowires lying on the embedded ZnS substrate after deposition of Au rectangular electrode. The bright region are covered by Au.

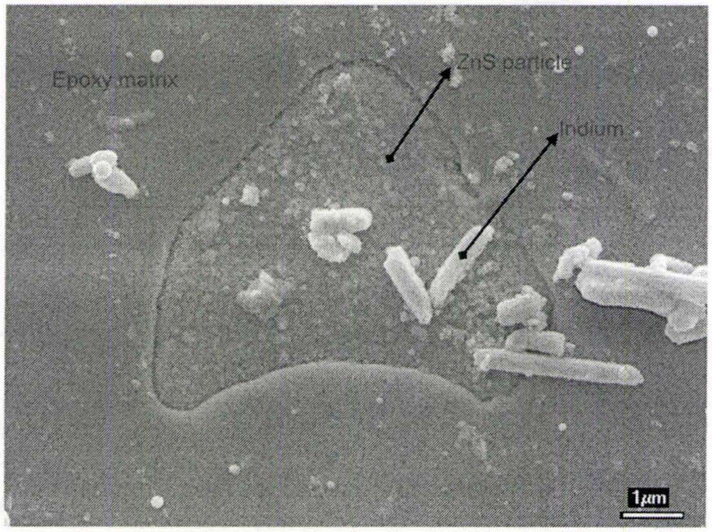

Figure 6.15 Indium nanowires fully covered by Au

6.8. Discussion

6.8.1 Mechanism of the light generation from the nanowire contact powder EL device

The explanation of light generation from the nanowire contact EL can be borrowed from the bipolar field-emission model.

If the metal nanowire is considered as a long isolated charged cylinder surrounded by vacuum in an electrostatic field, the intensity of the electric field on the surface of the nanowire can be expressed by equation (6-1) (Rogers, 1954, p181)

$$E = \frac{\lambda}{\pi \varepsilon_0 d} \quad (6\text{-}1)$$

Where λ - Linear charge density along the nanowire

ε_0 -Permittivity of vacuum

d– Diameter of the nanowire

It becomes clear in equation (6-1) that thinner nanowires can induce a higher field under the same linear charge density. But the exact field intensity is more complicated after the introduction of the ZnS phosphor. The distribution of the field in the ZnS, therefore, is not modelled in detail. However, if a voltage is applied to a metal nanowire placed on a ZnS particle, it can be firmly predicted that a higher electric field (at least ten times higher (Maeda, 1990)) will be formed in the phosphor region in contact with the indium nanowires compared to other regions as shown in Figure 6.16. (Note that this geometry occurs just outside the perimeter of the gold strip electrodes since the indium nanowires extend beyond the gold elelctrodes, but are electrically contacted by the gold electrodes.)

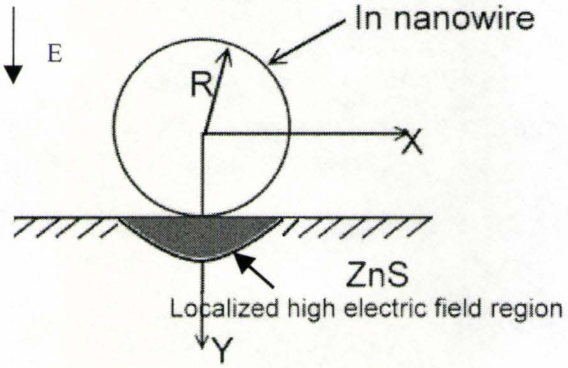

Figure 6.16 Illustration of the localized high electric field region in the ZnS phosphor due to the metal nanowire.

The localized electric field is strong enough (up to 10^8 V/m) to induce electron injection and avalanching in the ZnS phosphor lattice. The injected electrons are finally trapped at the donors (Al). When the polarity is reversed, the electrons recombine with the holes which are injected by the same process and are previously trapped at the acceptors (Cu). Therefore, EL emission is realized by the radiative recombination of electron-hole pairs through donor-acceptor pairs.

The role of conductive nanowires in the EL device can be confirmed by another EL structure, substrate/ITO/phosphor/Au, as shown in figure 6.17, in which the gold electrodes are directly deposited onto the ZnS phosphor particles and there is no nanowires exist (figure 6.17 b). Under the same driving conditions as the nanowire contact EL device, no luminescence is observed from the device.

6.8.2 Simulation of electric field in the ZnS phosphor

In order to quantitatively characterize the electric field in the phosphor, electric simulations were performed with electromagnetic field simulation software (Maxwell SV from An Soft Inc.). Here we assume: (1) no breakdown in the phosphor; (2) the single metal nanowire is infinitely long in the Z direction. An average nanowire diameter d of 330 nm is used in the simulation and the applied voltage V is set to 100 V between the electrodes.

As mentioned in Section 2.1, two geometries of indium nanowires are focus of interest after the deposition of Au rectangular electrodes (figure 6.18): (a) the nanowires from the inner area of the Au electrodes are separated from each other and connected by Au; (b) the nanowires extend beyond the perimeter of the Au electrodes, but are electrically contacted by Au electrodes. Corresponding these two geometries, two kinds of electric fields are simulated.

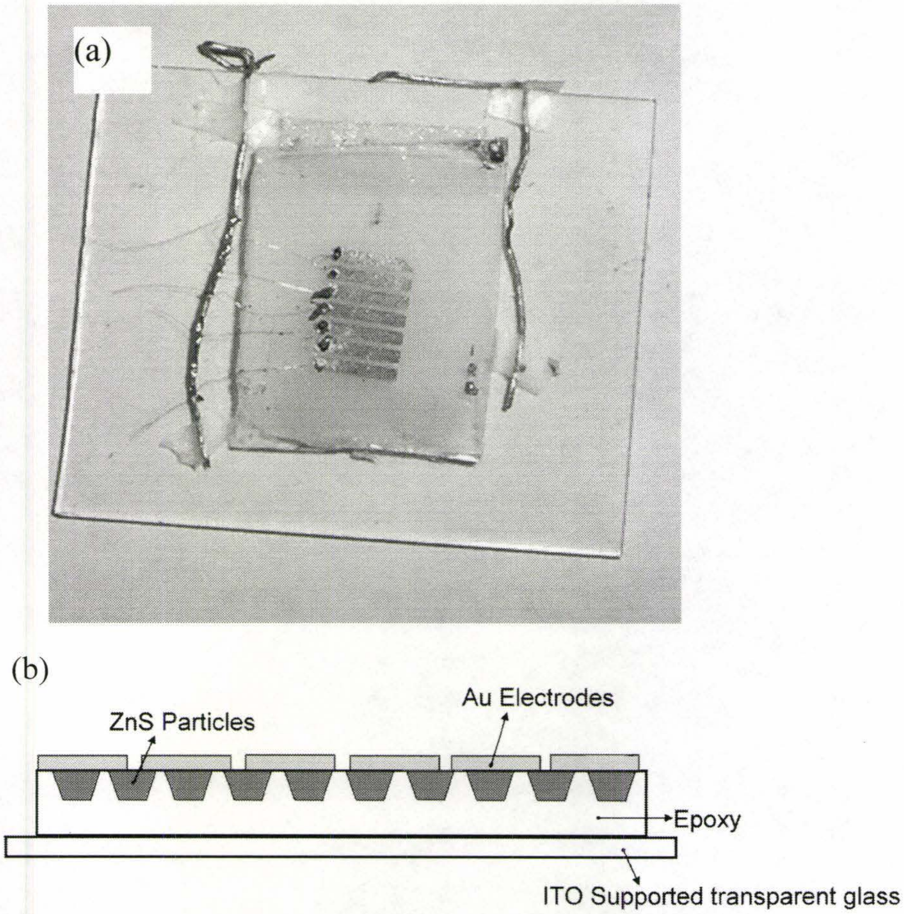

Figure 6.17. Powder EL device without indium nanowires. (a) Top view; (b) Illustration of the device structure. In this structure, the exposed surfaces of the phosphor particles are directly covered by the vacuum-deposited Au rectangular electrodes. As expected, no light is produced from the device under the usual driving conditions.

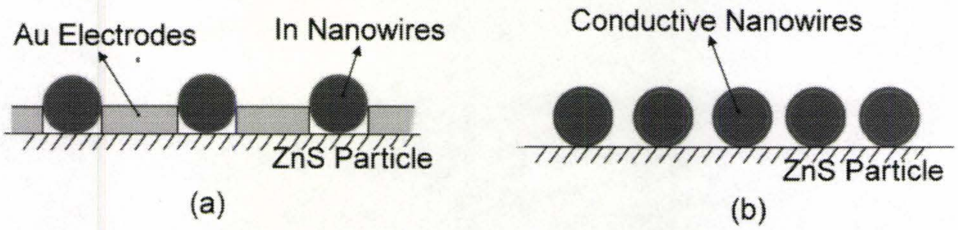

Figure 6.18 Indium nanowires on ZnS particle. (a) indium nanowires connected by Au; (b) Indium nanowires separate from each other

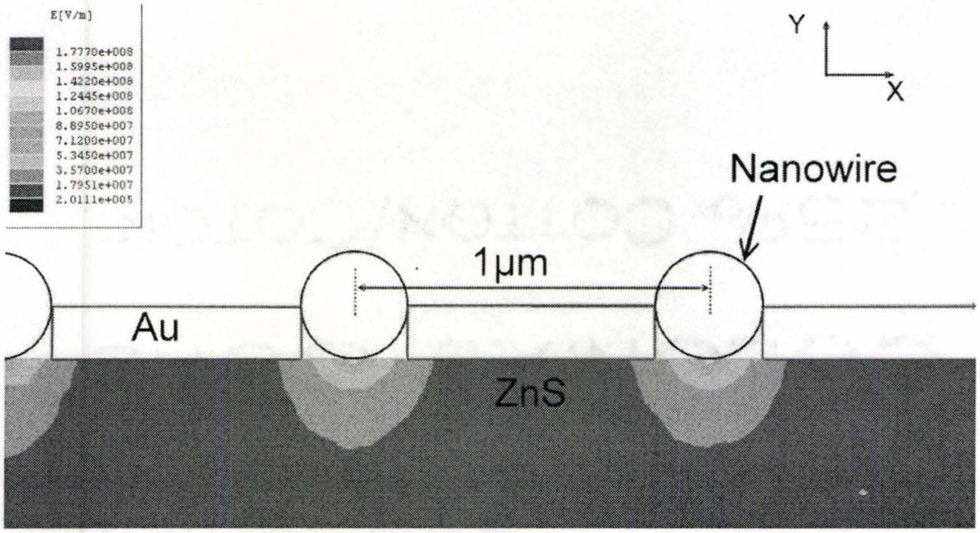

Figure 6.19 the distribution of the field in the ZnS phosphor due to the indium nanowires connected by Au

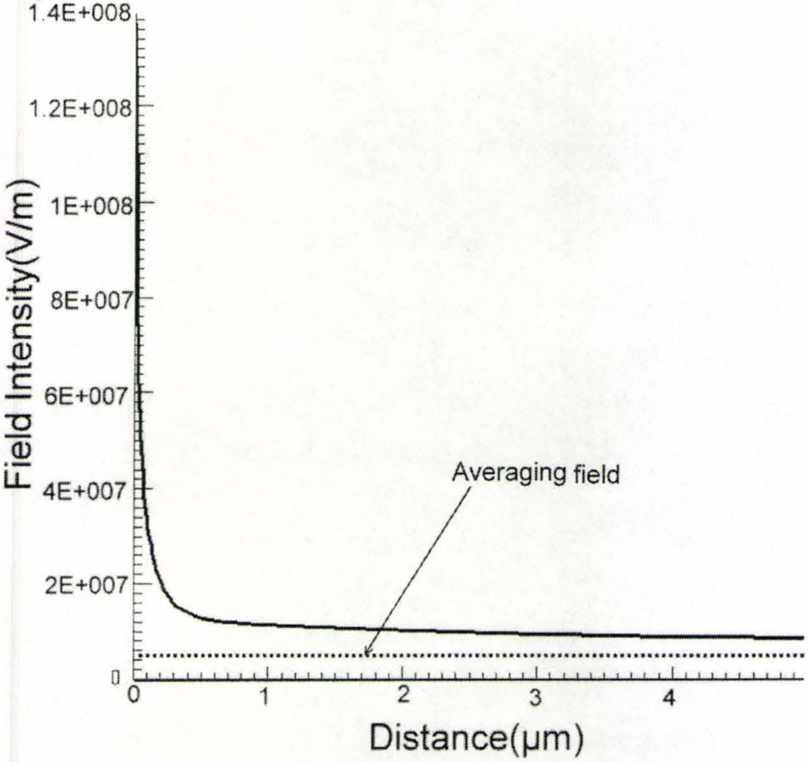

Figure 6.20 the distribution of the field in the ZnS phosphor with depth

(1) Simulation of the electric field caused by the nanowires from the inner area of Au

Figure 6.19 shows the distribution of the electric field in ZnS phosphor corresponding to the geometry shown in figure 6.18 a.

The dependence of the electric field on depth is shown in figure 6.20. In this case, the origin is the contact between the nanowire and the phosphor. The intensity of the electric field is on the order of 10^8 V/m, and then relaxes abruptly with depth. The averaging electric field, as shown by a dot line in figure 6.20, is calculated to be $\sim 5\times10^6$ V/m by assuming the device is with planar rear electrode and the thickness of the emissive layer is 20 μm . The electric field is gradually approaching to averaging field after 300 nm in depth.

(2) Simulation of the electric field caused by the nanowires from the edges of Au electrodes.

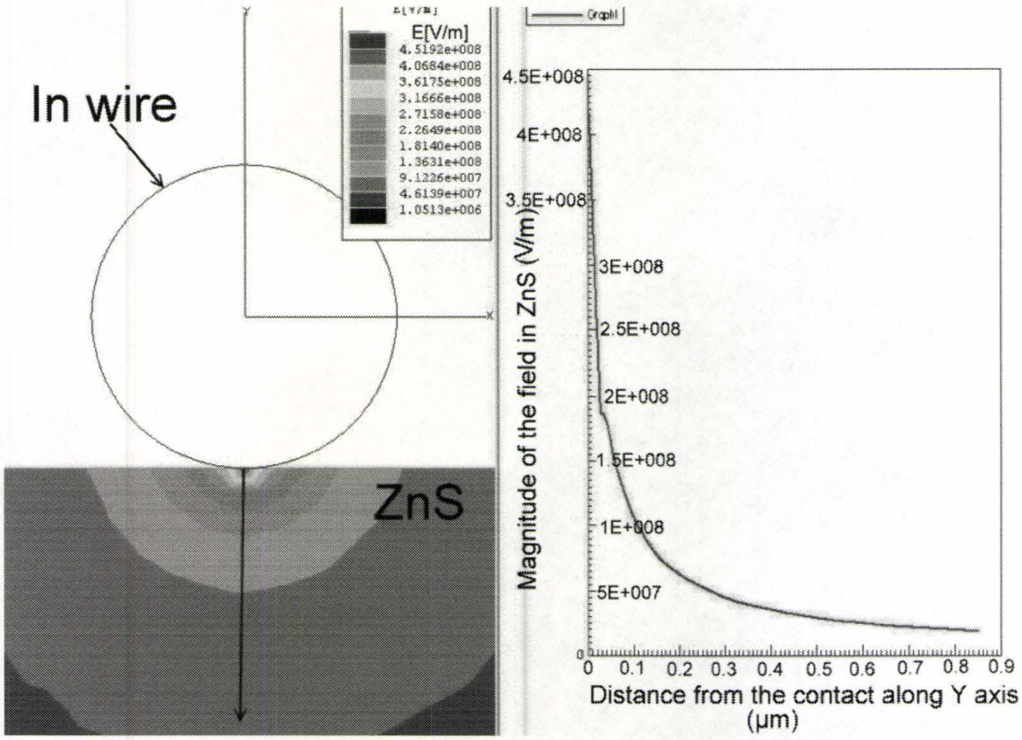

Figure 6.21 the distribution of the field in the ZnS phosphor due to a single contacted indium nanowire.

Similar results have obtained as shown in Figure 6.21 compared with the former case. However, the maximum electric field is higher under the same applied voltage. Furthermore, the depth for the averaging field is much more larger (~1 μm) compared with the former depth of ~ 300 nm.

Both simulations indicate that the indium nanowires can induce a field which is much higher than the applied external field. Hence, low average fields that are easy to produce can generate luminescence.

6.8.3 Effect of Diameter of the Nanowire on the Electric Field

According to equation (6-1), the electric field is proportional to *1/d*, where d is the diameter of the indium nanowires. Therefore, smaller nanowires can induce a higher localized field in the phosphor region under the same conditions compared to the large nanowires. Figure 6.22 shows the dependence of electric field on the diameter when the applied voltage is 100 V, calculated by the Maxwell software. Here the nanowires extend beyond the perimeter of the Au electrodes, but are electrically contacted by Au electrodes. So decreasing the dimension of the nanowires is an effective way to lower the operating voltage and increase the brightness of the device.

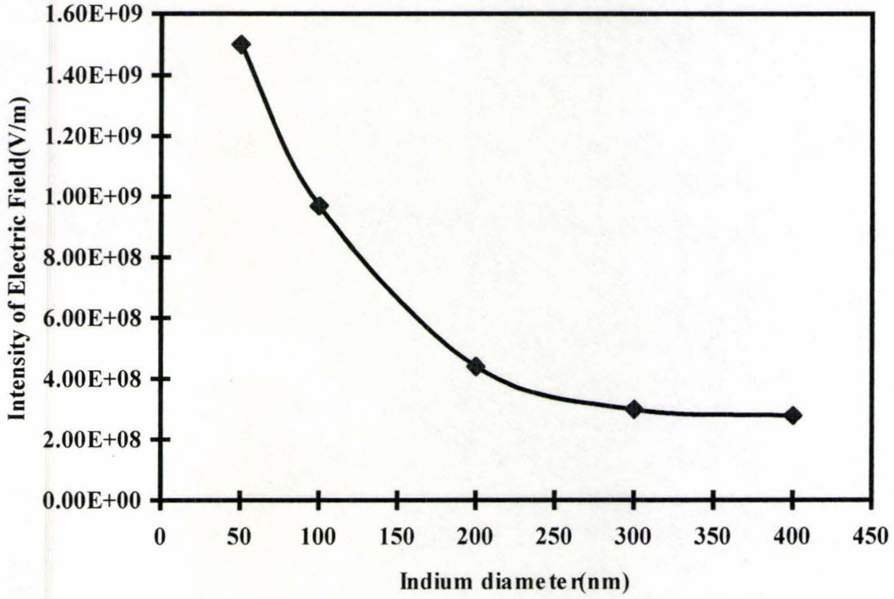

Figure 6.22 Dependence of electric field on nanowire diameters (the applied voltage is 100V and no breakdown in phosphor is assumed)

6.9 NCPEL Device Performance

6.9.1 Luminance-Voltage relationship for the nanowire contact EL device

The tests of the dependence of luminance on voltage with various frequencies for a nanowire contact EL device sample are performed as shown in Figure 6.23. In this case, the luminance from the edges of the Au electrodes is measured. The effective emission area is estimated from the product of the indium nanowire average length (~10 μm) and the total perimeter of the gold electrodes.

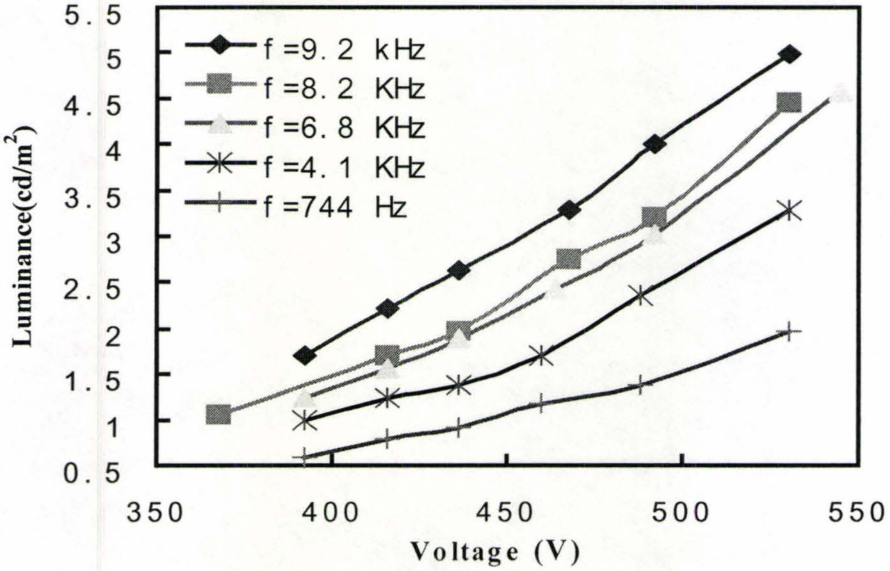

Figure 6.23. Luminance-voltage characteristic of a nanowire contact EL device at various frequencies driven by the sinusoidal waveform. The luminance from the edges of the Au electrodes is measured.

6.9.2 Rear Electrodes and Luminance

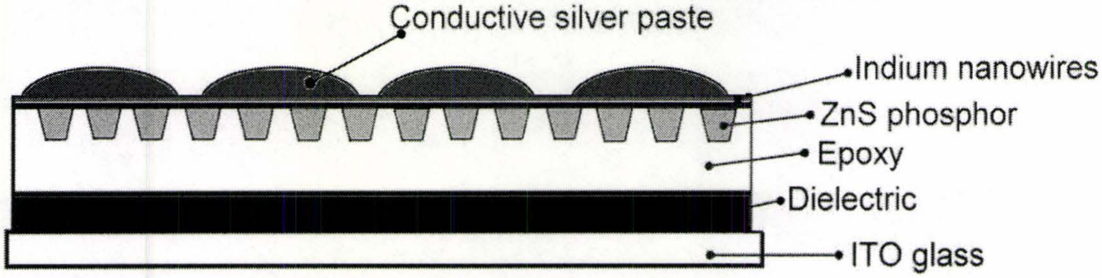

Figure 6.24 Nanowire contact EL device with conductive silver paste.

It should be noticed that the choices of rear electrodes which electrically connect with the indium nanowires have an important effect on the luminance of the device. In an alternative device structure, conductive silver paste (Epo-TEK H20S), which is a two component, solids silver-filled epoxy system, is used as the rear electrodes to replace the Au rectangular electrodes. In this case, isolated silver paste drops (~200 μm in diameter) spaced several microns away from each other are directly put onto the

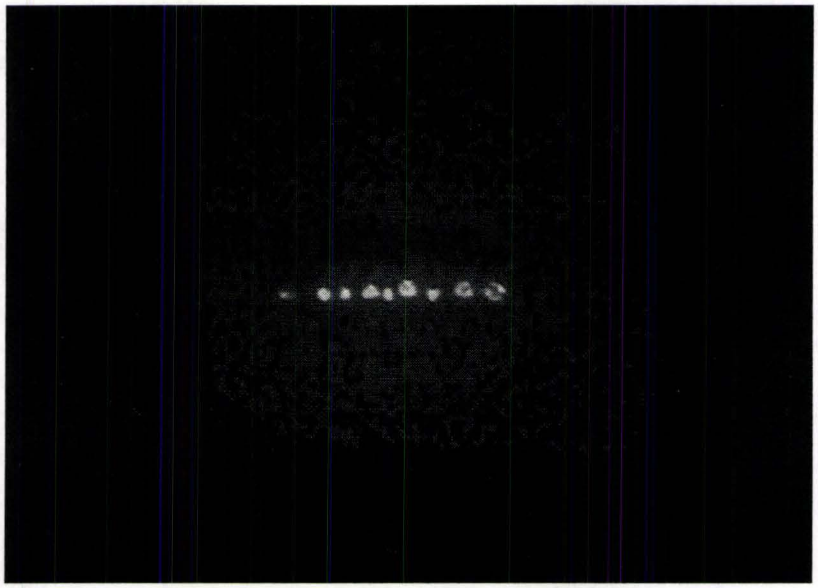

Figure 6.25 Nanowire contact powder EL device using a conductive silver paste as rear electrodes. The applied voltage is 450V with frequency of 8.2 kHz driven by a sinusoidal waveform.

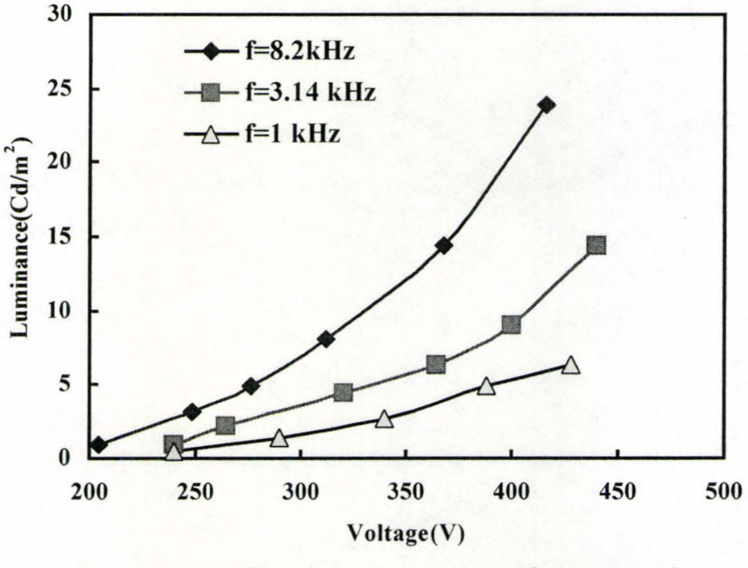

Figure 6.26 Dependence of luminance on voltage for a nanowire contact powder EL device using a conductive silver paste as rear electrodes

indium nanowires as shown in figure 6.24. The drops are finally connected together by a thin gold wire which is connected with the external drive voltage. The silver paste is cured at 100 ℃for 2 hours. In order to improve the reliability of the device, a $BaTiO_3$-filled dielectric (Luxprint®8153) layer is inserted between the phosphor layer and the ITO electrode. When the voltages are above the threshold voltage, light can be generated from the vicinity of the silver paste drops as shown in figure 6.25. Figure 6.26 shows the dependence of luminance on voltage with various frequencies for a silver-paste-contacted sample driven with a sinusoidal voltage waveform.

It appears that the conductive silver paste electrically connects the indium nanowires together and offers a better contact between the nanowires and the ZnS phosphor particles. As a result, the silver-paste device has a higher luminance, lower operating voltage compared to the device using Au as rear electrodes. This conclusion can be confirmed by the figure 6.27. An indium nanowire rests on a ZnS particle and is electrically connected with conductive silver paste. When a voltage is applied, localized high electric field can be formed around the nanowire, which excites the phosphor to luminesce. The peak luminance can be up to 25 cd/m^2, 5 times higher than the device using Au as electrodes. Therefore, the rear electrodes play a very important role in the nanostructured device as they can change the performance of the indium nanowires lying on the ZnS particles and then change the light output from the device.

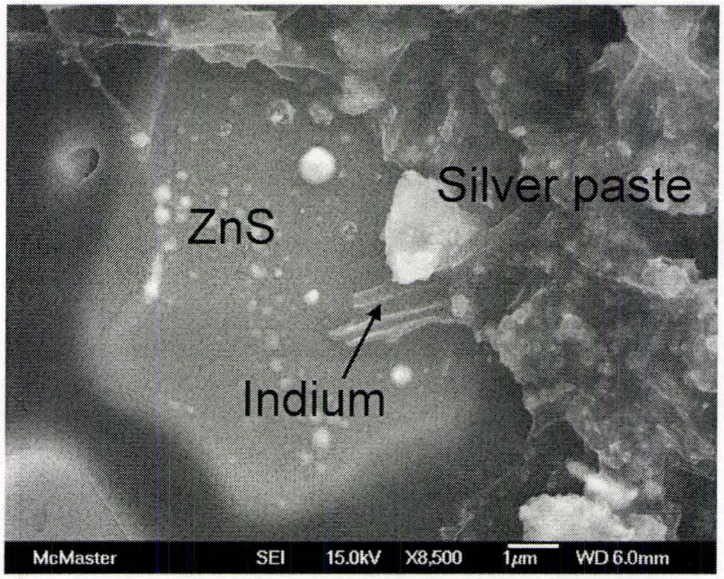

Figure 6.27. An indium nanowire rests on a ZnS particle and is electrically connected with conductive silver paste

6.9.3 Luminous Efficiency of the Nanowire Contact EL Device

Once the input power density P_{in} [W/m^2] and luminance L [cd/m^2] are obtained, the luminous efficiency η [lm/W] can be estimated from the following equation under the assumption of a perfectly diffuse EL emission surface:

$$\eta[lm/W] = \pi \times \frac{L[cd/m^2]}{P_{in}[W/m^2]} \quad (6\text{-}2)$$

A convenient method to determine the input power density P_{in} is to use the Sawyer-Tower circuit method to plot the charge-voltage curve (figure 6.28). The charge is derived from a small voltage across a sense capacitor C_s inserted in series with the EL device such that the voltage drop across the sense capacitor V_s is always much smaller (about 100 times smaller) than the voltage drop across the EL device.

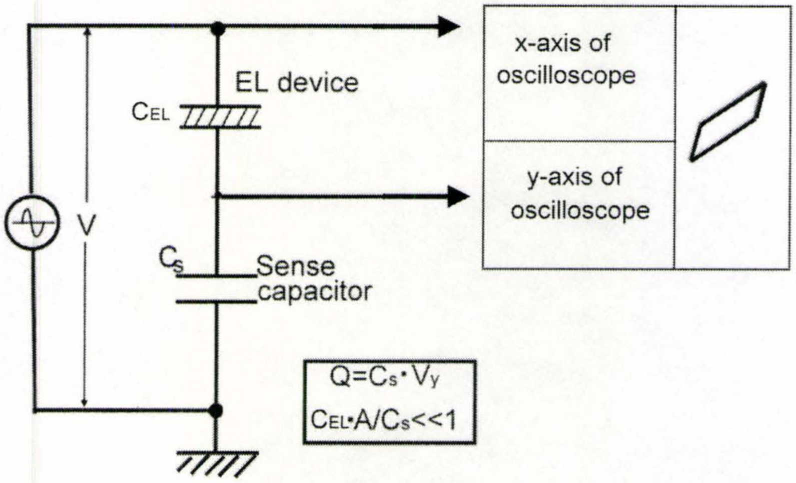

Figure 6.28. Charge density vs. voltage (Q-V) characteristic measuring circuit based on Sawyer-Tower circuit. The sense capacitor is chosen to be approximately 100 times larger than the EL device capacitance

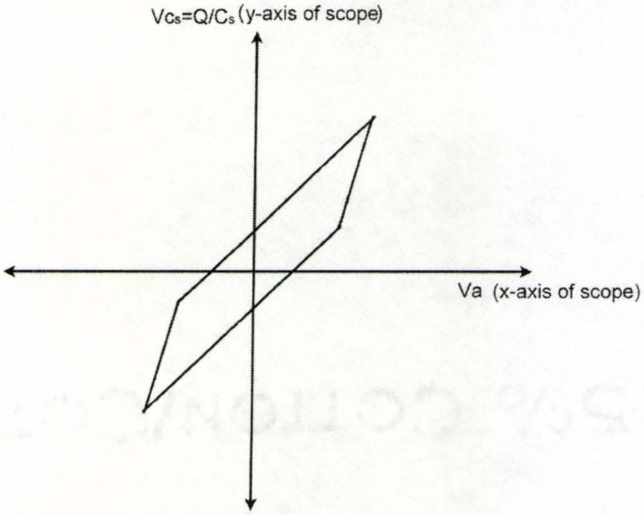

Figure 6.29 Charge vs. applied voltage relationship for an EL device. The charge is derived from the voltage across a sense capacitor according to $Q=C_sV_s$ and is plotted vs. applied voltage V_a. The area of the loop represent the power dissipated by the device per cycle

The *x*-axis of the oscilloscope is connected to the applied voltage, which is almost identical to the sample voltage, and the *y*-axis measures V_s. The oscilloscope is used in *x-y* mode. When the applied voltages are above the threshold of the EL device, Q-V loops can be obtained from the oscilloscope. The area encompassed within the Q-V loops represents the energy consumed by the EL device per cycle (figure 6.29). Therefore, the input power density P_{in} [W/m^2] is just this area times the frequency of the applied voltage and then divided by the area of the EL device. In practice, the Q-V loop as well as the sample brightness in cd/m^2 is recorded for each applied voltage. By measuring the loop area, the input power intensity P_{in} is determined and then the luminous efficiency is obtained.

Powder EL is a capacitance device. Below the threshold voltage, the relationship follows the simple equation Q=CV. The Q-V plot is a straight line instead of a loop. In other words, any loop obtained before the excitation of the phosphor indicates a current leakage across the device, which makes the estimation of the efficiency unreliable.

Sawyer-Tower method is employed to estimate the efficiency of the nanowire contact EL device. The Q-V loops as well as the luminance are recorded for a set of voltages. An example of the Q-V loop is shown in figure 6.30.

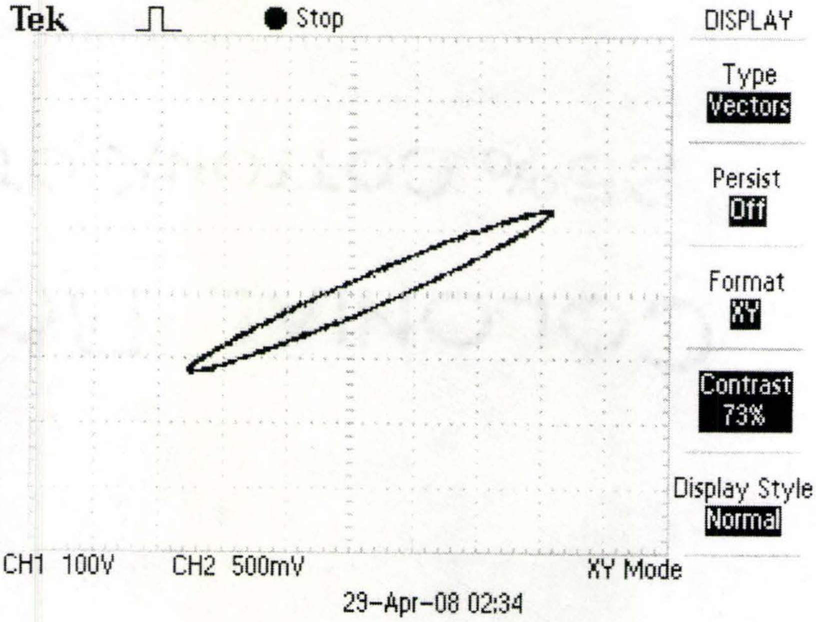

Type Vectors
Persist Off
Format XY
Contrast 73%
Display Style Normal
CH1 100V CH2 500mV XY Mode
29-Apr-08 02:34

Figure 6.30 Q-V loop for a nanostructured device driven by a sinusoidal wave at 284V and 8.27 kHz.

It should be noticed that leakage currents are observed across the nanostructured device. As a result, the electric power dissipated by the device includes both the power consumed by the luminescence and the power consumed by the leakage currents. In this case, the Q-V loop area represents the summation of these two power consumptions per cycle.

In order to extract the leakage power and precisely estimate the power dissipation that is used to produce luminescence, the input power (loop area) is plotted vs. applied voltage (V^2) as shown in figure 6.31. All loops, including the loops before and after the luminescence, are recorded for a set of voltages. For example, a Q-V loop can be

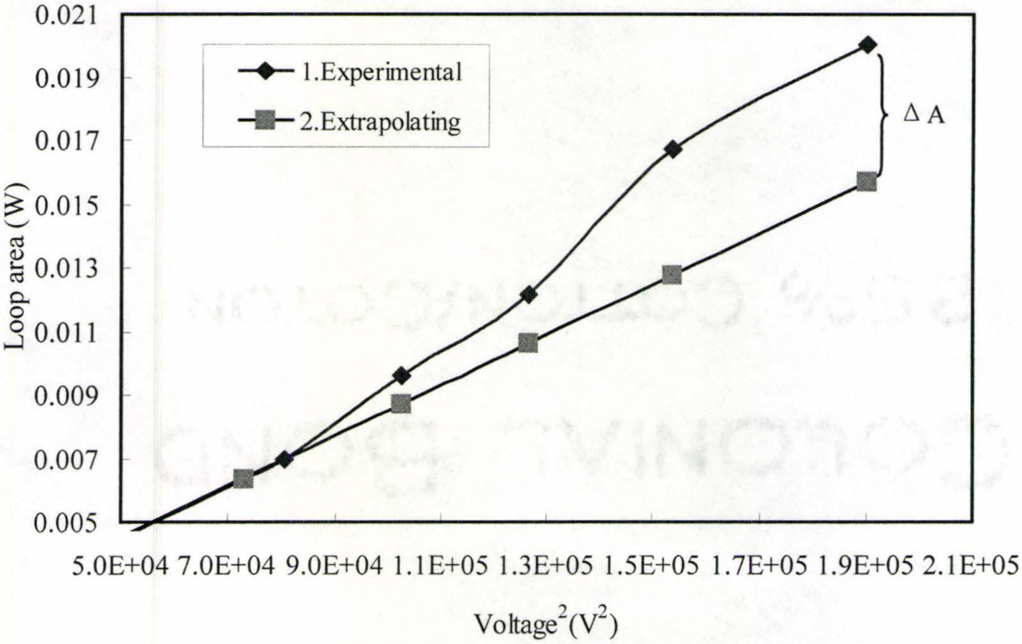

Figure 6.31 Dependence of Q-V loop area (W) on the applied voltage (V^2). The frequency is 8.3 kHz driven by a sinusoidal waveform.

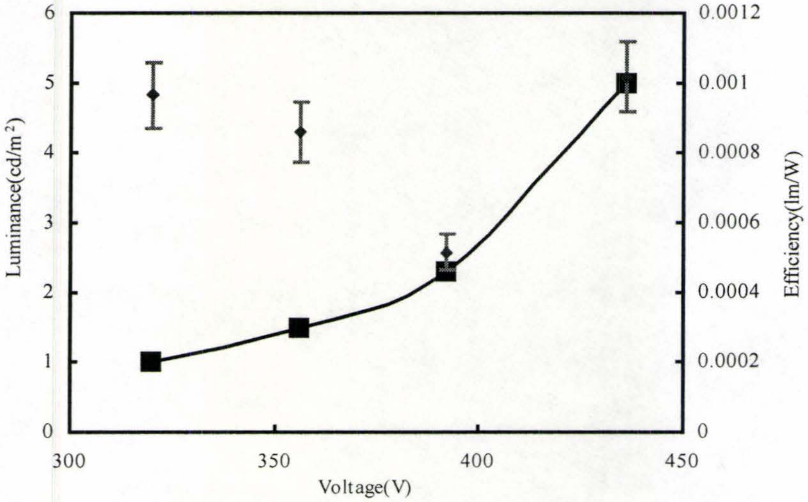

Figure 6.32. EL performance of the nanostructured powder EL device as a function of applied voltage. The line represents the L-V curve, while the dots with error bars indicate the dependence of efficiency on the operating voltage. The frequency is 8.3 kHz driven by a sinusoidal waveform.

obtained when the applied voltage is 270 V even though no light is produced from the phosphor. This loop is corresponding to the power consumed by the leakage current. However, if the applied voltage is up to 320 V, light is produced and the loop represents the power consumed by the leakage current as well as the excitation of the phosphor. Therefore, line 1 in the figure 6.31 represents the experimental dependence of the input power (loop area) on applied voltage (V^2). Line 2 indicates the power consumed by the leakage currents by extrapolating the loop areas obtained before the luminescence. This assumes that the leakage is linear with voltage. Therefore, the difference between the loop areas (ΔA) at the same applied voltage indicates the real power used to produce luminescence by comparing these two lines. The input power density (P_{in}) is just this loop difference (ΔA) divided by the luminescent area of the device. If the luminance (cd/m^2) is recorded at the same time, the luminous efficiency can be estimated according to the equation (6-2). Figure 6.32 shows the dependence of efficiency (lm/W) on the operating voltage obtained by the approached described above.

Generally, the presence of leakage currents causes the values of the luminous efficiency to be extremely low, inconsistent and unreliable. Reasons for the leaking include the relatively low dielectric constant of the polymer matrix (~3-4), as well as the low density of the embedded phosphor particles. The phosphor-free regions are easier to electrically break down compared to phosphor-embedded regions. Therefore, a material with high dielectric constant is expected to solve the leaking problem and improve the efficiency of the device. Typical values of the efficiency for powder EL are 1 to 10 lm W^{-1}(Shionoya and Yen, 1998).

Chapter 7. Conclusions and Future Work

7.1 Conclusions

By exploiting the contact EL idea and taking advantage of the concentration of electric field on indium nanowires, a new powder EL device based on green ZnS:(Cu, Al) phosphor has been fabricated in this paper. Compared to the traditional powder EL device, the novel device consists of a dilute layer of metal nanowires which directly contact with the phosphor particles and function as rear nanoelectrodes.

CRT green phosphor ZnS:(Cu, Al) which has no EL is used as the emission layer in the device. The phosphor is embedded into, but not covered by, a layer of polymer film which is supported by ITO transparent glass. Indium nanowires are directly put onto the exposed surface of the phosphor by a wet-coating method. Under an AC voltage, an intensified high electric field can be formed in the phosphors region contact with the nanowires, and, therefore, excite phosphor to luminesce.

The indium nanowires with 330 nm in diameter and several micron lengths are fabricated by impregnation of anodic aluminum oxide (AAO) templates using a hydraulic pressure injection method. AAO membranes (Whatman) formed by anodizing high-purity aluminum in an appropriate acid solution are used as the templates in the formation of nanostructures. The membranes with a nominal pore size of 0.1 μm and approx. 60 μm thickness are known to be self-organized structure with the pores normal to the surface and running through the entire thickness. In this thesis, indium metal foil is heated to its melting point and is injected to the membrane under a high hydraulic pressure. This method features easy handling and high repeatability. After complete dissolution of the membrane with NaOH solution, indium nanowires are released into the solution and transferred onto the embedded ZnS substrate. The final nanostructured device is completed by the deposition of Au rectangular electrodes on the top of the device. Correspondingly, metal nanowires with two different profiles are formed simultaneously at the vicinity of the Au rectangular electrodes: (a) the nanowires from the inner area of Au electrodes are separated from each other and are connected by Au; (b) the nanowires extend beyond the perimeter of Au or conductive silver paste electrodes, but are electrically contacted by Au or conductive silver paste electrodes.

The mechanism of the light generation from the nanowire contact powder EL device can be explained by the bipolar field-emission model. Under an average electric field, a concentrated electric field can be formed in the phosphor region in contact with the metal nanowires compared to that of other regions. This localized electric field is strong enough, in order of 10^8 V/m, to induce electron injection and avalanching in the phosphor lattice. The injected electrons travel in the phosphor lattice and finally trapped at the donors. When the electric field is reversed, the electrons recombine with the holes, which are injected and trapped at the acceptors previously by the same process, and therefore the visible light is generated.

In order to quantitatively characterize the electric field in the phosphor, electric simulations are performed with an electromagnetic field simulation software (Maxwell SV from An Soft Inc.). The results indicate that the indium nanowires can induce a field which is much higher than the applied external field. Hence, low average fields that are easy to produce can generate luminescence.

The tests of the dependence of luminance on voltage at various frequencies for a nanowire contact EL device sample are performed. A peak luminance of 5 cd/m^2 has been achieved for the device driven at frequency of 9.2 kHz and a voltage of 540 V.

Besides traditional applications of powder EL devices such as backlighting and lamps, the nanostructured powder contact EL devices may enable their application to displays due to potential low operating voltage, long lifetime, high luminance, as well the intrinsic high efficiency of powder EL. Because a polymer can be used as the vehicle for the powder phosphors, flexible nanostructured powder contact EL devices are possible. As a conclusion, low cost, self-supported nanowire contact EL devices with promising applications in displays and lamps have been fabricated in this work.

7.2 Future Work

In general, the performance of nanowire contact EL device is far from as good as the traditional powder EL device so far. However, the nanowire contact EL devices have the potential for a lower operating voltage with simultaneous long lifetime and high luminance with the help of the nanowires as long as the optimum structure and fabricating processes could be achieved.

First of all, the nanowires randomly lie down onto the phosphor and partially electrically connected or covered by Au. That means only a small fraction of wires works effectively as the contact material. In addition, the devices are less capable of repeatability in terms of the EL performance due to the random distribution of the nanowires. If all nanowires could be perpendicularly grown up from the surface of the phosphor with good control of dimension and position, the operating voltage could be much lowered, and hence the brightness could be increased, as each nanowire would have a significant contribution to the performance. However, a new technique is needed to grow the nanowires which are normal to the surface of phosphor particles. The technique itself has to be compatible with reliable optoelectronic device fabrication processes.

Secondly, the nanowires are deposited onto the phosphor surface by using a wet-coating method. Although this method features easy handling, it is a top-down technique and all nanowires loosely contact with the phosphor. As we know, an intimate contact, whether an ohmic contact or a schottky barrier, is highly desirable for the nanowire contact EL. Therefore, modification of the contact between the phosphor and the nanowires would be an effective way to improve the EL performance, as well as the stability, of the device.

Last but not least, the dimension of the nanowires is a critical parameter in the device, which determines the extent of how much the electric field can be intensified, as the electric field is proportional to $1/r$, where r is the radius of the nanowire. Therefore, smaller nanowires can induce a much higher electric field compared to large nanowires at the same operating voltage. In future, nanowires with decreasing diameter should be fabricated by using smaller templates made in our lab.

These improvements will also decrease leakage current since lower applied voltage will reduce stress on dielectric material.

Indium nanowires contact the phosphor and work as nanoelectrodes. Therefore, other nanowire or nanotube materials including carbon nanotube may be considered in place of indium nanowires.

Appendix I: Powder Contact Electroluminescence

1. Introduction

Powder electroluminescence was first reported by Lehmann in 1957 (Lehmann, 1957). In his experiment, powder phosphors which were unable to EL under usual conditions could luminesce in a strong alternating electric field after they were mechanically mixed with selective metal powders such as Ag, Cu, or nonmetalic powdered substances such as Cu_2S, Ag_2S or fired ZnO. The arrangement of the contact EL cell is shown in figure 1.12. The emission colours for some phosphors are different for photo- and electroluminescence which indicates the excitation of the phosphors caused by the strong electric field instead of u.v radiation generated by a glow discharge in device. Furthermore, the geometrical size and shape of the metal powders mixed were more critical compared to their other chemical and physical properties to work as effective contact substances with the phosphors. Metal powders with rounded shape were unable to excite phosphors, while powders with sharp edges were very effective to produce EL. All these features indicate that the contact substances (metal /non-metal) play a very important role in contact EL. The similarity of the contact EL to ordinary powder EL now is so clear that ordinary powder EL is also caused, or at least strongly favored, by the presence of second substance in addition to the phosphor itself. As a result, bi-polar field emission model was introduced to elucidate contact EL. It is proposed that metal powders with sharp edges and irregular shapes can cause a strong nonuniformity of electric field inside the phosphor particles when these are subjected to an external field. The strength of the electric field in the immediate neighbourhood of the sharp edges is much higher than the average electric (at least some 10^3 V/cm). Therefore, electrons can be injected into phosphors, causing avalanching of more electrons and finally trapped at lattice defects or impurities (Donors). When the applied electric field is reversed, the electrons recombine with holes, which are injected and trapped at acceptors previously injected by the same process; emissive light is produced and the colour of the light is determined by the bandgap of the donors and acceptors.

By exploring contact EL, a new EL structure has been proposed by our group (Sarah, 2005). Instead of mechanically mixing the metal powder with phosphor, the phosphor is firstly embedded, but not covered, into a polymer and then the metal powder contacts the phosphor by an external pressure (see figure 1.13). Similar results to Lehmann's powder EL have been obtained.

2. Experimental procedures

In the experiment, two phosphors are used: blue ZnS:Ag made by Phosphor Technology and CRT 1260 green ZnS:(Cu,Al) made by Silvania. Both phosphors have a very strong photoluminescence, but are unable to EL under usual conditions in a strong alternating electric field. The experiment starts with embedding a phosphor powder into a polymer. Various polymers were evaluated, but a polypropylene film with 23 μm thickness was chosen as the embedding medium based on low cost, availability, and the ability to peel off of a substrate. In order to get a fairly uniform single layer of phosphor powders in the polypropylene, they are pressed onto a sheet of tape (Gelpak). Meanwhile, a sheet of polypropylene is placed on the top of an ITO glass and both of them are heated until the polypropylene begins to melt. At this stage, the Gelpak with phosphor powders is placed at the top of polypropylene and pressure is applied by a weight to push the powder into the polypropylene as it cools. Too much pressure will push many of the powders below the surface and cause them to be covered by the polymer, but too little will not embed them far enough in. For a 1 inch square sample, it was found that about 1 kg was adequate. After it cools, the Gelpak is peeled off. The structure with powder embedded in a polymer is obtained.

Two kinds of metal powders, spherical silver powder with diameter of 1.3-3.2 μm (Alfa Aesar, 99.9%) and copper powder with diameter of 1-1.5μm (Alfa Aesar, 99%), are used as the contact substances with the phosphor. In practice, a layer of metal powder is spread across the exposed surface of the phosphor and pressed down using a conductive tape. Then one electrode is attached to the conductive tape touching the metal powder while the other is connected to ITO. When an AC voltage is applied, the resulting light is emitted through the glass substrate.

3. Experimental Results

3.1 Powder Phosphors embedded in polypropylene film

Figure 1 shows the powder phosphors embedded in the polypropylene films. The shape of the phosphors is quite irregular. All particles embed into, but are not covered by, the film. The exposed surfaces of the phosphors will contact with metal powders to produce light. As a result, a uniform single layer of phosphor powders with flat surfaces up is highly desirable so as to obtain more effective areas for points of contact of the metal powders. In addition, large particles are more favoured in contact EL than small particles.

3.2 Electric field inside phosphor particles due to the contact substances

The morphology, including the geometrical size and shape, and the conductivity of the contact substance plays a very import role in contact EL. The other chemical and physical properties of the contact substance seem to be unimportant for contact EL. It has been proved by previous studies that the particles with suitable geometrical size and sharp edges can work effectively in contact EL as the strong nonuniformity of the electric field inside the phosphor can only be induced by the particle of high electrical conductivity and sharp-cornered or sharp-edged shape when the phosphor is subject to an external field. If we assume that a contact substance with infinitely good conductivity surrounded by an ideally insulating phosphor crystal and an average electric field of F_0 is applied to this system, the highest local field F_{max} appears near sharp edges of the conducting particles, and the ratio F_{max}/ F_0 is the order of R/r, where r is the radius of curvature of the edge and R the particle diameter.

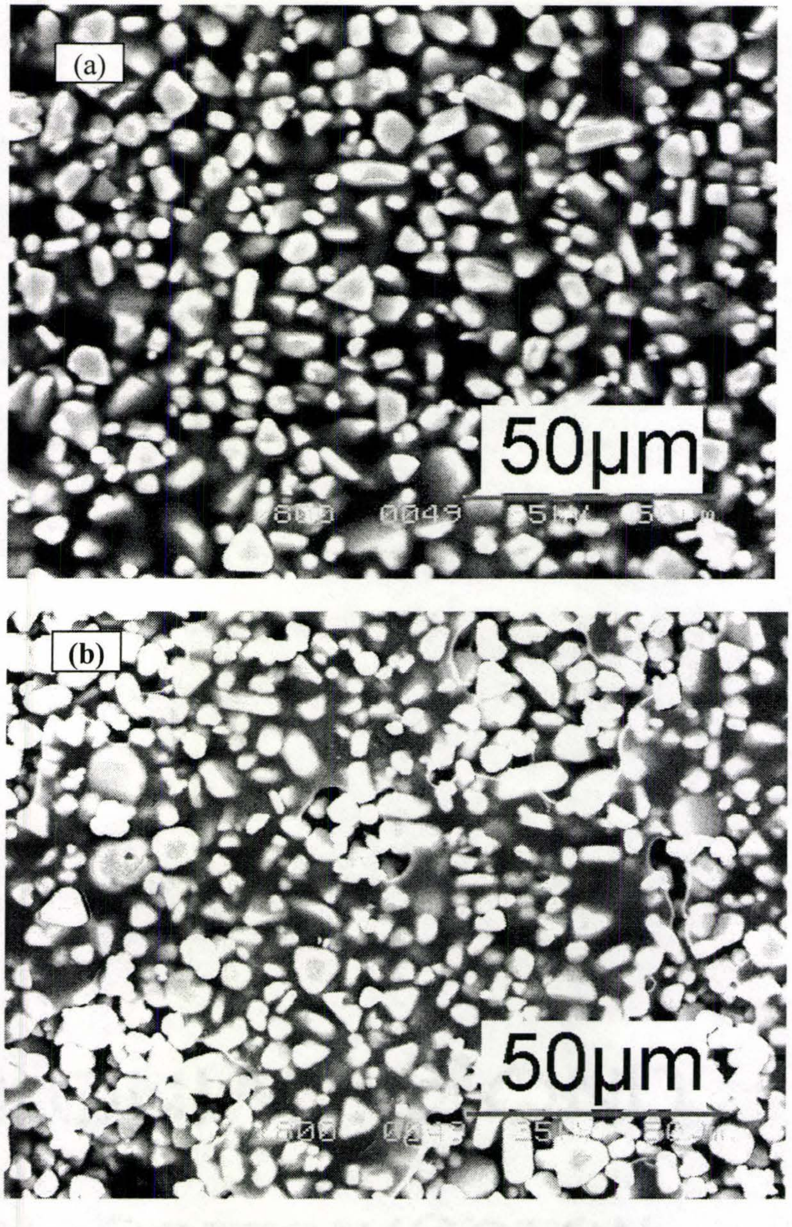

Figure 1. Powder phosphors embedded in polypropylene films, ZnS:Ag blue phosphor (a); ZnS: Cu, Al green phosphors (b)

According to Lehman's results, the largest possible geometrical dimension of a contact substance particle in a ZnS phosphor is the order of 1µm. Much larger dimensions can not work in contact EL because the phosphor particles themselves normally have average diameter of the order of several microns. Theoretically, the smallest possible radius of curvature can be considered to be the order of magnitude of the lattice constant of the crystalline material. Assuming, roughly, $R=3\times10^{-4}$ cm and $r=3\times10^{-8}$ cm as the most ideal case, one obtains

$$F_{\max}=10^4F_0$$

as the highest possible field strength in the phosphor particles under the best conditions. It also can be predicted that this highest possible field is only limited to a very small region near the sharp edges of the contact substance. The electric field will be gradually lowered down to the average electric field with the regions far away from the sharp edges. Therefore, the field in much the largest part of the phosphor is only of the order of F_0, the average field applied to the phosphor.

In our research, two metal powders, copper and silver with dimensions of the order of 1 μm, are testified to be the effective contact substances in powder contact EL. Figure 2 shows the powders imaged with SEM. Silver powder has a spherical geometry, while copper powder tends to have a faceted morphology. Both of these two powders are small enough and can form points of contact with the phosphor particles under a suitable pressure. Therefore, highly localized fields can be induced by these powders, causing light output from the phosphor particles.

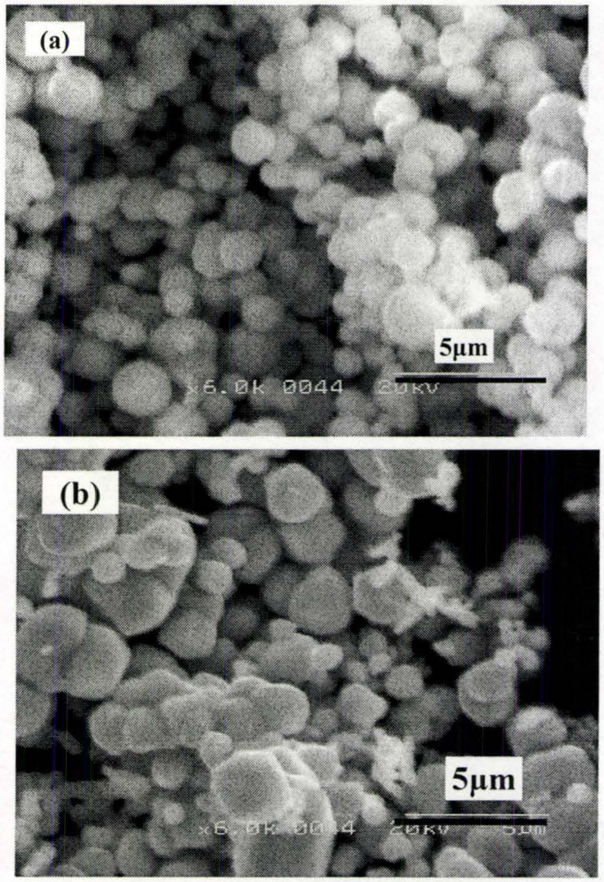

Figure 2. SEM images of the contact powders. Ag (a), and Cu (b).

3.3 Degradation characteristic of powder contact EL cell

Degradation is a key issue in applications of AC powder EL devices. One reason for the degradation is related to the escape of sulfur from the ZnS phosphor with the help of water, resulting in sulfur and zinc vacancies in the phosphor. It has been reported that the ZnS phosphor deteriorates when the number of sulfur vacancies increases (Hirabayashi, et al., 1983).

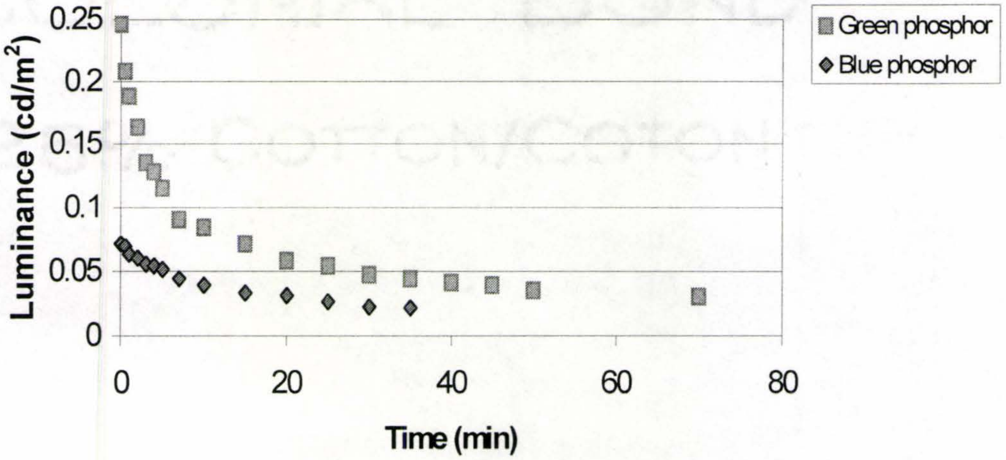

Figure 3. Brightness degradation in powder EL contacted with spherical silver powder, Vp-p=710V, f=488 Hz, under normal atmosphere

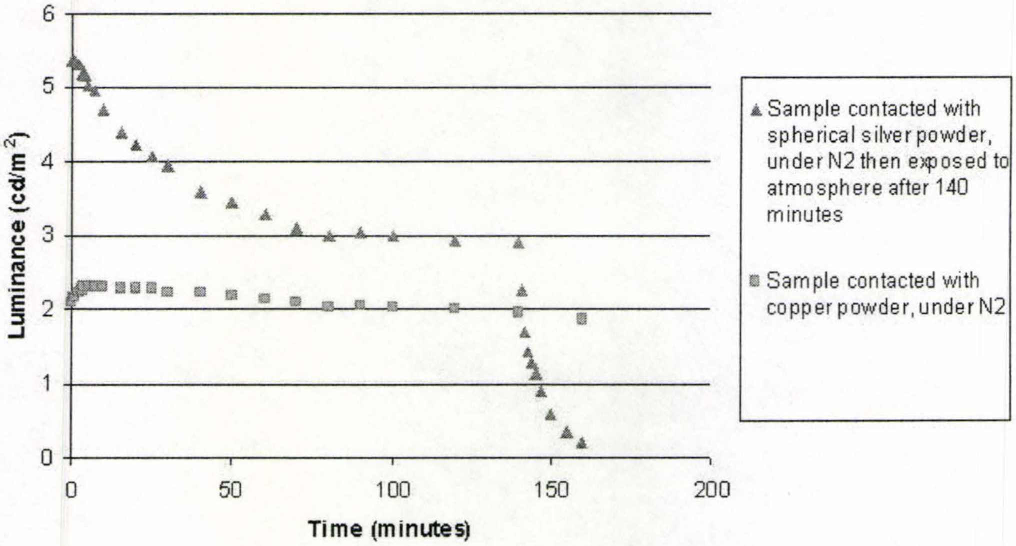

Figure 4. Decrease in brightness over time of green powder (ZnS:Cu,Al) EL (Vp-p=1.7kV, f=488 Hz)

Powder contact EL cells exhibit a similar degradation to normal powder EL devices as shown in figure 3. The brightness of each sample made in this experiment also decreased with operating time at a constant voltage. It also can be confirmed that moisture has a very bad effect on the brightness. Under normal atmosphere the decrease in brightness is fairly sharp, but under nitrogen protection, it is more gradual. Figure 4 illustrates the decrease in brightness for green phosphor while figure 5 shows the decrease for the blue phosphor.

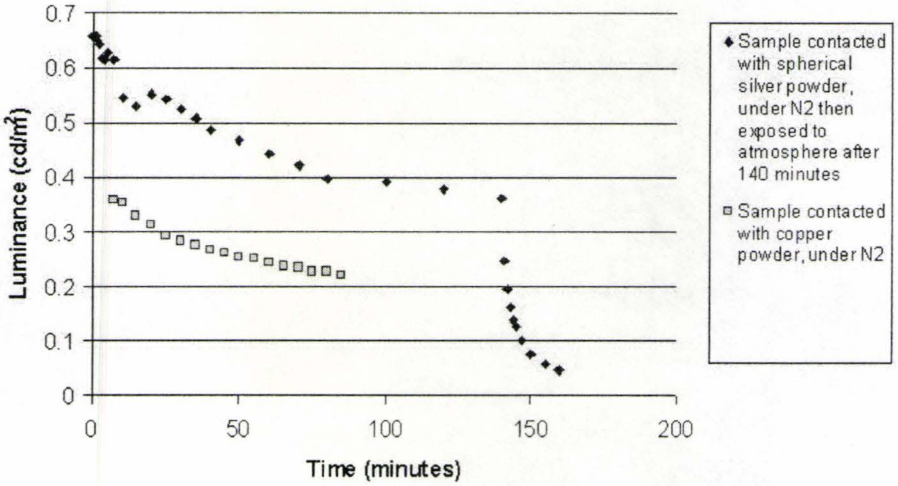

Figure 5. Decrease in brightness over time of blue powder (ZnS:Ag) EL (Vp-p=1.7kV, f=488 Hz)

3.4 Luminance and Luminous Efficiency of Powder Contact EL

The EL characteristics of powder contact EL cells were measured as shown in Figure 6-8. The luminance output of the powder contact EL cell is not as strong as that observed in the normal powder EL structure (Shionoya, 1998, P603). The voltages required to drive the powder contact EL are excessively large. However, similar to the normal powder EL, a very sudden onset of luminance at a specific threshold voltage is observed in powder contact EL cells. This is inherent in an avalanche process and validates the bi-polar emission model for powder contact EL.

The extremely high operating voltage of these powder contact EL devices is attributed to the fact that the polymer film is quite thick in comparison to the phosphor powder. If the polymer could be made thinner, more of the electric field would drop across the phosphor rather than across the polymer and the device could be run at significantly lower voltages. Several devices were prepared by using a spin-on polymer with thickness of 7 μm as embedding material, however, the light output from these devices was not bright enough to gather any meaningful data and higher voltages caused them to be short-circuited and burned out. Nevertheless, the threshold voltage for these devices with thinner polymer was found to be much lower than for those embedded using polypropylene.

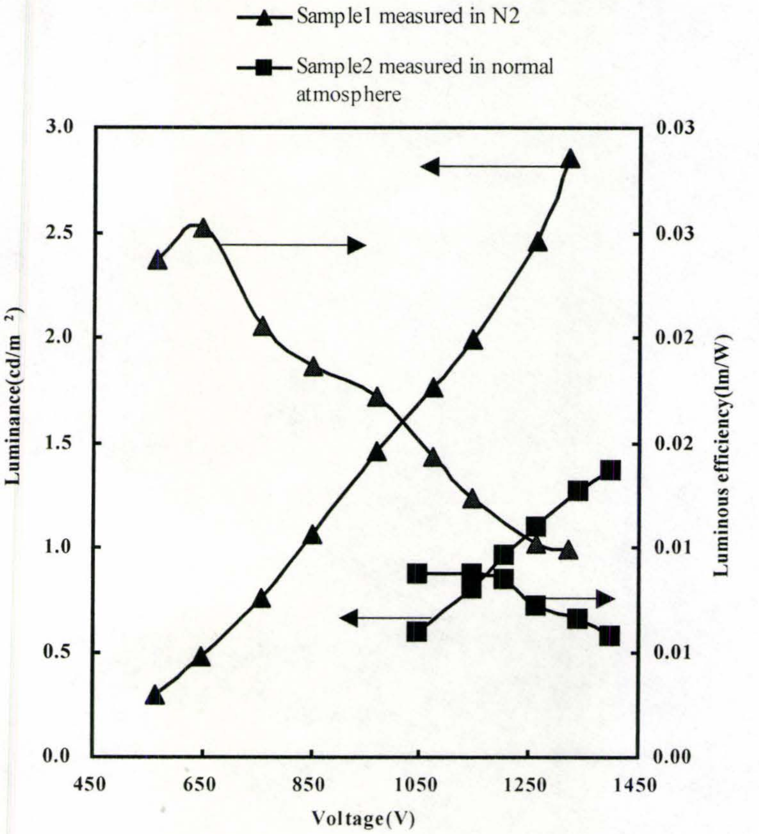

Figure 6 EL performance of blue powder EL (ZnS:Ag) contacted with copper powder Sample1: Measured in N_2; Sample 2: Measured in normal atmosphere (f=488 Hz)

It should be noticed that the luminance and the efficiency of the powder EL devices working in nitrogen are much higher than those working in the normal atmosphere. This is attributed to the humidity which in the air can interfere with the contacts between the phosphor and the metal. In addition, spherical silver powder was more effective that copper powder as a contact substance perhaps due to the fact that the silver powder has surface structures that more consistently make a sharp contact with the phosphor particles regardless of the orientation of the powders. Also the silver oxide formed on the silver powder surface is conductive.

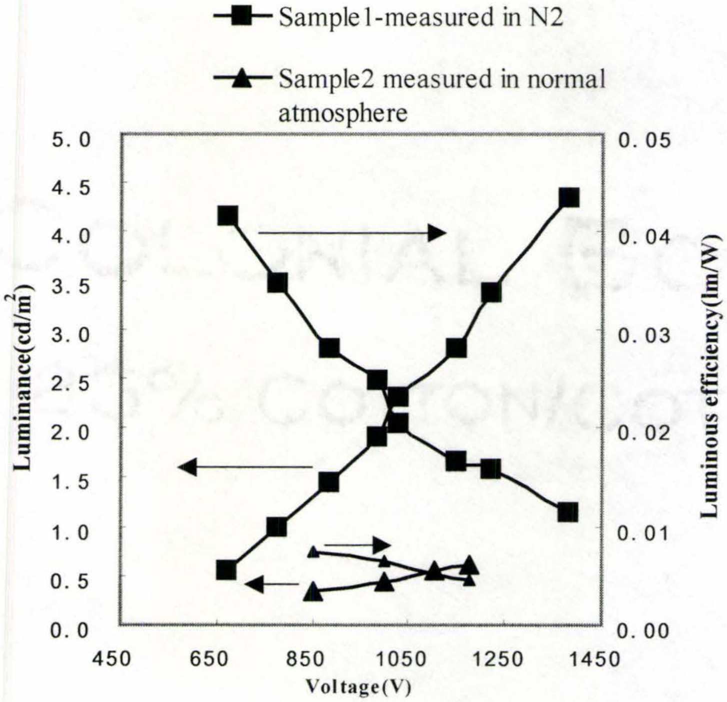

Figure 7 EL performance of blue powder EL (ZnS:Ag) contacted with silver powder Sample1: Measured in N_2; Sample 2: Measured in normal atmosphere (f=488 Hz)

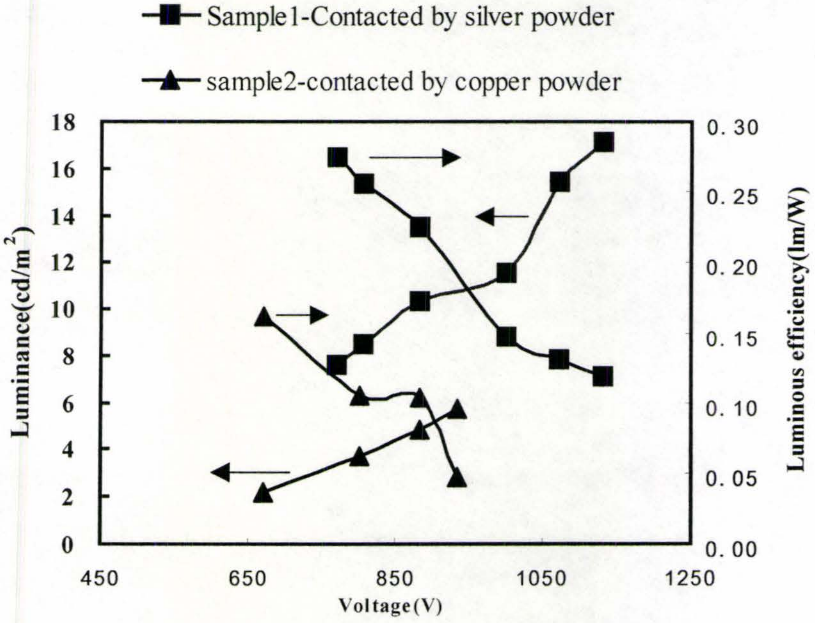

Figure 8 EL performance of green powder EL (ZnS:Cu, Al)in N_2 (f=488 Hz) Sample: contacted by Ag powder; Sample 2: contacted by Cu powder

4. Discussion

4.1 The Effect of Pressure on Brightness

The brightness of the powder contact device is found to have a slight dependence on the pressure. Initially, increased pressure on the powder increased the brightness somewhat, but after this first brightening there is no visible change as pressure continually increased. In some instances, repeatedly increasing and decreasing the pressure actually decreased the brightness quite significantly.

The slight pressure dependence is likely due to the number of points of contact. Initially, increased pressure pushes excess powder grains into the phosphor and increases the number of light-emitting contact points. However, after a certain point increased pressure does not create any new contact points and therefore does not change the brightness in any way. For faceted powders, it is believed that repeatedly increasing and decreasing the pressure actually causes the metal powder particles to lie flat against the phosphor rather than having a sharp point contact. This will lower the electric field at the point of contact and raise the threshold voltage as well as decrease the amount of light emitted from that area, which accounts for the observed decrease in brightness after such actions.

4.2 Improvement of the EL Performance of Powder Contact EL Device

Powder contact EL is far from as good as the normal EL powder device, however, one way to increase the brightness of the powder contact EL would be to increase the number and the flatness of the phosphor particles at the surface of the polymer. One way that this could be done is by using a sedimentation method to deposit the powder on the surface of the Gelpak® before embedding. If the powder is suspended in a solution and dropped on the surface of the Gelpak® and then allowed to evaporate, the powder particles should settle with a flat side facing down. Additionally, depending on the amount of phosphor in the solution, they should be more densely packed. Preliminary experiments using this method show this to be true as can be seen from figure 9. However, the extent of how much this will increase the brightness and efficiency was not determined.

There is a large size variation between particles in the phosphor powders used. If the smaller particles could be separated from the larger, then only the large grains could be embedded. These large particles might offer more areas for points of contact and increase the brightness.

Finally, the structure of the powder contact EL can be improved if the metal contact powders are held in place more firmly. This would ensure that individual particle would not rotate but would maintain a sharp contact point. This is less important for spherical powders but could greatly improve the performance of the faceted powders. A technique would also be needed to ensure the sharp points ended up oriented facing towards the phosphor. Based on this idea, powder EL with nanostructures has been developed. In that case, metal nanowires functions as nanoelectrodes and directly contact with the phosphor particles.

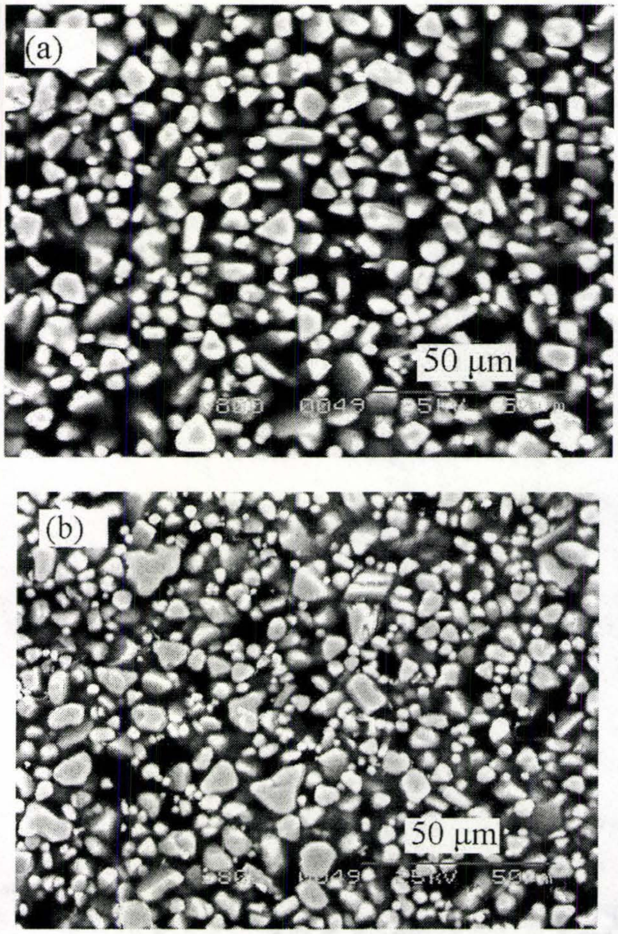

Figure 9. Phosphor particles embedded in polypropylene with different methods. (a) the powder is pressured into the Gelpak before they are embedded further embedded into the polymer; (b) the powder is deposited into the Gekpak by a sedimentation method before they are further embedded into the polymer

5. Summary

Powder contact EL devices using Ag and Cu powders as contact substances have been tested in this paper. All the results seem to be consistent with the bi-polar field emission model that has been proposed. Small metal powders can form sharp contacts with the phosphor. This intensified the electric field within the phosphor particles at the point of contact. As a result, electron injection and avalanching in the phosphor lattice can be induced by this localized electric field. Therefore, the threshold voltage can be lowered and the brightness can be increased. The luminance of the green-emitting devices can be as high as 18 cd/m^2 working in nitrogen and contacted by spherical silver powder. The EL performance could be improved by increasing contacts by a better embedding of the phosphor particles, smaller and sharper metal powders, and forming either an ohmic contact or a shottky barrier between the phosphor and the contact substance. The humidity in the air has a very noticeable effect on the EL performance of powder contact EL, as well as the degradation of the device. Metal nanowires have been considered to replace the metal powders as contact substances due to the intrinsic geometry of the nanowires, and the use of pressure to form the phosphor-metal contact points is not practical in real devices.

Appendix II:

Growth of Nanoporous Silicon Dioxide Thin Films Using Porous Alumina Substrates

1. Introduction

Nanoporous films show anomalous optical, electronic, magnetic and other properties different from those of their corresponding bulk materials (Hozumi, et al., 2001). Among the porous materials, porous silica films have recently attracted much attention due to applications ranging from low-k dielectric materials in electronics, to diffusion filters for molecule separation and fluid purification and biosensors for detecting biological molecules. SiO_2 aerogel film with 70% porosity was reported with dielectric constant as low as 2 (Jo, et al., 1997) which can be used as intermetal dielectrics to decrease the interconnection delay in ultralarge scale integration. Piezoelectric biosensors made from nanoporous silica can improve the sensitivity of the device to biological molecules due to the high surface areas of the nanoporous structure (Collings and Caruso, 1997) (Diaz and Balkus, 1996).

However, the fabrication of porous silica thin films seriously limits their development in application. So far, the methods include wet-based techniques, such as sol-gel (Liu, et al., 1999), free-radical aqueous polymerisation (Zhao and Zhu, 2003), electrochemical anodization of silicon in weakly alkaline low-buffered fluoride media (Frey, et al., 2005); and dry-based techniques such as evaporation or plasma enhanced chemical vapour deposition (PECVD) (Wu, et al., 2005). Recently, a method termed as plasma polymerisation which takes advantages of plasma-assisted deposition of silicon oxide and polymer colloid beads was reported by Chifen et al (Chifen, et al., 2007).

Porous alumina, which is formed by anodizing high-purity aluminum in an appropriate acid solution and has been studied extensively over the last five decades, is characterized as a self-organized porous structure with uniform pore diameter and depth (Shingubara, 2003). Nowadays, porous alumina is widely used as a template to grow nanowires, nanodots or nanotubes since the pioneering work of Martin (Martin,1994) (Wirtz, et, al., 2002). Taking advantage of the uniform nanoporous structures of alumina membranes and using a sputtering technique, nanoporous Pd (Ding, et al.2006), and WO_3 (Gorokh, et al., 2006) thin films have been prepared recently. It was reported that these films grown on the porous alumina membranes are highly sensitive to the specific gas and have promising sensor applications.

Similar to this approach, we report a cost-effective and highly reproducible method for the deposition of porous SiO_2 thin films in this work. Commercially available porous alumina membranes are used as a support. Due to the intrinsic nature of the alumina support, SiO_2 thin films with a self-organized porous structure are prepared by sputtering. These porous films have promise as microporous (<100nm) materials for catalysts and molecular separation.

2. Experimental details

SiO_2 thin films in this study have been prepared by sputtering on porous alumina substrates using a 2'' diameter SiO_2 sputtering target at a R.F. power of 100 W and pressure in the deposition chamber of 1×10^{-2} Torr. The distance from the target to the substrate was set to 60mm. The sputtering atmosphere consisted of Ar-O_2 mixed gas and its flow rate was controlled by separate gas flow meters to provide an Ar:O_2 flow ratio of 5:3. The porous alumina substrates were held in thermal contact with the substrate holder and were kept at 200℃ during the deposition cycle. The growth rate of the thin films was around 0.67Å/s. Under these conditions, SiO_2 thin films with a range of thicknesses from 80nm to 350nm grown on the PA substrates were achieved by varying the deposition time. The thickness of the films was measured with an Alpha-step Stylus Profiler on glass substrates. The structure and the morphology of the final thin films were characterized by a scanning electron microscope (FE-SEM, JEOL 7000F).

3. Results and discussion

3.1 Characterization of the porous alumina (PA)

In this paper, Whatman Anodisc membranes with 0.1μm pore size were used as the substrates to grow SiO_2 thin films. These membranes have two well-defined faces: a branched side formed by interconnected channels with a nominal diameter of 100nm (corresponding to the pore size claimed by the company) and a depth of approximate 1.6 μm. The other face (denoted as front side in this paper) was formed by unconnected cylindrical pores of 200nm mean diameter, with pore density of 1×10^9 pores/cm^2. The membrane thickness is about 58 μm. The porosity of the membranes is around 52%. The front side was used to grow the thin films because of its high regularity. The SEM images of the porous alumina membrane have been shown in figure 5.4.

3.2 Growth of thin films on porous alumina

The SEM images of the SiO_2 thin films grown on PA substrates as described in Section 2 are shown in Fig. 1. The porosity of the films is determined by porosity of the PA substrates as well as film thickness. When the thickness of the SiO_2 thin film is only 80nm, the film is not continuous as shown in figure 1(a), indicating that the growth of the thin film is in the nucleation stage. SiO_2 molecules prefer to nucleate on the top of the porous alumina and form discontinuous clustering along the vicinity of the pores when the film is not thick enough. During the growth of the thin film, large islands are formed and gradually coalesce together. A continuous self-organized porous network structure is formed with the thickness of the film increasing to 160 nm. The surface of the thin film is smooth and the pore size is a little bit smaller than the PA's pore size as shown in figure 1 (b). Growing the SiO_2 thin films to 250 nm and 350 nm respectively as shown in figure 1 (c) and (d), the mean pore size of the films can be decreased much smaller than 100 nm. The reason that the thickness of the thin films can be much larger than the pore size of the PA substrates is that the thin films will grow both parallel to the substrate by surface diffusion of the SiO_2 molecules, as well as perpendicular to it by direct impingement of the incident SiO_2 molecules. Due to the porous structure of the substrates and the low deposition temperature, the rate of the perpendicular growth can be much higher than the lateral growth. Therefore, thick porous SiO_2 films have been achieved on PA before the PA is fully covered.

As shown in figure 2, most SiO_2 molecules knocked out from the sputtering target prefer to nucleate at the open surface of the PA. Other SiO_2 molecules intend to go into the PA channels. Due to the high aspect ratio, defined as the ratio of the thickness to the channel diameter, of the PA channels (~300:1) and low PA substrates temperature (200℃), these molecules will deposit on the inside wall near the end of a channel instead of going through the channel. The first-arriving molecules form shadows which will block the other molecules from going into the PA channels. The

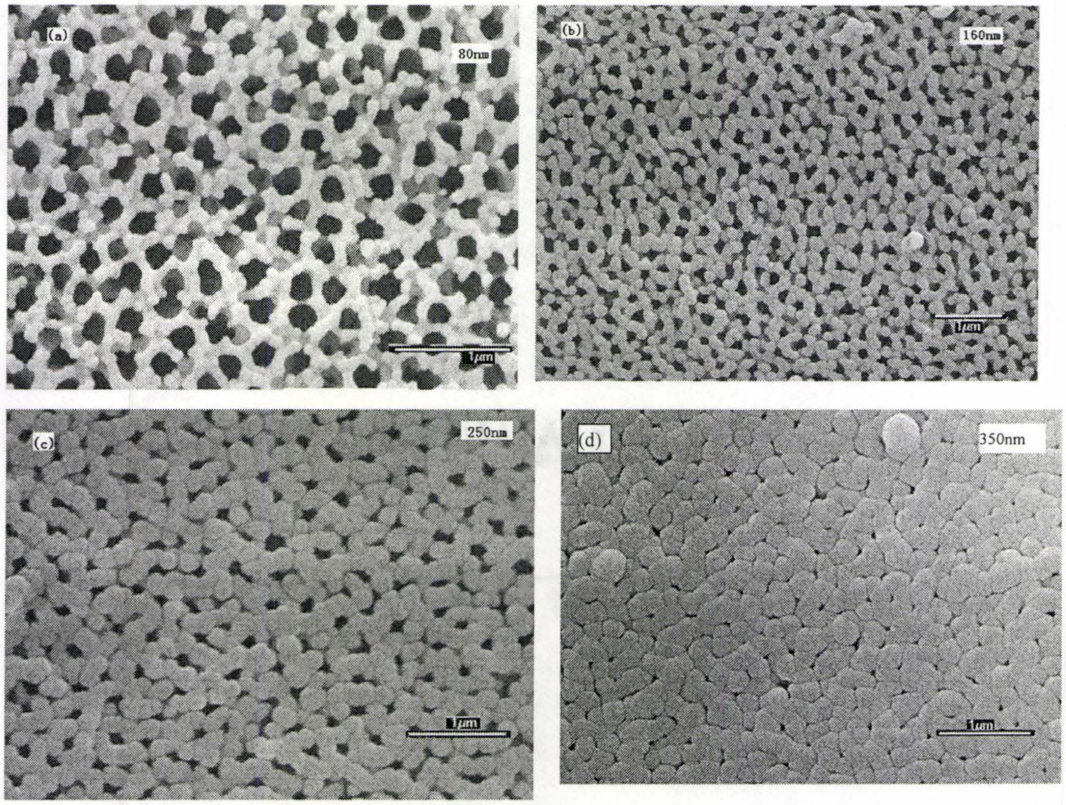

Figure 1. SEM images of SiO_2 thin films on PA with varying thickness. 80nm (a); 160nm(b); 250nm(c) ; 350nm(d)

pore size, therefore, will be narrowed with the growth of the film.

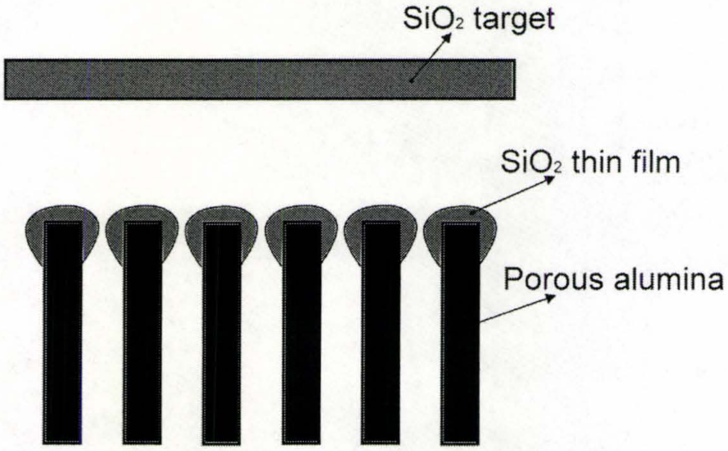

Figure 2 Schematic of the growth of SiO2 thin film on PA substrate using sputtering technique.

Figure 3 shows a micro detailed SEM cross-sectional analysis of the SiO_2 thin film grown on PA substrate with a thickness of 350 nm. Before the SEM analysis, the sample was fractured and embedded into epoxy. The epoxy stub was then polished with progressively finer grit sand papers to expose the cross-section of the sample. In order to increase the contrast of the SiO_2 thin film and the Al_2O_3 support, the sample was finally etched by a dilute NaOH (~0.2 wt%) solution for 12 hours.

The island coalescence of the film, with thickness of 350nm, is clearly shown in Fig. 3 (a). The SiO_2 film caps on the walls of the PA channels are clearly visible. With larger magnification and energy dispersive X-ray (EDX) analysis, Fig. 3 (b) and (c) further confirm that the morphology of the SiO_2 film is identical to that illustrated in figure 2. SiO_2 molecules first deposit on the inside wall. These first-arriving molecules then form shadows and prevent the other molecules from entering into the channels. As a result, the expected morphology is gradually obtained with this process. The EDX spectrum was obtained from the place labelled by an arrow in Fig. 3 (b).

Not only porous silica thin films, but also other thin films with porous structure can be prepared by the grown mechanism described above. Porous alumina thin films grown on PA, for instance, have been prepared by us under the similar sputtering conditions as that of the silica. The thicknesses range from 160nm to 300nm in this case as shown in Fig. 4 a-c. However, a detailed microstructural analysis is difficult since both substrate and film are Al_2O_3.

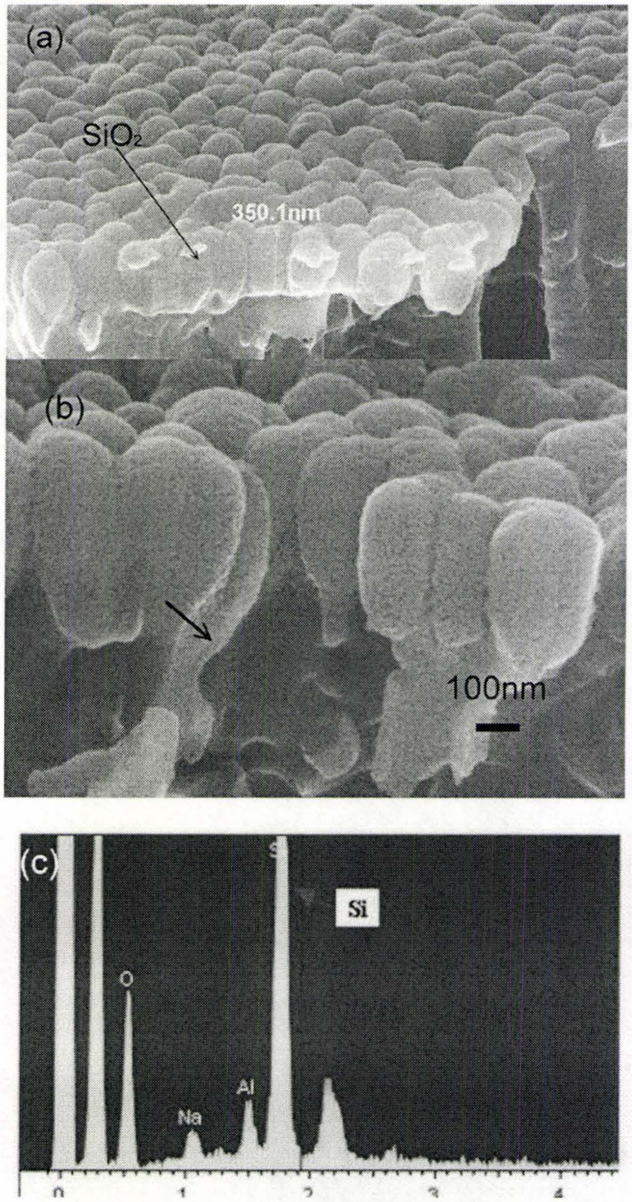

Figure. 3 SEM Cross-section of SiO2/Al2O3 composite. Low magnification (a), high magnification (b) and EDX spectrum(c) obtained from the place labelled by an arrow in (b).

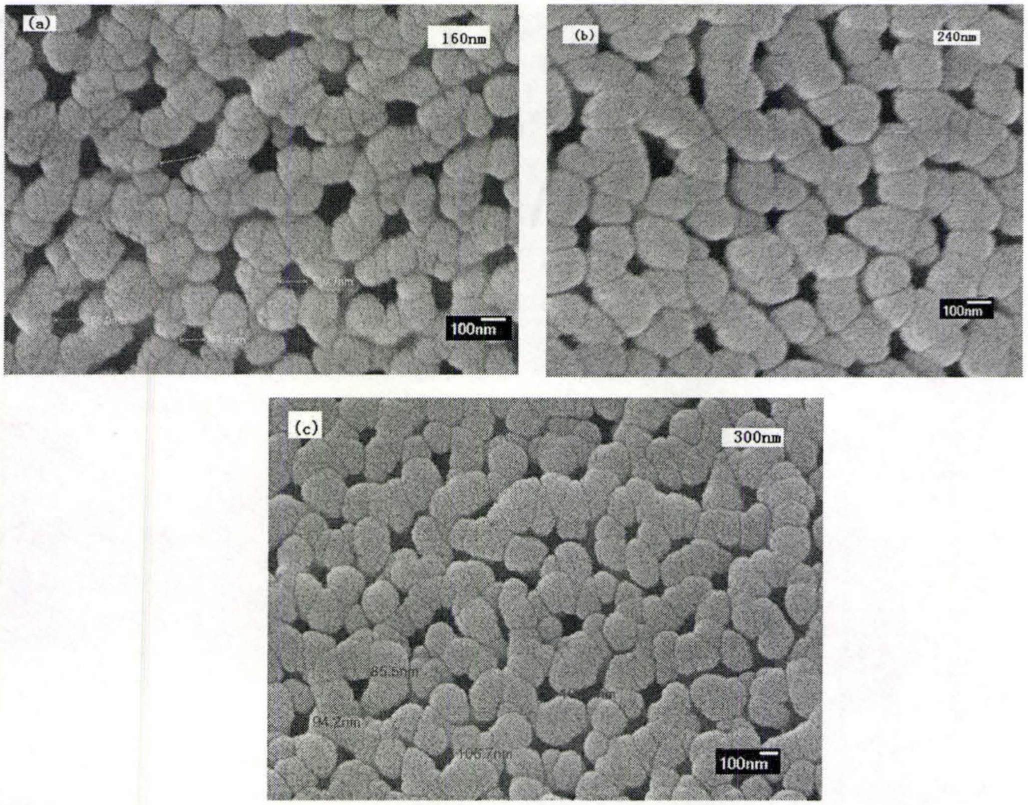

Figure 4. SEM images of alumina on PA with different thicknesses. 160nm(a) and 240nm(b) 300nm(c)

4.Conclusions

Using porous alumina membranes as the substrates, SiO_2 thin films were grown using the r.f. magnetron sputtering technique. Due to the unique porous structures of the substrates, the deposited thin films exhibit continuous self-organized porous morphologies. The pore size of the thin films depends on the film thickness. The growth process of the thin films can be understood as follows: Film growth occurs fastest perpendicular to the membrane surface. In addition, the first-arriving molecules deposited on the PA inside wall shadow and block subsequent molecules from going into the PA channels. With this mechanism, porous alumina thin films can also be grown on PA with similar morphology to the silica, indicating that PA is a good support for the deposition of a variety of thin films with the nanoporous structures.

Appendix III: List of Publications

Research Paper published in Journals:

- Feng Chen, A. Kitai, *Template Synthesis of Indium Nanowires using Aluminum Oxide Membranes*, J. Nanosci. Nanotech., 8, (2008), 4488–4493.
- Feng Chen, A.H. Kitai, *Application of Indium Nanowires to Donor-Acceptor Pair Luminescence*, J. Luminescence, 128 (2008), 1856-1862.
- Feng Chen, A.H. Kitai, *Growth of Nanoporous Silicon Dioxide Thin Films Using Porous Alumina Substrates*, Thin Solid Films,(2008), In press.

Research Papers/Abstract Published In International Conferences/Seminars:

- Feng Chen, A.H. Kitai, *Nanowire Contact Powder Electroluminescence Technology*, 2008 SID Inter. Symp. Dig. Tech. Papers, Los Angeles, May 15-23, 2008
- Feng Chen, A. H. Kitai, *Fabrication of Self-organized Nanoporous Thin Films using Porous Alumina*(abstract), 19th Canadian Materials Science Conference, June 20-22,2007, McMaster, Hamilton, Ontario, Canada.

Book Chapter:

- Feng Chen, Y. Xiang, *AC Powder Electroluminescence*, in Luminescence Materials and Applications, Ed. By A. Kitai, John Wiley & Sons, Ltd., 2008, P249-267

Ammar, I.A., Darwish, S., and Khalil, *P., Z.Werkstofftechn.,* **12** (1981) 421

Bard, P. A. M. E. A. J., *Encyclopedia of electrochemistry of the elements*, **vol.6**. New York and Basel: Marcel Dekker, 1973

Brody, T.P. and Yu, K.K., IEEE Trans. Electron Devices, **22**, 739(1975)

Chai, J. and Buriak, J.M., *ACS Nano*, 2(3), 489–501, 2008

Chen, C-C., Bisrat, Y., Luo, Z. P., Schaak, R. E., Chao, C-G and Lagoudas, D. C, *Nanotechnology.* **17**, 367-374 (2006)

Chen, C-C., Kuo, C-G. and Chao, C. G., *Jpn. J. Appl.Phys.,* **44**, 3, 1524-1528 (2005)

Chifen, A. N., Knoll, W. and Förch, R., *Mater. Lett.*, 61 (2007) 1722-1724

Choi, J, Sauer, G., Nielsch, K.,Wehrspohn, R.B. and Gösele, U., *Chem. Mater 2003*, **15**,776-779

Chou, S. Y., Krauss, P.R., and Renstrom, P. J., *Science*, 1996, 272, 85-87

Collings, A.F. and Caruso, F., *Biosensors: recent advances*, Rep. Prog. Phys. 60 (1997) 1397

Despic A., Parkhutik V., in: J.O.M. Bokris, R.E. White, B.E. Conway (Eds.), *Modern Aspects of Electrochemistry*, vol. **23**, Plenum Press, New York, 1989, pp. 401

Destriau G., J. Chim. Phys. (1937), **34**,327

Diaz, J. F. and Balkus, K.J., *J. Mol. Catal. B: Enzymatic* 2 (1996)

Ding, D., Chen, Z., and Lu, C., *Sens. Acutators, B,* 120(2006) 182-186

Elam, J. W., Routkevitch, D., Mardilovich, P. P. and George., S. M., *Chem. Mater. 2003*, **15**, 3507-3517

Frankl, R. D., *Electromagnetic Theory*, Prentic-Hall, Inc., Englewood Cliffs, New Jersey,1986, P19

Fischer, A.G., *J. Electrochem. Soc.,* **118**, 139c(1971)

Fischer, A.G., *J. Electrochem. Soc.,* **110**, 7, July (1963), 733

Fisher, A.G., *J. Electrochem. Soc.*, **109**, 11 (1962) 1043-1049

Fleisher, R.L., Price, P.B., and Walker, R.M., *Nuclear Tracks in solids*, University of California Press, Berkeley, CA,1975

Franceschetti, A., and Zunger, A., *J. Chem. Phys.*, 104 (1996),5572

Frey, S., Grésillon, B., Ozanam, F., Chazalviel, J.-N., Carstensen, J., Föll, H. and Wehrspohn, R.B., *Electrochem. and Soild-State Lett.*, 8 (9) B25-B29 (2005)

Fukushima, T., Fukuda, Y., Ito, G. and Shimizu, A., *J. Met. Finish. Soc. Jpn.* **25** (1974) 542

Gibson, J.M., *Phys. Today*, 1997, 56-61

Grimmeiss, H.G. and Allen, J.W., *J. Non-Crystalline Solids*, **352** (2006) 871

Gobrecht, H. and Gumlich, H.E. *J.Phys. Radium* (1956), 17, 754

Gobrecht, H., Gumlich, H.E., Nelkowaki, H. and Langar, D.Z., *Phys.,* **149**, 504 (1957)

Gooch C.H., *Injection Electroluminescent Devices* (New York: Wiley, 1973), p 2

Gorokh, G., Mozalev, A., Solove, D. I, Khatko, V., Llobet, E., and Correig, X., *Electrochim. Acta,* 52 (2006) 1771-1780

Guo, Y.G., Wan, L,J., Zhu, C.F., Yang, D.L., Chen, D.M., and Bai,C.L., Chem. Mater., 2003,15,664

Haynes, J.R. and Briggs, H.B., phys. Rev., 99, 1892, 1947

He H. and Tao N, *J 2003 Encyclopedia of Nanoscience and Nanotechnology,* Vol X, Ed H. S. Nalwa and R. Smalley(CA, USA: American Scientific Publishers)p1

Hirabayashi, K., Kozawaguchi, H., and Tsujiyama, B., *J. Electrochem. Soc.*, 1983, 130, p 2259

Hozumi, A., Sugimura, H., Hiraku, K., Kameyama, T. and Takai, O., *Nano Lett.*, 1(8) pp 395 – 399(2001)

Hu, J., Odom, T.W., Lieber, C.M., *Acc. Chem. Res.,* 1999, 32,435

Huber, T. E., Graf, M. J., Foss, C. A. Jr. and Constant, P., *J. Mater. Res.,* **15**, No. 8 1816-1821 (2000)

Huber, C. A., Huber, T. E., Sadoqi, M., Lubin, J. A., Manalis, S.and Prater, C. B., *Science.* **263**, 800-802 (1994)

Hulteen, J.C. and Martin, C.R., *J. Mater. Chem.*, 1997, 7(7), 1075-1087.

Jaffe, P.M., *J. Electrochem. Soc.,* (1961), **108**, 711

Jessensky, O., Müller, F., and GÖsele, U., *Applied Physics Letters*, vol. **72**, 1173–1175(1998)

Ji, R., Lee, W., Scholz, R., Gösele, U., Nielsch, K., *Adv. Mater.,*2006,18, 2593-2596

Jo, M.H., Park, H.H., Kim, D. J., Hyun, S. H., Choi, S.Y. and Paik, J. T, *J. Appl. Phys.* 82 (3) 1 August (1997) 1299

Jung, K-H., Yoon, J.-W., Koshizaki, N., and Kwon, Y.-S., *Jpn. J. Appl. Phys.*, 44, 7A, 2005, pp. 5300 - 5303

Kape, J. M., Survila, E. and Wernick, S., *Trans. inst. Met. Finish.* 62 (1984) 41.

Keller,F., Hunter, M. S., and Robinson, D. L., *ibid.*, **100**, 411 (1953)

Kitai, A. H., *Solid State Luminescence*, Chapman & Hall, 1993, p160

Kitai, A.H., *Solid State Luminescence*, Chapam &h Hall, 1993, p209

Kitai, A.H., *Luminescent Materials and applications,* John Wiley & Sons, p76 (2008)

Kitai, A.H., *Luminescent Materials and applications,* John Wiley & Sons, p62 (2008)

Kohli, P.,Wharton, J. E., Braide, O. and Martin, C.R., *J. Nanosci. and Nanotech* (2004), Vol **4,** No 6. 605-610

Lee, W., Scholz, R., Nielsch, K., and Gösele, U., *Angew.Chem. Int. Ed,* **44,** 6050-6054 (2005)

Lee, J., Shimoda, W. and Tanaka ,T., *Meas. Sci. Technol.* **16**, 438-442 (2005)

Lehmann, W., *J. Electrochem. Soc.*, **104**, 1, 1957 (January), 45-50

Lenzmann, F., Li,K., Kitai, A.H., and Stöver, H.D., *Chem. Mater*. 1994,6, 156-159

Leverenz, H. W., *An introduction to Luminescence of Solids*, Wiley, New York, (1950), p61

Lew, K-K and Redwing, *J. M., Journal of Crystal Growth,* **254,** 14-22 (2003)

Li, A. P., Müller, F., Birner, A., Nielsch, K., and Gősele, U., *Journal of Applied Physics*, vol. **84**, pp. 6023–6026, 1998.

Liang, W., and Martin, C.R., *J. Am. Chem. Soc.,* 1990,112, 9666

Liu, Z., Shen, Z., Zhu, T., Shou, S., Ling, Y., Shi, Z., and Gu, Z., *Langmuir*, 2000, 16, 3569

Lossev, O.V., "Wireless Telegraphy and Telephony," *Telegrafia i Telefonia bez provodor*, no. 18 (1923), p. 61 and no. 26 (1924), p. 403

Lossev, O.V., *Philosophical Magazine*, v. **6**, no. 39 (1928), 1024-1044

Liu, Y., Ren, W., Zhang, L.Y. and Yao, X., *Thin solid films* 353 (1999) 124-128

Maeda, K., *J. Phys.Soc.(Japan)*, **13**, 11, November (1958), 1352-1361

Martin, C. R., *Science.* **266**, 1961 (1994)

Mardilovich, P. P., Govyadinov, A. N., Mukhurov, N. I., RzhevskiF, A. M. and Paterson, R. *J., Membr. Sci.98*, 131-142 (1995)

Matsumoto, F., Harada, M., Koura, N., Nishio, K. and Masuda, H., *Electrochemical and solid-state letters*, **7** (11), E51-E53 (2004)

McClure, D.S., *J. Chem. Phys.*, **39**, 2850 (1963)

Milne, W. I., Teo, K. B. K., Chhowalla, M., Amaratunga, G. A. J., Pribat, D., Legagneux, P., Pirio, G., Binh, V. T. and Semet, V., *Curr.Appl. Phys*., 2 (2002) 509

Moreau, W. M., *Semiconductor Lithography: Principles and Materials*, Plenum: New York, 1988

Nakamura, S. and Fasol, G. *The blue laser diode*, Berlin: Springer-Verlag, (1997)

Nalwa, H.S. and Rohwer, L.S., *Handbook of Luminescence,* Display materials, and Devices, 3. Display Devices, American Scientific Publishers, P36.(2003)

Nien, Y. T., Chen, I.G., Hwang, C.S. and Chu, S.Y., *J. Elecroceram.*(2006), **17,** 299-303

Ono, Y.A., Kawakami, H., Fuyama, M., and Onisawa, K., *Jpn. J. Appl. Phys.* 26 (1987) 1482

Ono, Y., in *Encyclopedia of Applied Physics,* Vol.5, ed. G.L. Trigg (VCH publishers, Inc. American Institute of Physics, Weinheim and New York,1993) P.295; in *1993 SID Seminar Lecture Notes,* Vol. II. F-1 (1993) F-1/1; in *Progress in Information Display Technology,* Vol. 1, H.L. Ong and S. Kobayashi (eds.)(World Scientific Publishing Co., Singapore, 1995), Chap. 2

Ono, Y., *Electroluminescent Displays, Series on Informatin Display*, World scientific publishing Co. Pte. Ltd, 1995, Singapore, p11

Ono, Y., Shiraga, N., Kadokura, H., and Yamada, K., *Electron. Inform. Commun. Eng., Tech. Rep.*, **89**, No. 378, 1990.

Park, M., Harrison, C., Chaikin, P. M., Register, R.A., Adamson, D.H., *Science*, 1997, 276, 1401-1404

Possin G E, *Rev. Sci.Instrum*.,(1970) **41**,772

Poretics Corporation, Livermore, CA, Product Guide, 1995

Rahman, M. T., Lai, C., Vokoun, D. and Shams, N. N., *IEEE Transactions on magnetics*, VOL. **43**, NO. 6, JUNE 2007

Rao, C.N.R.FRS, and Govindaraj, *Nanotubes and Nanowires,* the Royal Society of Chemistry, 2005, p136

Riveros, G., Green, S., Cortes, A., Gómez, H., Marotti, R. E. and Dalchiele, E. A., *Nanotechnology.* **17**, 561-570 (2006)

Russ M.J. and Kennedy, D.I., *J. Electrochem. Soc.*, 114, (1976),p1066.

Rogers, W.E., *Introduction to Electric Field*: A Vector Analysis Approach, New York, McGraw-Hill Book Company, Inc., 1954, p181

Round,H. J., *Electrical World*, v. **19** (February 9, 1907), p. 309.
Sanger, w., *Principles of Nucleic Acid Structures*, Spingerverlag, New York, 1986

Sarah, M., Powder contact electroluminescence, summer project (2005).

Shankarn, K. S., and Raychaudhuri, A.K., *Materials Science and Engineering C*. 25, 738 – 751 (2005)

Shingubara, S., *J. Nanoparticle Research*, 5(2003) 17-30

Shionoya, S., Yen, W.M., *Phosphor handbook* (1998), p603

Shionoya, S., Yen, W.M., *Phosphor handbook* (1998), p129

Shrader, R.E., Larach, S., and Yocom, P.N., *J. Appl. Phys.*, **42**,4529 (1971)

Solak, H. H., David, C., Gobrecht, J., Golovkina, V., Cerrina, F. and Kim, S. O., *Microelectron. Eng.* , 67 - 68 (2003) 56.

Stratton, J. A., *Electromagnetic theory,* McGraw-Hill Book Co., New York, 1941.

Sung, S.L., Tsai, S.H.,Tseng, C.H., Chiang, F.K., Liu, X.W., and Shih, H.C., *Appl. Phys. Lett.,* 1999, 74, 197

Suzuki, A., and Shionoya, S., *J. Phys. Soc. Janpan,* **31**, 1455,1971

Tannas, L., *Flat-panel Displays and CRTs*, New York: Van Nostrand Reinhold, (1985) p271

Thompson, G.E. and Wood, G.C., in *Treatise on Materials Science and Technology,* Vol. **23**, Ed by J.C. Scully, Academic, New York, 1983, p. 205

Thornton, W.A., *Bull. Am. Phys.Soc.* (1958), 3, 233

Timp, G., *Nanotechnology*, Springer-Verlag, New York(1999).

Toyli,D., *NNIN REU 2006 Research Accomplishments, MATERIALS*, 86-87

Trau, M., Yao, N., Kim, E., Xia, Y., Whitesides, G. M., *Nature*, 1997,390, 674-676

O. Vazquez-Mena, V. Savu, K. Sidler, G. Villanueva, M.A.F. van den Boogaart, J. Brugger, *Proceedings of the 3rd IEEE Int. Conf. on nano/Micro Engineered and Molecular Systems*,January 6-9, 2008, Sanya, China

Vecht, A. and Chadha, S.S., *Powder EL displays*, CompEuro '89., 'VLSI and Computer Peripherals. VLSI and Microelectronic Applications in Intelligent Peripherals and their Interconnection Networks', Proceedings

Vecht, A., *British Journal of Applied Physics*, vol. **1**, Ser. 2 (January 1968), 134-136.

Vecht A., Smith, D.W., Chadha, S.S., Morton, D.C., and Miller, M.R., *Electrochem. Soc. Extended Abstracts*, Oct. 1990, No. 525, pp. 896-897

Vlasenko, N.A. and Popkov, I. A., *Optics & Spectroscopy*, v. **8** (1960), 39-42.

Vlassiouk, I., Krasnoslobodtsev, A., Smirnov, S. and Germann, M., *Langmuir* (2004), 20, 9913-9915

(a) Wagner, R.S.,*Whisker Technology* ed. Levitt, A.P., Wiley-Interscience, New York, 1970 (b) Wagner, R.S., and Ellis, W.C., *Appl. Phys. Lett.*, 1964, 4, 89.

Wernick, S. and Pinner, R., *Finishing of Al*, Ed. By R. Draper, London, 1976

Weichold, O., Hsu, Shou-Chian and Mölle,M., *J. Mat. Chem.*,2006,16, p 4475-4479.

Whitesides, G.M., Mathias, J.P., Seto, C. T., *Science*, 1991, 254, 1312-1319
Wirtz, M., Parker, M., Kobayashi, Y., and Martin, C.R., *Chem.Eur. J.*, 8, No.16 (2002) 3572-3578

Wu, C.-G., and Bein, T., *Sicence*, 1994,264,1757

Wu, Y., Yan, H., Huang, M., Messer, B., Song, J. H., and Yang, P., *Chem. Eur. J.*, (2002), 8, No.6. p1261

Wu, Y., and Yang, P., J. Am. Chem. Soc.,2001, 123,3165

Wu, Q., Ross, A.D., and Gleason, K., *Plasma Process. Polym*. 2(2005) 401

Xia, Y., and Whitesides, G., M., *Angew. Chem. Int. Ed.* 1998, 37, 550-575

Xia, Y., Zhao, X.-M., Whtiesides, G.M., Microelectron. Eng., 1996, 32, 255-268

Xu, J., Petkov, N., Wu, X. Y., Lacopino, D., Quinn, A. J., Redmond, G., Bein, T., Morris, M. A. and Holmes, J. D., *ChemPhyschem,* **8**, 235-240 (2007)

Yang, C.J., Chen, C., Wu, P.W.,, Shieh, J.M., Wang, S.M. and Liang, S.W., *J. materials research*, (2007) vol.**22**, iss.4, 1064 –1071

YASUI, K., NISHIO, K.,and MASUDA, H., *Jpn. J. Appl. Phys.*, 44, 37, 2005, pp. L 1181 - L 1183

Yoon, H., Deshpande,D.C., Ramachandran, V., and Varadan, V., K., *Nanotechnology*, 19 (2008), 2, p53

Zhang, Z., Ying J.Y., and Mildred, S.J., *J. Mater. Res*. **13**, 1745 (1998)

Zhang, Z.,Gekhtman, D., Dresselhaus, M.S., and Ying, J.Y., *Chem.Mater.* **11**, 1659 (1999)

Zhao, Q. and Zhu, Q., *Mater. Lett.* 57 (2003) 3606